Fundamental Studies of Refined Polyelectrolyte/Surfactant Nanoparticles- Bulk and Interfacial Properties

By

Yan Gao

Submitted to the graduate degree program in Department of Chemical and Petroleum Engineering and the Graduate Faculty of the University of Kansas in partial fulfillment of the requirements for the degree of Doctor of Philosophy.

Committee members:

_____
Prajnaparamita Dhar, Ph.D.
(Chairperson)

_____
Jenn-Tai Liang, Ph.D.
(Co-chairperson)

_____
Stevin H Gehrke, Ph.D.

_____
Edward Peltier, Ph.D.

_____
Jyun-Syung Tsau, Ph.D.

Date defended: 08-04-2014

The Dissertation Committee for Yan Gao certifies that this is the approved version of the following dissertation:

Fundamental Studies of Refined Polyelectrolyte/Surfactant Nanoparticles-Bulk and Interfacial Properties

Committee members:

_____
Prajnaparamita Dhar, Ph.D.
(Chairperson)

_____
Jenn-Tai Liang, Ph.D.
(Co-chairperson)

_____
Stevin H Gehrke, Ph.D.

_____
Edward Peltier, Ph.D.

_____
Jyun-Syung Tsau, Ph.D.

Date approved: 09-07-2014

Abstract

Novel surfactant/polyelectrolyte complexes have been the focus of recent research efforts due to their applications in consumer products, petroleum engineering and biotechnology. The interaction between surfactant and polyelectrolyte results in considerable system property change, such as foam stability, wettability and coating properties. Currently, most research efforts on this topic focus on the behavior of the complex system (including nanoparticles, free surfactants, dispersed surfactant and polyelectrolyte aggregates) with very few studies aimed at understanding the bulk properties and interfacial behavior of the self-assembled nanoparticles alone.

In this dissertation, the bulk properties of refined polyethylenimine(PEI)/sodium dodecyl sulfate (SDS) nanoparticles with and without salts were first investigated. The self-assembly of positively charged nanoparticles had a narrow particle size distribution. Particle size, surface charge and the stability of the nanoparticle solution are controlled by pH, stock solution ratio as well as ionic strength. Additionally, in the presence of salts, both co-ions and counter-ions affected the stability of these refined colloidal particles. The observed results were different from the effect of salt on polyelectrolyte/surfactant mixtures where the salts interact with the individual compound not the particle as a whole. Moreover, the electrostatic interactions and solvation forces are important for the interaction between the salts and refined nanoparticles.

To study the interfacial properties, surface tension measurements was employed as a first step to investigate the adsorption of PEI/SDS nanoparticles to the air/water interface. These results were correlated with the interfacial microrheology and microscopy data to study the details of the short and long term interfacial behavior of these surfactant-like

particles. In this study, we discovered an interfacial induced disassembly of these refined nanoparticles. Such novel phenomena can lead to several potential applications.

Also, adsorption of these refined nanoparticles at solid/liquid interface was investigated by means of quartz crystal microbalance with dissipation (QCM-D) and atomic force microscopy (AFM) techniques. First, it was found that gold surface with low charge density rendered loose binding between nanoparticles and gold surface allowing rearrangement of the adsorbed nanoparticles. Further, the negatively charged silicon dioxide had stronger electrostatic attraction with the positively charged nanoparticles, leading to tight binding of nanoparticles on the surface, it was then hard for the nanoparticles to rearrange themselves on the surface.

Acknowledgement

First and foremost, I would like to express my gratitude to Prof. Prajna Dhar and Prof. Jenn-Tai Liang who are not only excellent researchers but also superb educators. Their continuous motivation supported me during the entire period of this study. They have taught me a lot about critical thinking and how to approach research problems analytically. Their many insights have been a critical part of this work, and I thank them for contributing many great ideas. This work would have not been accomplished without their guidance and support.

Deep appreciation is also extended to Prof. Cory Berkland and Dr. Stephen Johnson for being so generous in their time and being very helpful in discussing this work, especially in the area of colloidal stability.

I would like to thank Dr. Ying-Ying Lin for her great help in optimization of the PEI/SDS nanoparticle system, and Nicolas Joseph Mucci for his help in operating the AFM equipment. I would also like to thank Dr. Huili Guan, Dr. Kaixu Song, Dr. Shengxue Xie, and Dr. Ying Wang for their insightful comments that greatly improved the whole research. I am also thankful to Dr. Qiang Ye for providing access to their lab instruments.

I extend my appreciation to Prof. Stevin Gehrke, Prof. Edward Peltier, and Dr. Jyun-Syung Tsau for serving in my committee.

My deep appreciation is also extended to Dr. Phil Sullivan and Dr. Alhad Phatak in Schlumberger for their instructions that help me further understand polymer rheology.

I greatly appreciate Dr. Karen Peltier for all her assistance with construction and operating laboratory equipment and procedures. I also thank all my fellow students in Dr. Dhar's lab for their help and friendship.

Finally, I would like to dedicate this document to my beloved parents and my husband, Weiwei Li, for their love and support.

Table of Contents

List of Figures

List of Tables

1 Introduction

1.1 Motivation and objectives

Complexes of polyelectrolytes with surfactants of opposite charge form through combination of cooperative electrostatic interactions and hydrophobic interactions. Due to the ease of assembly of these complexes, they have been widely used in various applications such as consumer products, petroleum engineering and biotechnology. In the complex mixtures, the polyelectrolyte/surfactant nanoparticles, free surfactants, dispersed surfactant and polyelectrolyte aggregates are all included. The refined polyelectrolyte/surfactant nanoparticles are defined as resuspended nanoparticles obtained after centrifugation of polyelectrolyte/surfactant mixtures. The behavior of the complex system (including nanoparticles, free surfactants, dispersed surfactant and polyelectrolyte aggregates) has been studied extensively over the past few years [1-4]. In contrast, studies reported on the refined polyelectrolyte/surfactant nanoparticles are very limited.

Until recently, the featured properties of self-assembled nanoparticles without any excess surfactant or polyelectrolytes have been pinpointed [5, 6]. The refined nanoparticles have well-controlled size and charge, low polydispersity [6], ultra low interfacial tension, adhesive properties [7]. These properties make them of great interest for potential industrial applications such as nanocarriers for pharmaceutical purposes [6], flocculation of colloidal nanoparticles, or even as delivery vehicle for control release of oil field chemical agents [8]. In spite of their great potential for various end-uses, the bulk and interfacial properties of these refined nanoparticles are not well understood.

Muller and co-workers [5, 6, 9] have demonstrated that the behavior of these refined nanoparticles is significantly different from that of polyelectrolyte surfactant mixtures. In the

mixtures, the complexes are usually treated as individual components and the external stimuli (pH, ionic strength) do not only change the interactions between the bound polyelectrolyte and surfactant, but also alter the equilibrium between the unreacted component and bound polyelectrolyte and surfactant. Contrarily, the resuspended nanoparticle can be treated as a whole soft permeable particle. Besides, the adsorption refined nanoparticles on solid substrate showed large dissimilarity in conformation on the surface when compared to the mixtures [5, 10]. As a consequence, fundamental studies on both intrinsic bulk and interfacial properties and dependence of these properties on the external environmental change (pH and ionic strength) as well as the correlation between nanoparticle properties and practical applications need to be studied and explored systematically.

Additionally, for the interfacial property test at liquid/liquid interface, a surface rheometer is needed to characterize the interparticle interactions between the nanoparticles at the surface. However, due to the low sensitivity of commercial surface rheometer, it is difficult to measure the surface viscosity accurately, even harder to decouple the response of the two-dimensional interfacial film from that of the three-dimensional subphase [11-14]. Therefore, a more sensitive surface rheometer is needed for quantifying the interfacial viscosity at the surface accurately.

The objective of this dissertation is to understand both bulk and interfacial properties of refined self-assembled polyelectrolyte/surfactant nanoparticle. Considering the potential application environment, we also studied the effect of different salts on the stability, surface activity as well as solid/liquid interface adsorption. These understandings help to provide an engineering guideline for designing polyelectrolyte/surfactant nanoparticles with specific properties for industrial formulations.

1.2 Overview of the dissertation

Chapter 2 reviews the existing literature pertaining to polyelectrolyte and surfactant systems, and briefly introduces the refined nanoparticles composed of polyelectrolyte and surfactant and the methods that were used in the following chapters. Chapter 3 focuses on the bulk properties of refined polyethylenimine (PEI)/ sodium dodecyl sulfate (SDS) nanoparticles, and attempts to provide comprehensive characterizations of these nanoparticles, including particle size, zeta potential, and particle stability. This chapter also reports on investigations on the influence of different salts on the stability of the refined nanoparticles. Chapter 4 explores the interfacial properties of PEI/SDS nanoparticles at the air/liquid interface by measuring the surface tension using wihelmy plate as well as evaluating the surface conformation by a self-designed microrheology technique. In chapter 5, I report on the interfacial behavior of the same system at a solid-liquid interface. The mechanism of interactions between nanoparticles and different solid substrates with different surface chemistry was investigated. Chapter 6 provides an overall summary in which both bulk and interfacial properties are linked to potential applications as well as an outline for future studies.

References

[1] C.D. Bain, D. Langevin, R. Meszaros d, T. Nylander, C. Stubenrauch, S. Titmuss, R. V. Klitzing, Advances in Colloid and Interface Science 155 (2010) 32.

[2] X. L. Zhang, R. K. Thomas, J. Penfold, Journal of Colloid and Interface Science 356 (2011) 656.

[3] B. A. Noskov, S. Y. Lin, G. Loglio, R. Miller, Langmuir 23 (2007) 9641.

[4] L. Chiappisi, M. Gradzielski, Soft Matter 9 (2013) 3896.

[5] T. Reihs, M. Muller, K. Lunkwitz, Journal of Colloid and Interface Science 271 (2004) 69.

[6] M. Muller, T. Reihs, W. Ouyang, Langmuir 21 (2005) 465.

[7] J. Qin, R. Farina, S. L. Perry, L. Leon, J. Whitmer, K. Hoffmann, M. Tirrell, J. J. de Pablo, ACS Macro Letter 3 (2014) 565.

[8] C. Berkland, J. T. Liang, G. P. Willhite, University Of Kansas, US Patent 8 183 184, 2012.

[9] T. Reihs, M. Muller, K. Lunkwitz, Colloids and Surfaces A: Physicochem. Eng. Aspects 212 (2003) 79.

[10] S. Ondaral, L. Odberg, L. Wagberg, Langmuir 26 (2010) 14606.

[11] P. G. Saffman, M. Delbruck, Proceedings of the National Academy of Sciences, USA 72 (1975) 3111.

[12] T. M. Fischer, P. Dhar, P. Heinig, Journal of Fluid Mechanics 558 (2006) 451.

[13] V. Prasad, S. A. Koehler, E. R. Weeks, Physical Review Letter 97 (2006) 176001.

[14] M. H. Lee, D. H. Reich, K. J. Stebe, R. L. Leheny, Langmuir 26 (2010) 2650.

2 Background & Techniques

In this chapter, polyelectrolyte, surfactant, and self-assembled polyelectrolyte surfactant nanoparticle are reviewed. In section 2.1, a general introduction to polyelectrolyte is presented. In section 2.2, basic information about surfactant is introduced. In section 2.3, the main focus is about oppositely charged polyelectrolyte and surfactant. The binding mechanism and phase behavior of polyelectrolyte/surfactant complex are explained in details in 2.3.1, 2.3.2 and 2.3.3. The interfacial properties of polyelectrolyte/surfactant complex and the techniques for characterization of interfacial properties are briefly introduced in 2.3.4. The refined polyelectrolyte/surfactant nanoparticle is then defined in section 2.3.5 following general information about polyethylenimine/sodium dodecyl sulfate system in section 2.3.6.

2.1 Polyelectrolyte

2.1.1 Polyelectrolyte classification

Polyelectrolytes are polymers containing multiple ionic groups. In polar solvents such as water, these groups can dissociate, releasing counter ions into the aqueous phase, and making the polymer chains charged [1]. There are two opposite forces control this process: the counter ions-releasing driving force and the electrochemical potential, which attracts the oppositely charged counter ions to the polyelectrolyte chain. Count ions driven by those two forces develops two states of “free” and “condensed” counter ions around the polyion chain in dilute solutions, similar to the electrical double layer for dilute colloids [2-4] (Figure 2.1). Some polyelectrolytes in aqueous solution are completely dissociated into macroion and counter ion in the whole pH range, i.e., Sodium-polystyrene and poly(diallyldimethylammonium chloride). Some polymers

remain undissociated at a certain pH range. These polymers are defined as "weak" polyelectrolytes since they cannot exhibit typical polyelectrolyte characteristics in all pH ranges [5]. Typical examples are poly(acrylic acid) (PAA) and poly(ethylenimine) (PEI). PAA is not dissociated at low pH while PEI is charge-neutral at high pH. Polyelectrolytes can also be classified into polyanions, polycations and polyampholytes according to their charges (Figure 2.2) [1].

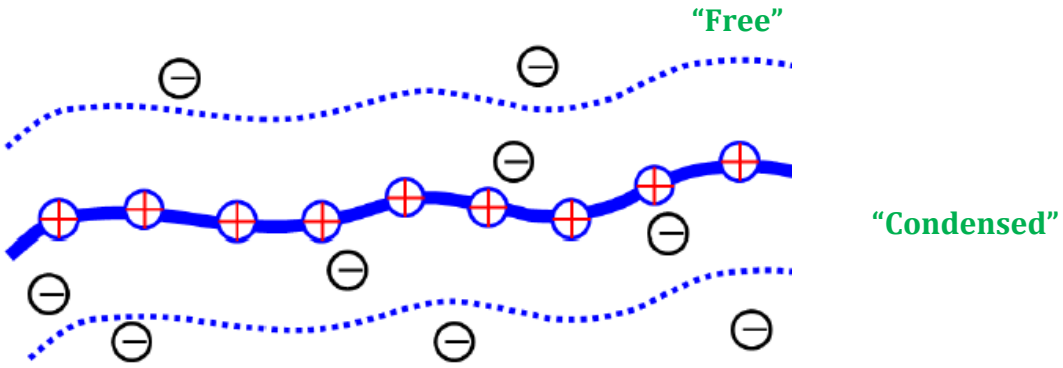

Figure 2.1 Schematics of the polyelectrolyte with "condensed" and "free" counterions [2]

Polyelectrolytes carrying both anionic and cationic groups are called "polyampholytes". For example, proteins belong to polyampholytes. They possess positive charge in acid media, negative charge in alkaline media and become charge neutral at the "isoelectric point".

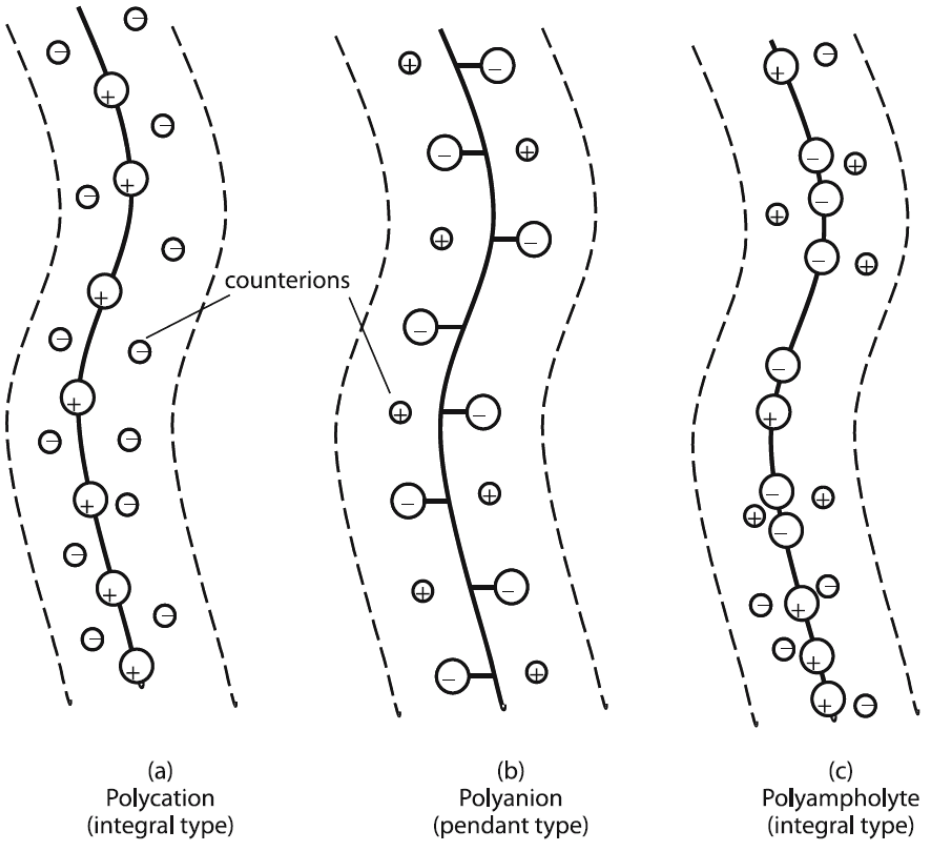

Figure 2.2 Classification of polyelectrolytes in terms of their charge [1]

2.1.2 Factors that affect polyelectrolyte properties

The ionic groups on the polymer chains determine the charge of the polyelectrolyte. The functional group attached to a polymer include:

$-COO^-$, $-CSS^-$, $-OSO_3^-$, $-SO_3^-$, $-OPO_3^{2-}$, $-NH_3^-$, $=NH^-$, $\equiv NH^-$, $-NR_3^-$

The ionization of the polyelectrolyte indicates the proportion of charge groups in the macromolecule. In the particular case of polysaccharides such as guar gums and starches, a limited number of the hydroxyl groups present on each sugar unit are active for substitution reactions. In this case it is customary to use the degree of substitution (DS) to express the number of charged groups per monomer (sugar) unit. For synthetic polyelectrolytes the charge density is often used to express the molar percentage of charged monomers in the copolymer. The charge density of these polyelectrolytes

depends on the dosage and reactivity of the respective monomers used in the polymerization steps of the manufacturing process. As a rule, the polymer is defined as polyelectrolyte if more than one tenth of the monomer sites are charged.

2.2 Surfactants

Surfactants are surface-active agents, which can lower the surface tension by adsorbing at air/liquid interface. The surfactant is characterized by its tendency to absorb at interfaces. The adsorption of surfactant to an interface is driven by the free energy decrease on the phase boundary. Interfacial tension is used to define free energy per unit area. Whenever the surface is covered by the surfactant, the surface tension is reduced [6].

Surfactants are amphiphilic in nature [7]. They consist of a hydrophilic head group and a hydrophobic alkyl tail group (Figure 2.3). The tail part may contain one or more alkane chains or ring structures. It can be either linear or branched. The composition of the hydrophobic tail can be a hydrocarbon, fluorocarbon or a siloxane while the hydrophilic head group can be anionic, cationic or neutral. The head group determines the properties of the surfactant. The surfactants are classified as non-ionic, ionic, or zwitterionic based on the charge carried by the head group (Figure 2.4) [8-10].

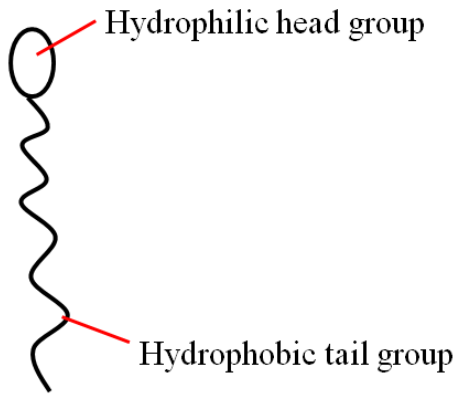

Figure 2.3 Schematics of surfactant structure

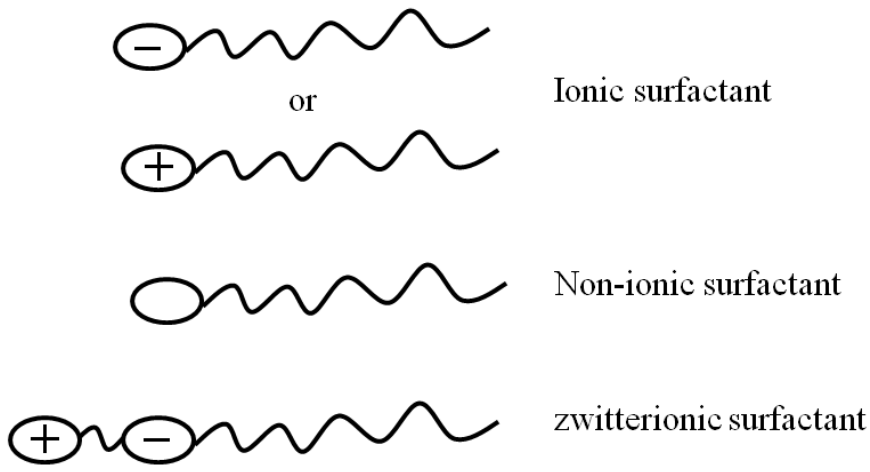

Figure 2.4 Classifications of surfactants in terms of the charge of their head groups

In aqueous solutions, surfactants are soluble as monomers, as the concentration increases above their critical micelle concentration (CMC), these molecules prefer to self assemble into aggregates, shielding the hydrophobic tail group in order to minimize the contact with water. Self-assembly of amphiphilic molecules is a physicochemical process by their amphiphilic molecular structure [3]. During self-assembly, various structures are found depending on the concentration, pH, salt, pressure and temperature. Micelles are simple structures that are formed by surfactants at CMC in aqueous media. Critical micelle concentration (CMC) is an important parameter for surfactants. Micelles can self-assemble into spherical, cylindrical shapes and vesicles/lamellar phases (Figure 2.5). The relationship between the micelle shapes and packing number p can be found in Figure 2.5. In a non-polar solvent, the hydrophobic tails point in the direction of the solvent and the core is formed by the hydrophilic groups. Such structures are known as reverse micelles, which also have spherical or cylindrical shapes.

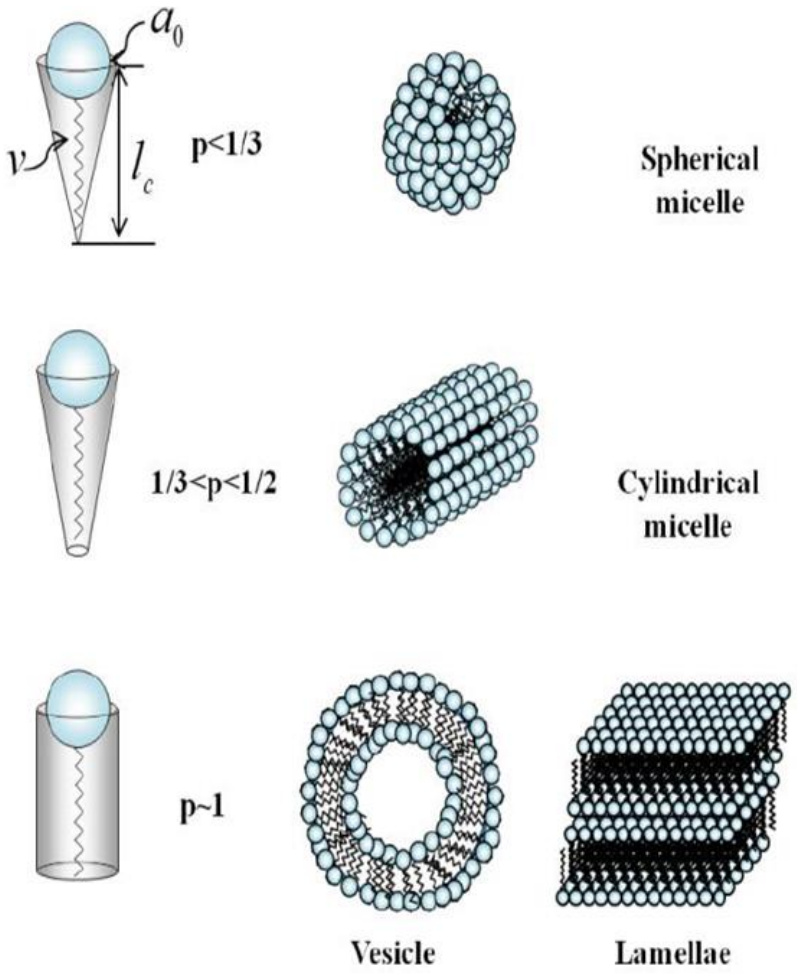

Figure 2.5 Relationship between different micelle structures and packing parameter p (p is a dimensionless packing parameter, which is expressed in terms of geometrical parameters as $\frac{V_S}{a_0 l_C}$, where V_S is the hydrophobic tail volume, a_0 is the optimal head group area, and l_C is the length of the surfactant tail at its full extension [2]

2.3 Oppositely charged polyelectrolyte/surfactant system

The interaction between water soluble polymers with surfactants has been extensively studied due to the importance of these systems in applications in laundry, personal care, coating, electronics, and pharmaceutics [11]. These application systems can be broadly divided into three categories: nonionic water-soluble polymer/surfactant systems, polyelectrolyte/surfactant systems and hydrophobically modified polyelectrolyte/

surfactant systems [12]. In this dissertation, the oppositely charged polyelectrolyte/ surfactant systems are the main focus.

2.3.1 Mechanisms of polyelectrolyte and surfactant binding

Polymer/surfactant binding was first studied by Saito in the 1950s [13]. The conceptual framework for this system was established by Jones in 1967 [14]. The electrostatic force and hydrophobic force are considered to be the dominate contributions to the molecular forces relevant for interaction between the polyelectrolyte chain and free, aggregated or micellized surfactants in dilute solution [15, 16]. These forces have been intensively studied and shown to be important for many different polyelectrolyte-surfactant systems [17-20].

The electrostatic interaction not only exists in the direct attraction between the oppositely charged polyelectrolyte and surfactant, but also involves the release of counterions [16]. In this way, although the direct electrostatic force is enthalpic, the ion-exchange process for polyelectrolyte-surfactant binding is usually accompanied by a significant entropy gain due to counterion release [19, 21].

A large gain in system entropy on the liberation of unfavorably organized water molecules surrounding the hydrophobic regions during the binding process results in the hydrophobic force [22]. The hydrophobic interaction can be proven by the formation of polyelectrolyte-surfactant complex at a pH of polycation neutralization. It is largely dependent on surfactant hydrophobicity [19, 22] and other parameters, such as the ionic strength and pH [18].

Significant work has been done to describe these association mechanisms. The models fall into two categories: the polyion-micelle interactions [21, 23-25] and the specific ion-

ion interactions [10, 16, 17, 26]. In the former case, a competition between electrical attractions and entropy effects is emphasized; distinct micelle-like surfactant clusters along the polymer backbone, known as string of pearls model, is observed (Figure 2.6 [27]). Goddard *et al*. [28] proposed a model which involves site-site specific ion-ion interactions. This ion-ion interaction model is based on small micelle-like aggregates of surfactant nested within a polyion with neutralization of the charges on the surfactant aggregates by adsorption of the polyion [28]. These molecular models support the coarse-grained description of the overall process in the former, polyion-mediated micellization theories. This model has also been observed and proven by small angle neutron scattering results, which show micelle-like structures of surfactants intercalated by polymer chains [29].

However, the real case of surfactant polymer mixtures is less simple, because the variation of the size and the shape of the surfactant aggregates in the polyelectrolyte/ surfactant complexes, micelles are bound to the polymer chains; sometimes their degree of aggregation is different from that of the pure micelles, depending on the properties of the polyelectrolytes [30]. The binding of surfactants with the polyelectrolyte can reduce the electrostatic interaction between surfactant head groups leading to formation of micelle at lower concentration in the complex.

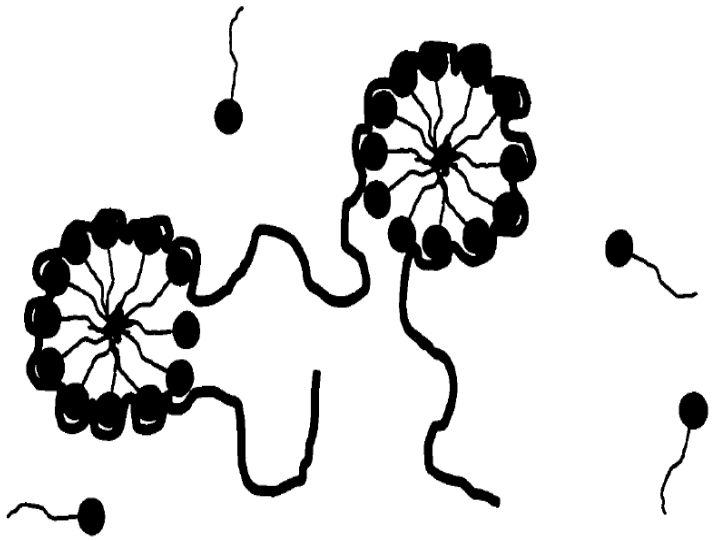

Figure 2.6 The structure of string of pearls model [27]

2.3.2 Phase behavior of polyelectrolyte/surfactant mixtures

The phase behavior of the mixtures depends on surfactant-to-polyelectrolyte charge ratio (Z). The equation for Z is listed below:

$$Z = \frac{Charge\ desity\ of\ the\ Surfactant}{Charge\ density\ of\ the\ Polyelectrolyte} \qquad (2.1)$$

A scheme for the phase behavior is given in Figure 2.7. From the phase diagram, at low surfactant-to-polymer ratios, where the polyelectrolyte charge is in excess or Z < 1, the polyelectrolyte binds with either individual surfactant molecules or micelles. The surfactant head groups can bind to the polymer charge sites without significantly reducing the solubility of the resulting complex. Thus the first region of the phase map is a transparent, non-birefringent phase which is termed isotropic [31]. At this stage, the polyelectrolyte-surfactant association is mainly entropy-driven, with the release of the simple monovalent counterions (e.g., Na^+ and Cl^-) [32-36]. At total surfactant concentrations below critical micelle concentration (CMC), the increasing concentration of surfactant around a polyelectrolyte chain leads to the formation of surfactant

aggregates (micelles). This cooperative binding occurs at critical aggregation concentration (CAC) [20, 37]. The CAC is always 1~3 orders of magnitude lower than the CMC in the absence of polymer. When the surfactant concentration is increased above CAC, the amount of surfactant bound to polymer increases until a saturation concentration, or C_{sat}, is reached [14]. C_{sat} is found to be directly proportional to polymer concentration. Beyond C_{sat}, free micelles form when the surfactant monomer concentration reaches the CMC. There is debate in the literature as to whether or not the surfactant monomer concentration increases between CAC and C_{sat} [38].

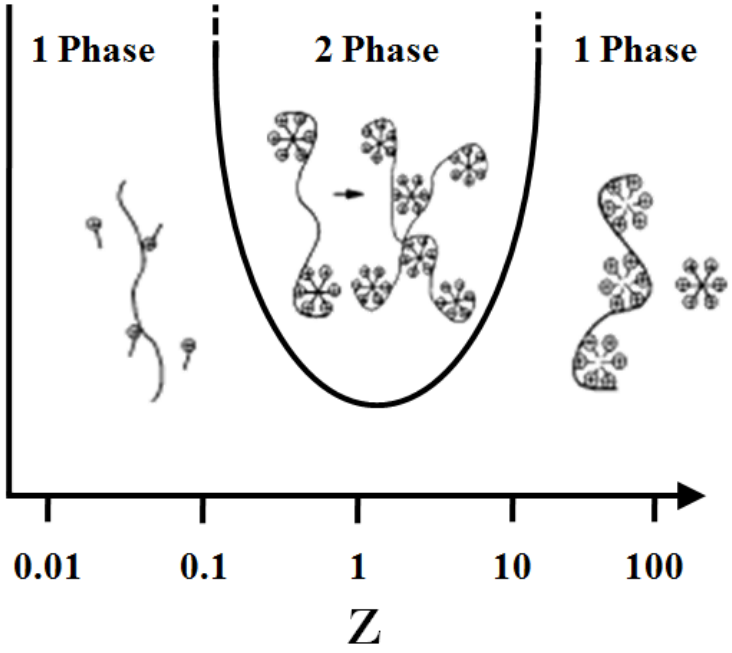

Figure 2.7 Phase diagram of polyelectrolyte-surfactant mixtures as a function of the charge ratio (Z) [36]

At equal charge ratio (Z=1), a two-phase region with precipitated complex and excess water forms. As the surfactant-to-polymer ratio increases, the total charge from the surfactant begins to approach the complimentary charge from the polymer. There is then a tendency for the complex to divide into a liquid-like (coacervate) and a solid-like

(precipitate) phase in equilibrium with very dilute solution [39]. In this way, the second characteristic region of the phase diagram is marked by turbidity or the presence of a definitive second phase. There is also a maximum "precipitation" representing the stoichiometric 1:1 surfactant/polymer charge unit neutralization. However, the phase separation region sometimes spans a range of surfactant-to-polymer charge unit ratio, depending on the nature of the polyelectrolyte-surfactant system [39, 40]. Zhou et al. [41] reported a lower limit about Z = 0.8 for cationic hydroxy ethyl cellulose/SDS. Upper limits range from 3:1 (reported by Goldraich *et al* [42]) for Polymer JR-400/SDS to 10:1 for cationic modified acrylamide/SDS. This second phase is observed to have a gel-like consistency [33, 43] consistent with the dehydration of the surfactant/polyelectrolyte ion pairs. Figure 2.8 shows the phase map for the Sodium dodecyl sulfate (SDS)/ poly(dimethyl diallyl ammonium chloride (pDMDAAC) system [44]. Open diamonds indicate one phase of polyelectrolyte/surfactant mixture; closed triangles mean the occurrence of a second phase on the colloidal size range; and solid squares represent solutions with clear supernatant and solid sediments; and open squares are the indication of solid suspension. The dotted line denotes 1:1 charge stoichiometry between the polyelectrolyte subunits and the SDS. It is observed from this graph that the two-phase region does not exist only at a polyelectrolyte: surfactant charge ratio of 1:1, but can be observed in a range of polyelectrolyte: surfactant ratios.

For Z > 1, there is excessive surfactant, therefore the free surfactant has the potential to dissolve the polyelectrolyte-surfactant precipitates and make them resuspended in the suspension. At this stage, the polyelectrolyte is surrounded and stabilized by the surfactant in a micelle solution; the mixture becomes clear again. Also, since the excess

surfactant may bind onto the neutralized polyelectrolyte and surfactant micellar core, the polyelectrolyte-surfactant complex will carry the same charge as the surfactant.

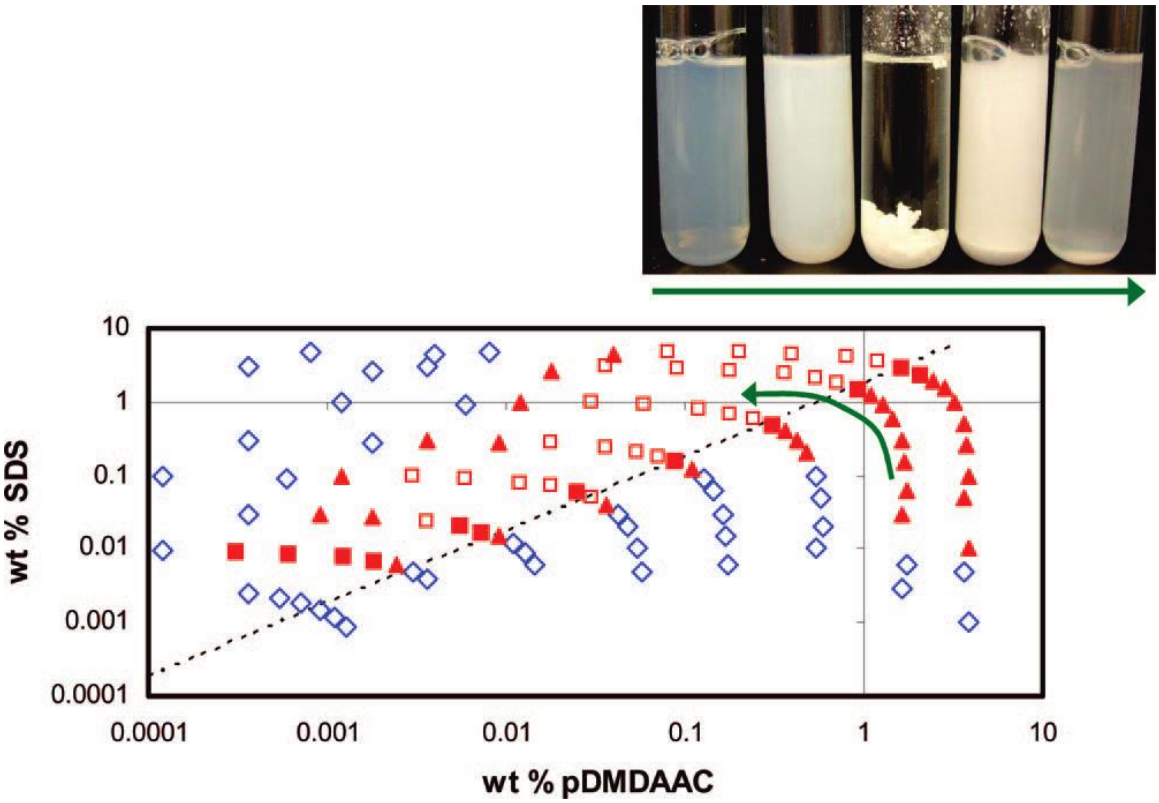

Figure 2.8 Phase map for the SDS/pDMDAAC system, showing the two-phase region at 23 ℃ [44]

2.3.3 Non-equilibrium state of polyelectrolyte/surfactant complexes

In the phase behavior study of polyelectrolyte-surfactant complex, a very distinguished feature is long-lived nonequilibrium redissolution states [45-49]. The nonequilibrium states often depend on the mixing procedure. For example, Naderi *et al*. [45] reported that the order of addition has a great impact on the size of the polyelectrolyte-surfactant complex aggregates. Adding either polyelectrolyte to surfactant or surfactant to polyelectrolyte and different surfactant/polyelectrolyte mixing ratio may lead to different

properties of complexes. Figure 2.9 shows a schematic graph of turbidity as a function of different surfactant/polyelectrolyte ratio or polyelectrolyte/surfactant ratio. Adding excessive surfactant into polyelectrolyte solution will redissolve the complex aggregates, while adding polyelectrolyte to surfactant will not observe the same phenomena. Meszaros *et al*. [29, 47, 49] proposed that the redissolution of complex precipitates leads to formation of water-like solution with low turbidity and such system is not a one-phase, thermodynamically stable system but a kinetically stable colloidal system. It has been pointed out that only very low molecular weight polyelectrolyte is preferred to form one-phase thermodynamically stable solution [50].

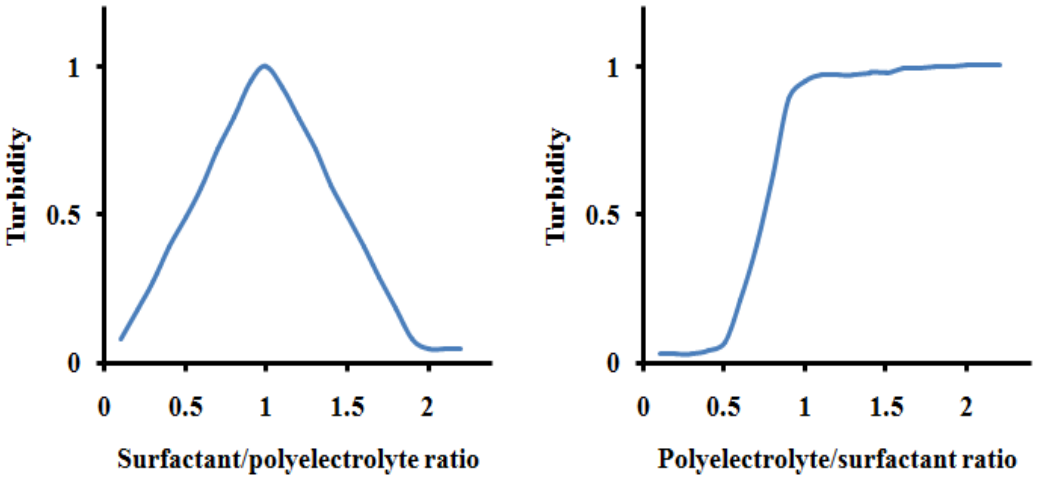

Figure 2.9 Schematics of the complex turbidity based on order of addition [51]

2.3.4 Interfacial properties of polyelectrolyte/surfactant complexes

2.3.4.1 Air/water interface

Surface tension is the cohesive forces between liquid molecules; this force will allow the liquid surface to resist an external force [52]. Usually, the reduction of surface tension is an indicator of the formation of surface complexes since surface tension is very sensitive

to small variations of the absorbed complex on surface. Meanwhile, surface tension also reflects the formation of polyelectrolyte/surfactant aggregates in bulk.

Figure 2.10 shows the conditions in the bulk and on the surface of a polyelectrolyte/surfactant mixture. The solid line shows the surface tension as a function of surfactant concentration when no polyelectrolyte is added. Surface tension decreases as the surfactant concentration increases, till a plateau is observed at critical micelle concentration (CMC) and beyond. When the surfactant concentration is increased at a constant polyelectrolyte concentration, the surface tension variation is shown in the dash line curve. Surface tension starts decreasing upon addition of the surfactant and reaches a plateau at a concentration at critical aggregation concentration (CAC), which is caused by the adsorption of surfactant monomers with or without polymer. After this plateau, a second decrease is observed, which is followed by another plateau, the onset of which is the CMC, same as the case without polyelectrolyte.

However, not all oppositely charged polyelectrolyte/surfactant systems show the same trend of surface tension. The changes of the degree of charge or solution pH can result in different results of surface tension curves. Depending on the relative stabilities of the surface complexes and the complexes in the bulk phase, the surfactant can either coadsorb with polyelectrolyte or adsorb alone at the surface, giving rise to discontinuity in surface tension.

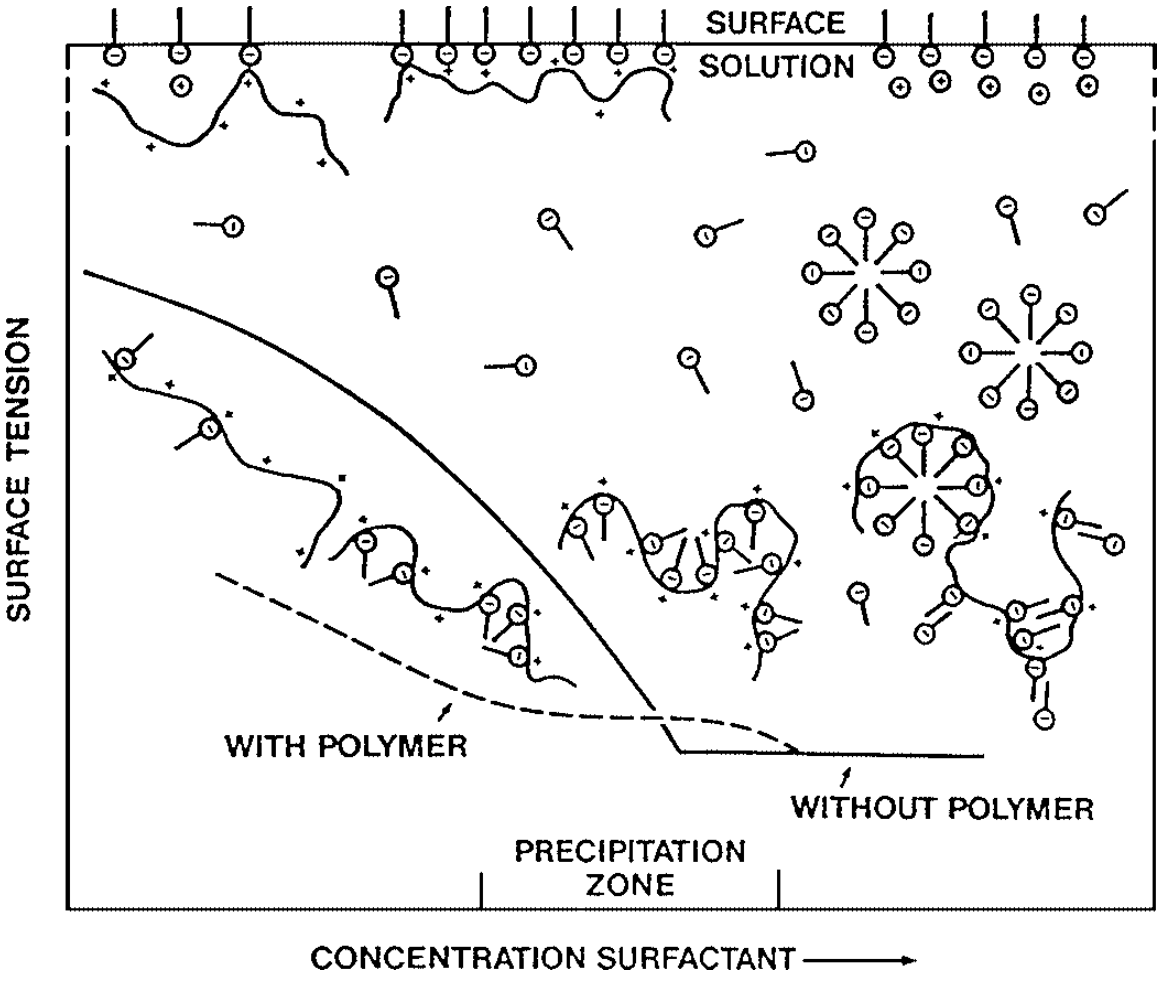

Figure 2.10 Schematics of surface tension and system composition change over surfactant concentration in the polyelectrolyte/surfactant mixture [53]

Another feature of the surface tension of polyelectrolyte/surfactant complex is the slow decrease of surface tension during the adsorption process. The formation of polyelectrolyte/surface complexes adsorption layers takes long time to reach equilibrium. Such slow kinetics of surface tension reduction may be associated with the slow unfolding of the macromolecules in the adsorption layers, increasing penetration layers and the formation of multilayers [54, 55]. According to Lankveld *et al* [56], the slow kinetics of the surface tension reduction depends on a slow differentiation in polarity of the macromolecular chains. In addition, the adsorbed layer is initially randomly packed

and then with increase of complex concentration, the diffusion process is accelerated, therefore the equilibrium surface tension is reached faster.

2.3.4.2 Solid/liquid interface

The association behavior (adsorption/deposition) of polyelectrolyte/surfactant complexes at solid surface is applied to different applications, which involve the adsorption/deposition of complexes on the surface and the control of the surface layer composition, from paints, drilling muds to personal care products and pharmaceuticals. In all of these applications, three major interactions will be carefully considered: surface-polymer interaction, surface-surfactant interaction, and surface-polymer/surfactant complexes interaction. The interaction between polyelectrolyte and surfactant is also important to adjust the adsorption properties of polyelectrolyte [29, 30, 57]. These surface properties of polyelectrolyte/surfactant complex are influenced by several factors: polyelectrolyte chain flexibility, hydrophobicity, charge density, the surfactant tail length and salt concentration. For example, the polyelectrolyte chains associate with surfactant molecules residing at the surface or in the bulk, which result in solubility decrease and the adsorption to a surface/interface [58]. When the surfactant concentration exceeds the expected phase separation concentration, the maximum adsorption on surfaces occurs. Also, when the surfactant concentration is more than sufficient, polyelectrolyte/surfactant complexes can desorb from the surface (see Figure 2.11). The methods for adsorption of polyelectrolyte/surfactant complexes at either air/liquid surfaces or solid-liquid interfaces will be reviewed in the following sections.

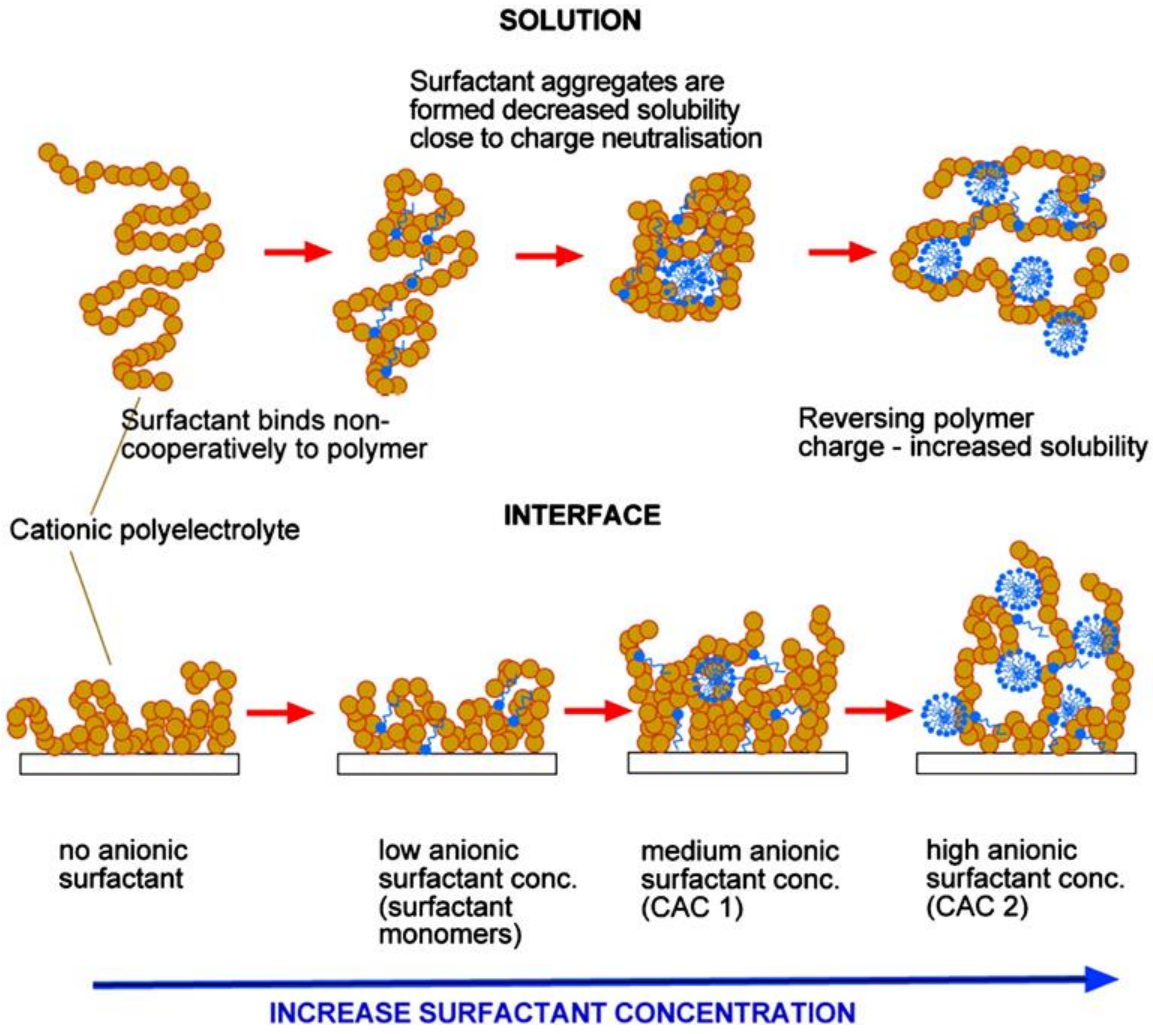

Figure 2.11 Schematic illustrations of the configuration change in the surface layer composed of a polyelectrolyte and an oppositely charged surfactant [29]

2.3.4.3 Methods for adsorption studies at air/water interface

2.3.4.3.1 Wihelmy plate technique

Different techniques have been used to study the interfacial behavior of polyelectrolytes, surfactants and their mixed solutions. Although the interfacial tension is not capable of fully describing the interfacial behavior, it is still the classical and standard method to investigate the polyelectrolyte/surfactant mixtures at the liquid/gas or liquid/liquid interfaces.

The adsorption equilibrium can be affected by surfactant concentration, alkyl chain length in the surfactant, etc. The interactions between surfactant and polyelectrolyte would alter the conformation of polyelectrolyte significantly at the surface The association of polyelectrolyte with surfactant can cause a change in hydrophilic–lipophilic balance of the adsorbed film. This can be indicated by the kinetics of surface tension reduction of polyelectrolyte/surfactant complexes when compared with pure surfactant solutions. However, the surface tension measurements are not very sensitive to the surface layer structure change, more dedicate technique is required in order to acquire addition information of the complex formation at the surface.

2.3.4.3.2 Surface rheology

Surface rheology is another important detecting method for surface behavior. It provides information about the viscosity and elasticity of the surface layer of solutions. As for surface tension measurements, the surface tension behavior for oppositely charged polyelectrolyte/surfactant mixtures is complex, so it is difficult to describe the mixture adsorption in terms of surface tension alone. More direct methods (e.g. surface rheology) for investigating the surface activities are required to interpret the interfacial properties.

The combination of surface rheology with surface tension measurements allows some insights about the rheological behavior of polyelectrolyte/surfactant complex. In general, two types of surface rheology are discussed: dilational rheology and shear rheology. Here, the dilational rheology provides information about the relaxation process and inter-molecular interaction of surface complexes, while the shear rheology refers to the structure formation at interfaces. In this dissertation, we mainly focus on the shear viscoelasticity of the surface layer.

Oftentimes, there is no clear boundary between two-dimensional surface and the bulk, the surface is adjacent to three-dimensional fluid reservoirs and it is difficult to differentiate 2D surface from 3D bulk [59-62]. The Boussinesq number B ($\eta_s/(\eta_B a), \eta_s$ is surface viscosity, η_B is bulk viscosity, a is the characteristic length of the probe) is a very important parameter to qualify this differentiation. In order to differ 2D surface layer from 3D bulk solution, B has to be greater than 1. This number is dependent on probe size. For commercial rheometer, the B is relatively small; it is not sensitive to the surface structure change. In this dissertaion, I self designed an active microrhometer, with smaller scale probes, which is capable of testing the surface viscosity as low as 10^{-9} [7].

2.3.4.4 Method for adsorption studies at solid/liquid interface-QCMD

In the 1990s, most of the studies on polymer/surfactant interaction on solid surfaces focused on analytical determination of the extent of adsorption[38]. With different variable conditions: order of addition, concentrations, surface properties, etc., recently elevated uptake of one or other of the components is a success. Also new methods used for these studies are developed with the updated knowledge, for instance, Quartz crystal microbalance (QCM-D) in Figure 2.12. It is observed that crystals can be coated with rigid material and experiments can be conducted in air or liquid such that adsorption kinetics can be monitored on a number of materials under many different conditions [9]. QCM-D measures the adsorbed mass to a surface per unit area. This factor is reflected by the resonant frequency of a vibrating quartz crystal. Modeling of the differential of frequency and mass per area at different overtones also allows for calculation of thin film viscosities of the adsorbed layers.

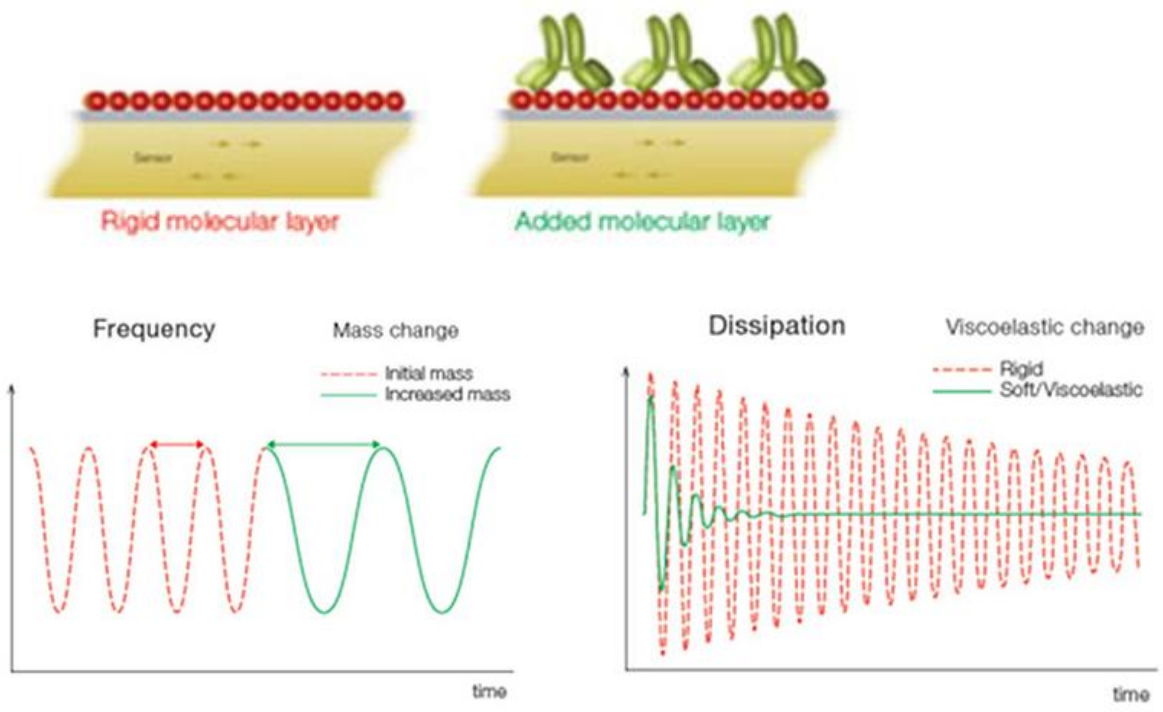

Figure 2.12 Schematic of adsorption studies on QCM-D[63]

2.3.5 Refined polyelectrolyte/surfactant nanoparticle

Electrostatic interactions usually lead to the formation of solid, lyophilic aggregates in polyelectrolyte/surfactant mixtures [64]. Once prepared, the mixture generally has two parts: (i) free polyelectrolytes and surfactants, and (ii) dispersed colloidal particles of aggregated polyelectrolyte/surfactant nanoparticles. Since the polyelectrolyte/surfactant complex exist as a mixture of complex and free compositions, the properties of pure complex (no free polyelectrolytes or surfactants), here we call it "nanoparticle", are seldom been studied. If the polyelectrolyte/surfactant mixture is centrifuged, it will be manually separated into two phases: the supernatant containing free polyelectrolytes, free surfactants and extreme small size nanoparticles; the relatively large nanoparticle precipitates. In some cases, the precipitated nanoparticle can be resuspended by vortexing or sonicating to form a pure polyelectrolyte/surfactant suspension without any free

compositions. In this research, my work focuses on the bulk and interfacial properties of the pure polyelectrolyte/surfactant nanoparticle.

In the bulk, as mixture, polyelectrolyte/surfactant complexes are commonly considered as individual compositions, for example, in the presence of salts, it is generally believed that the salt affect the equilibrium between free and bound surfactants; it induces growth of micelles as well as screens the attractive interactions between the polyelectrolyte and surfactant resulting in dissociation of the complexes. At air/water or liquid/solid interface, excessive free polyelectrolyte or surfactant in the mixture usually has priority to adsorb at the surface due to their small molecular weight and large diffusion rate. This will totally change the surface properties and further influence the subsequent adsorption of polyelectrolyte/surfactant nanoparticles [65, 66]. Therefore, interfacial behavior of refined nanoparticles free of unbound polyelectrolyte and surfactant after centrifugation are expected to be totally different from the mixtures.

2.3.6 Polyethyleneimine (PEI) / Sodium Dodecyl Sulfate (SDS) system

Among the studies on the systems of polyelectrolytes and oppositely charged surfactants, polyethyleneimine (PEI) have been widely investigated because of its intensive usage as an ingredient in pharmaceutical formulations, personal care products, food products, and household and industrial detergents. PEI exists in either linear or branched form. At low pH, the amine groups in PEI are protonated making it a highly positively charged polyelectrolyte, but at high pH, it is essentially a neutral polymer.

There have been many studies on the solution behavior of PEI/SDS mixture system. Winnik et al.[67] investigated the complex formation between branched PEI and SDS and interpreted an unusual increase in the conductivity of SDS in the presence of

hyperbranched PEI in terms of cooperative ion transport processes across the polyamine/surfactant complex. Their results identified both monomeric and micellar binding of SDS to branched PEI and provided evidence for both hydrophobic and electrostatic interaction. Yui et al.[68] showed that the electrostatic interactions between SDS and linear PEI led to an increase in the hydrophobicity of the linear PEI. Li et al.[69] found that SDS had a remarkably high affinity for PEI. The appearance of precipitation was explained by 1:1 charge neutralization, whereas the resolubilization at higher surfactant concentration was interpreted in terms of repulsive micellar interactions. To our best knowledge, no research has been done on either bulk or interface adsorption properties of refined PEI/SDS nanoparticles.

References

[1] J. Koetz, S. Kosmella, Polyelectrolytes and Nanoparticles, Springer Laboratory, 2007, 5-46.

[2] D. Li, Toward Rational Design of Polyelectrolyte-Surfactant Complexes: Thermodynamics, Microstructure and Property, University of Delaware, Delaware, 2013.

[3] O. J. Kwon, D. Lee , J. M. Park, Progress in Polymer Science 34 (2009) 1261.

[4] C. Berkland, M. Cordova, J. T. Liang, G. P. Willhite, US 11/515,580, University Of Kansas, US, 2012.

[5] J. L. Barrat,. I. Prigogine , S. A. Rice, Advances in Chemical Physics: Polymeric System, John Wiley, New York, US, 2009.

[6] K. Holmberg, B. Jönsson, B. Kronberg, B. Lindman, Surfactants and Polymers in Aqueous Solution, John Wiley & Sons Ltd., London, England, 2003.

[7] J. Penfold, D. J. F. Taylor, Current Opinion in Colloid & Interface Science 11 (2006) 337.

[8] E. D. Goddard, Colloids and Surfaces 19 (1986) 301.

[9] E.D. Goddard, Journal of Colloid and Interface Science 256 (2002) 228.

[10] K. K. Hayakawa, Journal of Physical Chemistry B 87 (1983) 506.

[11] E.D. Goddard, J. V. Gruber, Principles of Polymer Science and Technology in Cosmetics and Personal Care, Marcel Dekker Inc., New York, 1999.

[12] S. Ulrich, M. Seijo, S. Stoll, Current Opinion in Colloid & Interface Science. 11 (2006) 268.

[13] K. Hayakawa, J. C. T. Kwak, Journal of Physical Chemistry B 87 (1983) 506.

[14] M.N. Jones, Journal of Colloid and Interface Science. 23 (1965) 36.

[15] K.C. Taylor, Marcel Dekker, Inc. (1998).

[16] B. Lindman, A. Khan, E. Marques, Pure & Applied Chemistry 65 (1993) 953.

[17] K. Hayakawa, J. P. Santerre, J. C. T. Kwak, Macromolecules 16 (1983) 1642.

[18] K. Hayakawa, J. C. T. Kwak Journal of Physical Chemistry 86 (1982) 3866.

[19] D. Matulis, I. Rouzina, V. A. Bloomfield, Journal of the American Chemical Society 124 (2002) 7331.

[20] Y. Lapitsky, M Parikh, E. W. Kaler, Journal of Physical Chemistry 111 (2007) 8379.

[21] P. Hansson, M. Almgren, The Journal of Physical Chemistry 100 (1996) 9038.

[22] J. Israelachvili, Intermolecular and Surface Forces (2^{nd} ed.). Elsevier, San Diego, US, 2011.

[23] P. Hansson, Current Opinion in Colloid & Interface Science 11 (2006) 351.

[24] L.P. Wallin, Journal of Physical Chemistry 100 (1996) 17873.

[25] T. Wallin, Langmuir 12 (1996) 305.

[26] H. Okuzaki, Y. Osada, Macromolecules 27 (1994) 502.

[27] A.D. Baker. Colloidal and Interfacial Phenomena in Polymer/Surfactant Mixtures. Carnegie Mellon Unviersity, Pittsburgh, Pennsylvania, 2001.

[28] E.D. Goddard, Journal of Colloid and Interface Science 55 (1976) 73.

[29] C.D. Bain, D. Langevin, R. Meszaros d, T. Nylander, C. Stubenrauch, S. Titmuss, R. V. Klitzing, Advances in Colloid and Interface Science 155 (2010) 32.

[30] D. Langevin, Advances in Colloid and Interface Science 89-90 (2001) 467.

[31] J. Merta, T. Ikonen. R. Serimaa, P. Stenius, Macromolecules 34 (2004).

[32] S. Ranganathan, J. C. T. Kwak, Langmuir 12 (1996) 1381.

[33] F. Bai, Journal of Physical Chemistry B 108 (2004) 405.

[34] C. Wang, K. C. Tam, Langmuir 18 (2002) 6484.

[35] T.Chakraborty, I. Chakraborty, S. Ghosh, Langmuir 22 (2006) 9905.

[36] H. Wang, Y. Wang, H. Yan, J. Zhang, R. K. Thomas, Langmuir 22 (2006) 1526.

[37] M. Kasseh, E. Keh, Colloid and Polymer Science 284 (2006) 489.

[38] E. D. Goddard, Interactions of Surfactants with Polymers and Proteins. CRC Press: Boca Raton, FL, 1993.

[39] Y. Wang, K. Kimura, P. L. Dubin, W. Jaeger, Macromolecules 33 (2000) 3324.

[40] M. K. Miyake, Colloid and Polymer Science 280 (2002) 18.

[41] S. Zhou, C. Xu, J. Wang, P. Golas, J. Batteas, L. Kreeger, Langmuir 20 (2004) 8482.

[42] M. Goldraich, J. R. Schwartz, J. L. Burns, Y. Talmon, Colloids and Surfaces A 125 (1997).

[43] O. M. Anthony, C. M. Marques P. Richetti, Langmuir 14 (1998) 6086.

[44] O. Carnali, P. Shah, J. Phys. Chem. B 112 (2008) 7171.

[45] A. Naderi, P. M. Claesson, M. Bergstrom, A. Dedinaite, Colloids and Surfaces A-Physicochemical and Engineering Aspects 253 (2005) 83.

[46] A. Mezei, R. Mészáros, I. Varga, T. Gila´nyi, Langmuir 23 (2007) 4237.

[47] R. Mészáros, Journal of Colloid and Interface Science 338 (2009) 444.

[48] A. Mezei, A. Abraham, K. Pojjak, R. Mészáros, Langmuir 25 (2009) 7304.

[49] K. Pojjak, E. Bertalanits, R. Meszaros, Langmuir 27 (2011) 9139.

[50] S. dos Santos, C. Gustavsson , C. Gudmundsson , P. Linse , L. Piculell, Langmuir 27 (2011) 592.

[51] A.B. Zezin, V. A. Kabanov, Russian Chemical Reviews 51 (1982) 1447.

[52] W. J. Miller, Physical Chemistry (4th ed.). Lowe & Brydone Ltd, London, Great Britain, 1963.

[53] E. D. Goddard, Journal of the American Oil Chemists Society 71 (1994) 1.

[54] V.S. Alahverdjieva, K. Khristov, D. Exerowa, R. Miller, Colloids and Surfaces A 323 (2008) 132.

[55] I. M. Tucker, J. T. Petkov, C. Jones, J. Penfold, R. K. Thomas, S. E. Rogers, A. E. Terry, R. K. Heenan, I. Grillo, Langmuir 28 (2012) 14974.

[56] J.M. G. Lankveld, J. Lyklema, Journal of Colloid and Interface Science 41 (1972) 454.

[57] J.F. Taylor, R.K. Thomas, J. Penfold, Advances in Colloid and Interface Science 132 (2007) 69.

[58] S. dos Santos, L. Piculell, O. J. Karlssona, M. da Graça Miguel, Soft Matter 7 (2011) 1830.

[59] I. Langmuir, Journal of the American Chemical Society 38 (1917) 2221.

[60] L. Ivine, Transactions of the Faraday Society 15 (1920) 62.

[61] K.B. Blodgett, Z. Kolloid, Journal of the American Chemical Society 38 (1934) 2221.

[62] B.K. Baker, Journal of the American Chemical Society 57 (1935) 729.

[63] http://www.biolinscientific.com/q-sense/technologies/

[64] P.G. Saffman, M. Delbruck, Proceedings of National Academy of Sciences USA 72 (1975) 3111.

[65] T. Reihs, K. Lunkwitz, Journal of Colloid and Interface Science 271 (2004) 69.

[66] S. Ondaral, L. Odberg, L. Wagberg, Langmuir 26 (2010) 14606.

[67] S. M. Bystryak, M. A. Winnik,, J. Siddiqui, Langmuir 15 (1999) 3748.

[68] K. B. Musabekov, V. G. Pal'mer, T. I. Yui Tsun-sin, Polymer Science U.S.S.R. 30 (1988) 1779.

[69] Y. Li, J. Warr, D. M. Bloor, J. F. Holzwarth, E. Wyn-jones, Langmuir 16 (2000) 3093.

3 Bulk Properties of Refined Self-Assembled Nanoparticle System

3.1 Abstract

We report on the effects of nine different monovalent and multivalent salts on the stability of a refined positively charged nanoparticles formed as a result of centrifugation and resuspension of nanoparticles formed due to electrostatic interactions between oppositely charged polyelectrolyte (polyethylenimine, PEI) and surfactant (sodium dodecyl sulfate, SDS). Particle size and zeta potential measurements of these soft colloidal particles as a function of various salt concentrations show that beyond a certain critical concentration, addition of all salts leads to flocculation and precipitation. We found that the critical anion concentration (C_{cr}) where flocculation occurred demonstrates a power law dependence on anion (counter-ion) valence (Z^{-n}), establishing the validity of Schultz-Hardy rule for these soft colloidal systems. However, unlike the case of hard colloids where co-ions have relatively little effect on particle aggregation, co-ions (cations) also significantly alter the C_{cr} for these soft colloids. For cations, the C_{cr} increases in the order $K^+ \approx Na^+ > Ca^{2+} > Mg^{2+} > Al^{3+}$, suggesting the possible importance of hydration of these cations on colloidal complex stability. These hydration effects also hold for multivalent anions; C_{cr} decreases in the following order: $NO_3^- > Cl^- > HPO_4^{2-} > SO_4^{2-} > PO_4^{3-}$. Moreover, we find that the entrapped SDS micelles are shielded from the effect of salts. This behavior is in contrast with the effect of salts on polyelectrolyte/surfactant mixtures where the addition of salts typically causes an interaction with the individual components leading to differences in complex formation including dissociation of complexes. These fundamental studies provide an insight into the ability of refined self-assembled systems to maintain their stability in applications involving varying

salinity.

3.2 Introduction

Self-assembled colloidal particles composed of oppositely charged polyelectrolytes and/or surfactants are becoming increasingly important in various industrial, biological and commercial applications [1-5]. The ease of assembly and disassembly of these polyelectrolyte complexes make them attractive as potential drug delivery vehicles that enable controlled release of drugs, small molecules and also as non-viral gene delivery vectors [3, 6-8]. Some of us have extended the use of these particles for enhanced oil recovery as well, where polyelectrolyte/ surfactant nanoparticles are used to control the release of oil field chemical agents [2]. Oftentimes, these nanoparticle complexes are trapped in a non-equilibrium state[9, 10], making them sensitive to their environment, particularly changes in pH or salinity. Therefore, in order to maintain the stability of these nanoparticles, colloidal forces that dominate the bulk properties of these nanoparticles need to be understood.

The effect of salts on the stability of polyelectrolyte/surfactant mixtures as well as formation of polyelectrolyte/surfactant complexes has been studied extensively over the past few years [11-20]. Using mixtures with various concentrations of PEI and SDS, Mészáros and coworkers showed that the addition of moderate concentration of NaCl caused a decrease in the kinetic stability of PEI/SDS particles, due to suppression of free SDS onto PEI/SDS particles triggered by NaCl [21].In a more recent publication, Pojjak et al. showed that “at small and moderate NaCl concentrations”, these electrolytes can cause a “reduction of the kinetically stable composition range” in the case of “PSS/CTAB mixtures” that “are trapped in the non-equilibrium colloidal dispersion state” [22]. Further, it was shown that the salts interact

with the excess components, rather than the particles as a whole to alter their interactions. The role of the hydration of ions on complex formation have also been also argued for [18, 23].

In many recent applications, advantages of using self-assembled nanoparticles without any excess surfactant or polyelectrolytes have been highlighted [24, 25]. Muller and co-workers have termed these nanoparticles "refined polyelectrolyte complexes" and demonstrated that the behavior of these complexes is significantly different from that of polyelectrolyte surfactant mixtures or aggregates with free excess polyions [24]. An understanding of the effects of salinity on the stability of these refined nanoparticle complexes, once formed, is currently limited. In the absence of free surfactant or polymer, these refined nanoparticles can be treated as soft permeable complexes. In this paper we report on the addition of a series of monovalent and multivalent salts to these refined nanoparticles that demonstrates significantly different behavior than the addition of salts into polyelectrolyte/surfactant mixtures. Furthermore, we explored the possible role of salts in the Hofmeister series on the stability of these colloidal systems. To ensure absence of free components, that may impede nanoparticle interactions with salts, the nanoparticles were prepared in water solution, centrifuged, the supernatant of free polyelectrolytes and surfactants removed and the complexes resuspended in water. We have previously shown that these colloidal particles in water are stable over several months [26], ascertaining that the effects described in this paper are as a result of the addition of salts.

The Derjaguin–Landau–Verwey–Overbeek (DLVO) theory in terms of balance between van der Waals forces and electrical double-layer forces is mostly used to qualitatively describe the inter-particle forces between colloidal particles in the presence of salts. However, most of these studies focused on the investigation of solid nanoparticles [27-30]. Shultz-Hardy rule derived

from DLVO theory states that the counter ion of the colloidal particle plays a decisive role in determining the coagulation behavior of charged particles. The critical coagulation concentration (CCC) is scaled as z^{-6} where z is the counter ion valence [31, 32]. However, such correlation is only valid for symmetric electrolytes and colloids with high surface charge density (>1000 mC/m^2) [28, 33].In many practical examples of charged colloids, the surface charge of the particles cannot reach such high value. In such cases, the CCC is expected to demonstrate a weaker dependence on the valence of counter-ions, z^{-n} where $n \cong 1.6 - 4.5$ is expected [29, 34-36]. Results from theoretical modeling based on Poisson- Boltzman equation also showed that in addition to counter-ions, CCC shifts to higher values with increasing valence of co-ion [35]. Further, the porous nature of the colloidal polyelectrolyte/surfactant systems suggests that the DLVO theory alone cannot accurately describe interparticle interactions. Diffusion of small ions into the polyelectrolyte/surfactant nanoparticles leading to specific interactions with the individual components may also be important [17, 18]. Specific ion effects including ion binding to micelles [37], ion interactions with charged group in polyelectrolyte due to ion hydration [23, 38-43] need to be included as well.

In this study, changes in size and zeta potential of positively charged PEI/SDS nanoparticles in the presence of monovalent and multivalent salts are investigated by dynamic light scattering and phase analysis light scattering. The dependence of bulk properties of PEI /SDS nanoparticle on the concentration of different salts with either same cation or anion is discussed. Our results show that the stability of cationic PEI/SDS nanoparticles in electrolyte solutions is affected by both the charge of the anions and cations. The critical counter-ion concentration beyond which precipitation occurs follows power-law dependence on its valence as expected

by the Schultz-Hardy rule. However, unlike hard colloids the stability of the nanoparticles is also influenced by the valence of cations. The polyelectrolyte complexes seem more stable at higher valence cations. Furthermore, for anions of same valence, the critical concentration is found to follow the same trend as salts in the Hofmeister series. This is also true for cations of same valence; more hydrated cations form hydrogen bond with water molecules around the PEI chain, reducing the solubility of the aggregates. In summary, our results together suggest that in addition to electrostatic interactions, hydration forces also play an important role in the stability of these soft colloidal systems.

3.3 Materials and methods

3.3.1 Chemicals

Surfactant sodium dodecyl sulphate, SDS (MW: 288.38 g/mol, purity: >99.9%) and branched polyelectrolyte polyethylenimine, PEI (MW: 25 kDa) were purchased from Sigma Aldridge and used without further purification. The inorganic salts including sodium chloride (NaCl), potassium chloride (KCl), sodium nitrate ($NaNO_3$), calcium chloride ($CaCl_2{\cdot}2H_2O$), magnesium chloride ($MgCl_2{\cdot}2H_2O$), aluminum chloride ($AlCl_3{\cdot}2H_2O$), sodium sulfate (Na_2SO_4), disodium phosphate (Na_2HPO_4) and sodium phosphate (Na_3PO_4) were used as received from Fisher Scientific. Millipore water with initial pH = 7.0 was used for making the solution during the experiment.

3.3.2 Methods

Nanoparticle synthesis: Stock solutions of SDS and PEI at desired concentration were prepared by dissolving the required weighed amount in Millipore water. To make the nanoparticles, SDS (conc:26.6 mM) was added drop-wise to a solution of PEI (2500 ppm) in a glass-beaker being

stirred at 1200 rpm at room temperature for about 5 minutes, such that the ratio of SDS to polyelectrolyte by weight was either 2:9, 3:9, 5:9, 7:9. After the addition of SDS, the mixture was allowed to sit for one minute, after which it was allowed to centrifuge at 15000 rpm for 1.5 hours. The supernatant with free SDS, and dispersed PEI was removed and the collected nanoparticles resuspended with Millipore water (see Figure 3.1 for a schematic of the NP synthesis process). The centrifugation steps were followed several times to remove free SDS or dispersed PEI molecules. The residual free SDS in resuspended nanoparticle solutions is found to be negligible (less than 0.75%). The resulting nanoparticles formed a stable nanoparticle dispersion that does not settle out of solution even after 6 months. The final concentration of all entrapped surfactant (SDS) is calculated by estimating the entrapment efficiency of the polyelectrolyte complex. Once the particles have been characterized for the various SDS to polyelectrolyte ratios, only one combination (3:9) was chosen, based on our results (discussed below), for the rest of the studies described here. The stock nanoparticle solutions are at a final SDS entrapped concentration of 15 mM. Millipore water (pH = 7.0) is used to dilute the stock nanoparticle solution to the desired concentration of interest.

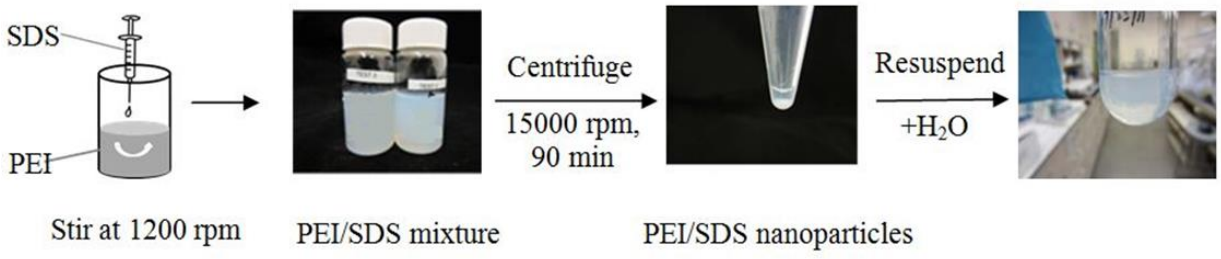

Figure 3.1 Schematics of the steps involved in preparation of refined PEI/SDS nanoparticles

Entrapment Efficiency: The entrapment efficiency is defined as $(C_{bulk}-C_{supernatant})/C_{bulk}$, where C_{bulk} is the bulk SDS concentration in PEI/SDS mixture, $C_{supernatant}$ is the SDS concentration in

the supernatant after centrifugation. The SDS concentration in supernatant was determined by using a standard spectrophotometric method to determine the presence of ionic surfactants. Anionic surfactants (AS) interact with methylene blue (MB) to form an ionic pair AS-MB, and can be extracted into a solvent phase using methylene chloride. UV absorbance of the ionic pair at wavelength 650 nm can then be used to estimate the concentration of surfactant in solution. For our measurements, 5 ml of the diluted sample (supernatant) was placed in an amber vial along with 200 µl of 50 mM sodium tetraborate buffer at pH 10.5, 100 µl of stablized methylene blue(0.1 g of methylene blue dissolved in 100 mL 10mM borate buffer, pH 5-6) and 4 ml methylene chloride. After shaking for 1 min, the sample was allowed to settle for 5 min before transfering the methylene chloride phase to a cuvette. UV absorbance of the ionic pair at 650 nm was recorded by using PerkinElmer UV-Vis Spectrophotometer and the concentration of free SDS in the supernatant estimated by using a standard calibration curve.

Nanoparticle Characterization: Particle size and particle size distribution of the nanoparticles were measured by dynamic light scattering using Brookhaven 90 Plus/BI-MAS(Brookhaven Instruments Corp., Holtsville, NY, USA). All the measurements were performed at 22±2℃. 0.8 ml of the nanoparticle samples was placed in polystyrene cuvettes and then diluted with Millipore water. A detector positioned at 90° was used to measure the scattered light. The zeta potential of the nanoparticles was determined by using ZetaPlus (Brookhaven Instruments Corp., Holtsville, NY, USA. Values of the particle size, particles size distribution and zeta potential are directly recorded using the in-built software.

3.4 Results

3.4.1 Bulk characterization of the nanoparticle system in pure water

The particle size and zeta potential of the synthesized nanoparticles are shown in Figure 3.2 as a function of different concentrations of total entrapped SDS. Each of the SDS concentration represents nanoparticles obtained from a different starting ratio of SDS: PEI used to synthesize the nanoparticles. 2:9, 3:9, 5:9, and 7:9 are the four concentrations shown in Figure 3.2(a) in increasing order of SDS concentration. The graph shows that these polyelectrolyte complexes form uniform nanoparticles of size 110-120 nm with a net positive charge distribution, and that the size of the nanoparticles was independent of the concentration of total entrapped SDS molecules in the system below the critical micelle concentration (CMC). However, for concentrations of SDS closer to 2 CMC, the size of the particles was found to increase to twice their size below CMC. The particle size distribution for each of these concentrations shows a very narrow size distribution (see supplementary data). On the other hand, our results showed that the zeta potential decreases linearly with the concentration of entrapped SDS up to the CMC, beyond which a sharp decrease in the zeta potential was observed. At this lower zeta potential, we also found that the particles precipitated out of solution. Based on these observations, the surfactant to polymer ratio of 3:9 was chosen for preparation on nanoparticles for all further studies. Figure 3.2(b) shows the effect of aging on the nanoparticles obtained from an initial mixture of 3:9 SDS:PEI ratio. The total concentration of entrapped SDS in this system is 3.8 mM. Our results show that even after 90 days, the particle size and zeta potential of the nanoparticle solutions did not change.

3.4.2 Effect of Monovalent and Multivalent Anions

The effect of different anions (Cl^-, NO_3^-, HPO_4^{2-}, SO_4^{2-}, PO_4^{3-}) is illustrated by comparing the hydrodynamic radii of these nanoparticles in different sodium salts at different concentrations

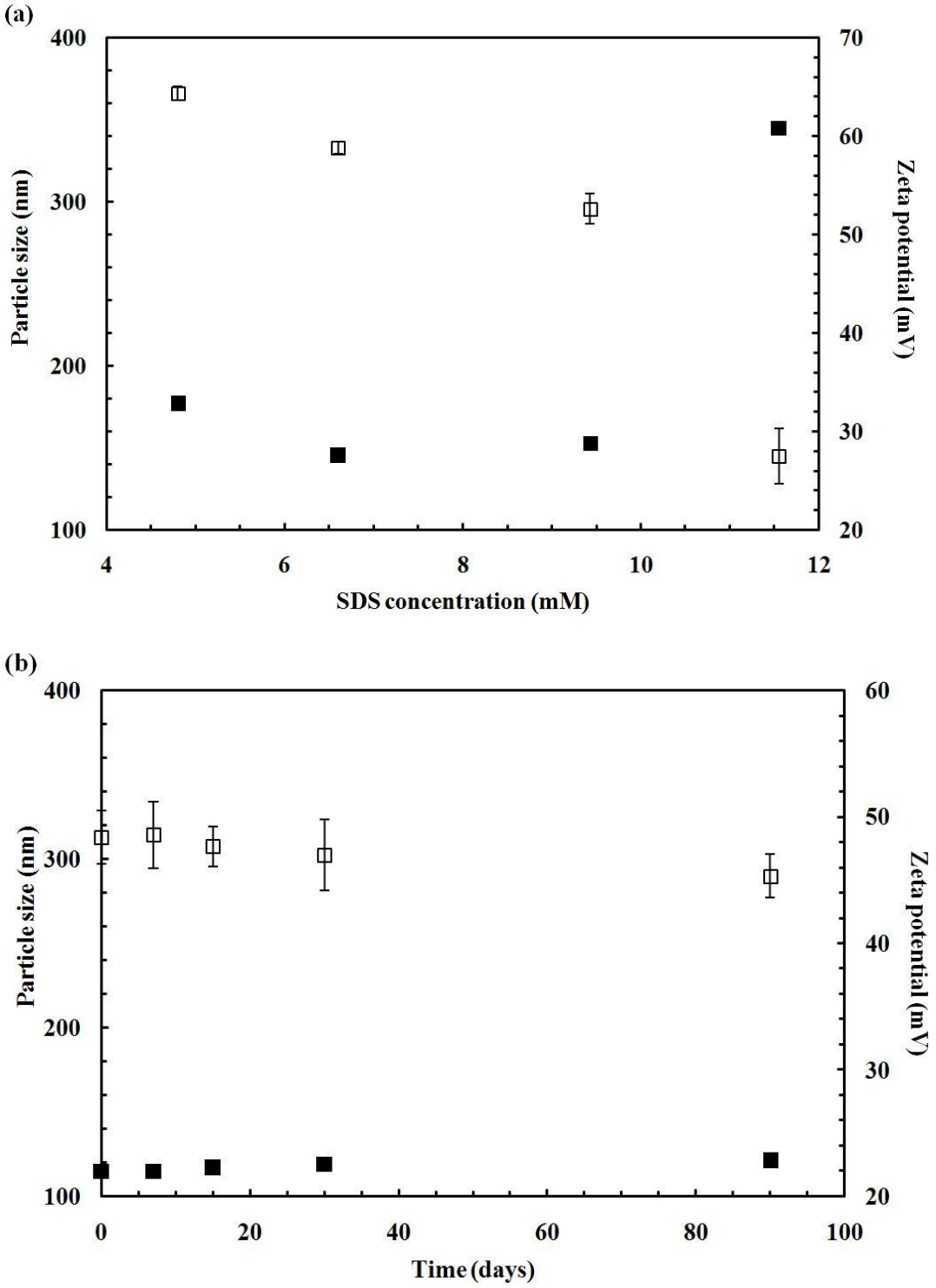

Figure 3.2(a) The particle size (■) and zeta potential (□) of PEI complexes as a function of different concentrations of total entrapped SDS at a solution pH=7.0. Our results show that the size of the nanoparticle complexes remain uniform up to a concentration of ~10 mM beyond which we see a sudden increase in size. Further, at this concentration, particles settle out of solution. (b) The particle size and zeta potential of a PEI complex as a function of time for a representative set of particles containing a total entrapped SDS concentration of 3.8 mM. These colloidal particles form a stable dispersion even after 90 days. (Note: the CMC for SDS solution is 8.31 mM)

of salt and nanoparticles. Figure 3.3 a(i), b(i), c(i) shows the hydrodynamic radius as a function of three different anion concentrations (NaCl, Na_2SO_4, Na_3PO_4).Three different concentrations in the figure represent the entrapped SDS concentration in our PEI/ SDS nanoparticles, which in turn is a measure of the nanoparticle concentration. We find that for monovalent Cl^- ions at low SDS concentration [Figure 3.3 a(i)], the particle size is almost constant up to 75mM [Cl^-]. At higher anion concentrationsthe particle size increases gradually but non-linearly with increases in the anion concentration followed by precipitation when the anion concentration exceeds 200 mM [Cl^-]. Figure 3.3 a(ii), b(ii), c(ii) represent observed changes in the zeta potential at the same salt concentrations. In Figure 3.3 a(i), the zeta potential decreases slightly with the concentration of Cl^- up to a concentration of about 125 mM, beyond which it sharply reduces from 37 mV to 21mV. We find the increase in particle size and decrease in zeta potential to be higher for multivalent ions, or in other words a lower anion concentration causes a larger increase in particle size. For example, Figure 3.3 a(i) shows that the particle size almost doubles at a concentration of 125 mM for SO_4^{2-} and 75 mM for PO_4^{3-}; a sharp decrease of zeta potential is also observed. Beyond these concentrations, the system becomes unstable leading to precipitation of the complexes. We define the critical anion concentration at the onset of this precipitation as C_{cr}. Colloidal stability in the presence of different salts decreases drastically with increasing anion valence (Figure 3.3 a, b or c). Further, our results show that with increase in the bulk SDS concentration (Figure 3.3 b and c), the macroscopic flocculation occurs at lower anion concentration. This dependence of the C_{cr} is further illustrated in Figure 3.4, where we plot the C_{cr} as a function of anion concentration for three different concentrations of PEI/SDS nanoparticles. With increasing counter-ion valence, C_{cr} shifts to lower

concentrations and follows a power-law dependence on the anion valence in the form of Z^{-n} where n increases with entrapped SDS concentration. Moreover, at the same ion valence, the C_{cr} is significantly higher for 1.4 mM SDS compared to 9 mM SDS.

a (i)

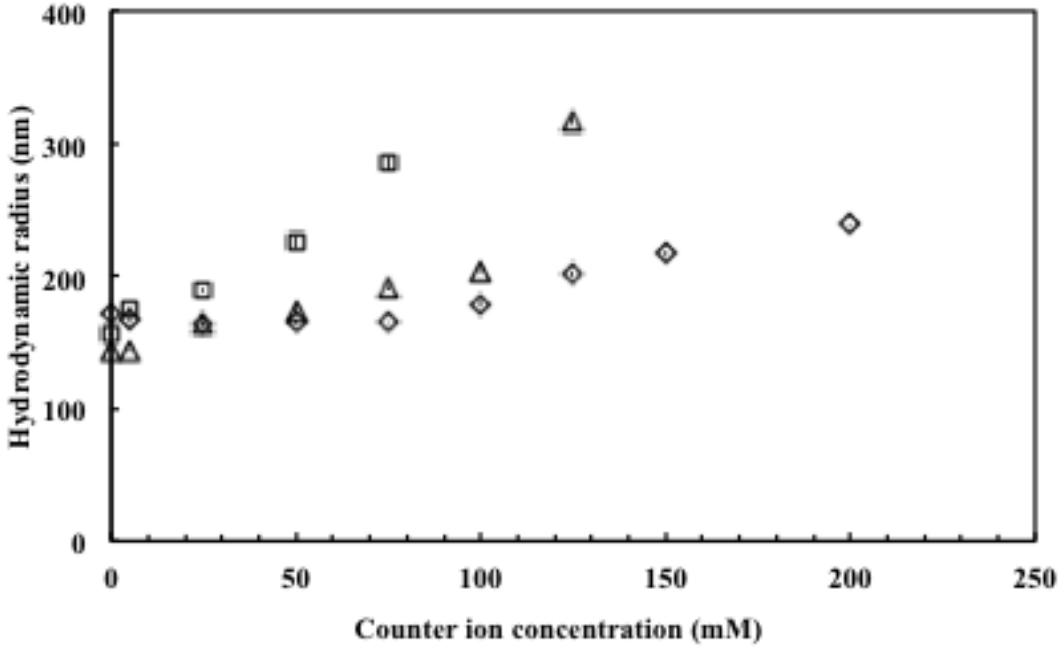

a (ii)

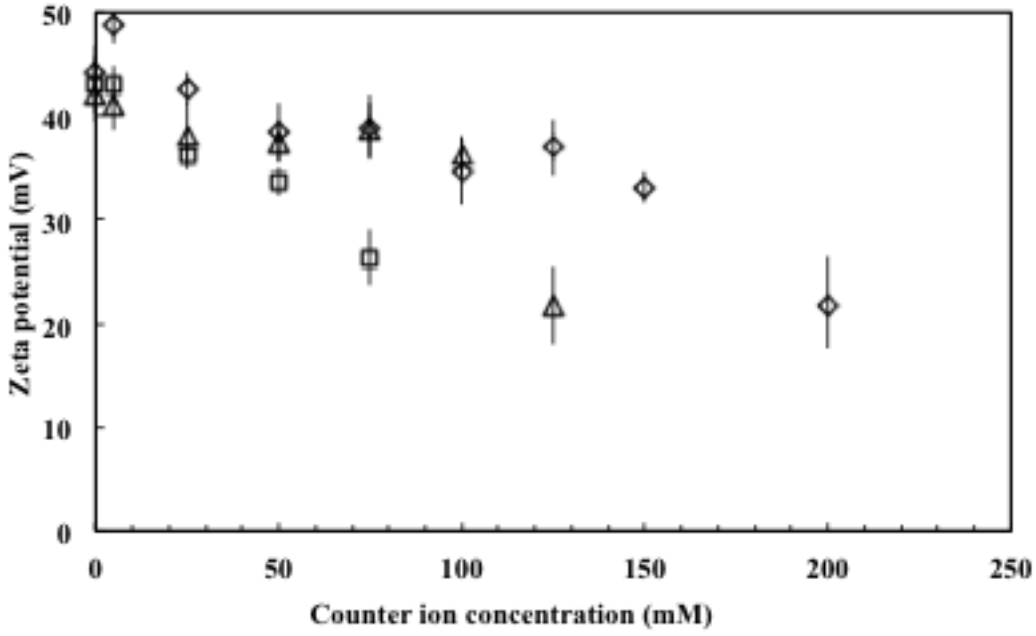

b (i)

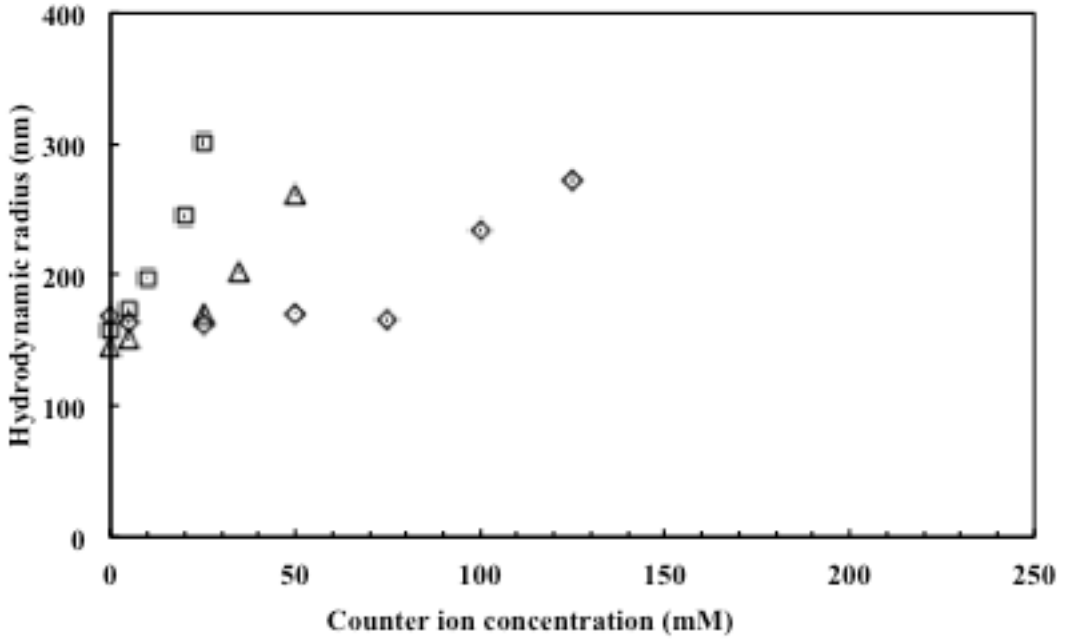
Hydrodynamic radius (nm)
400
300
200
100
0
0
50
100
150
200
250
Counter ion concentration (mM)

b (ii)

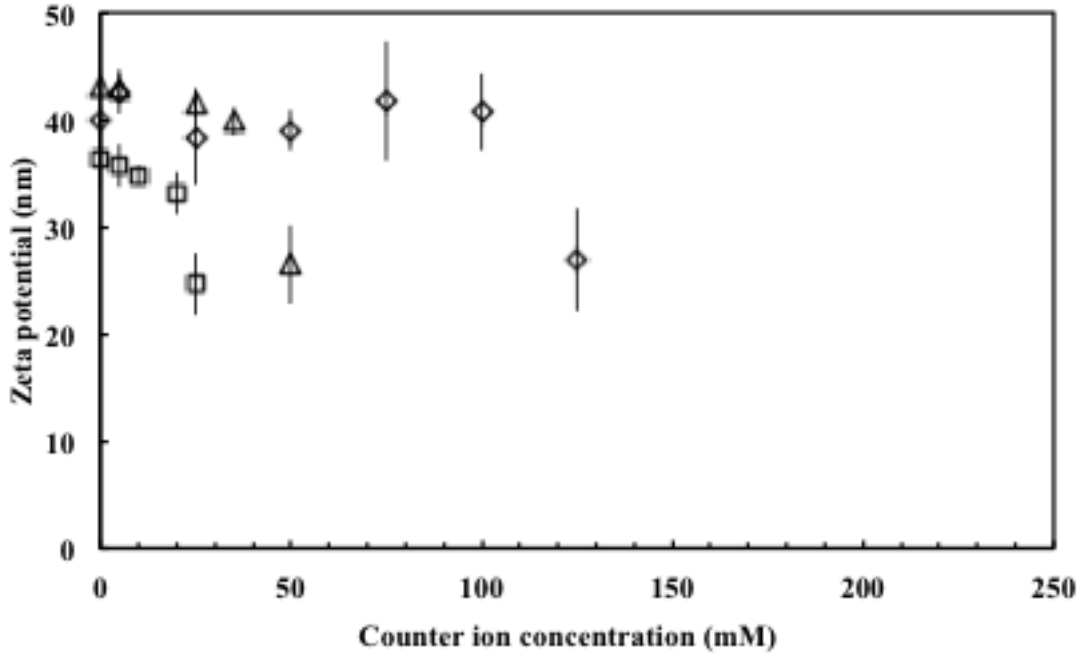
Zeta potential (nm)
50
40
30
20
10
0
0
50
100
150
200
250
Counter ion concentration (mM)

c (i)

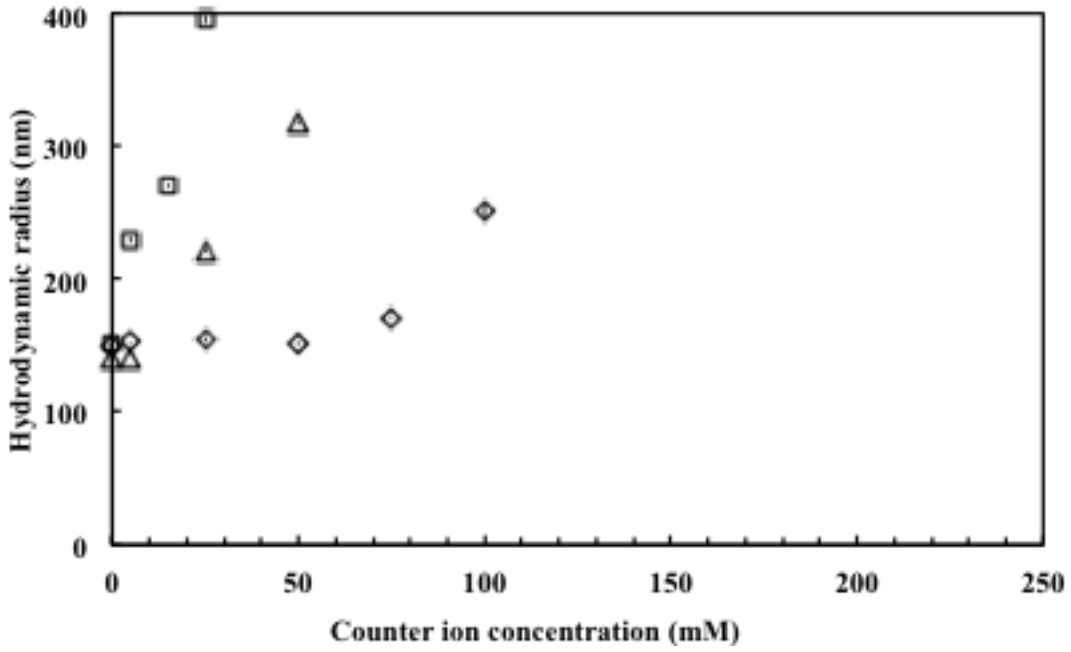

c (ii)

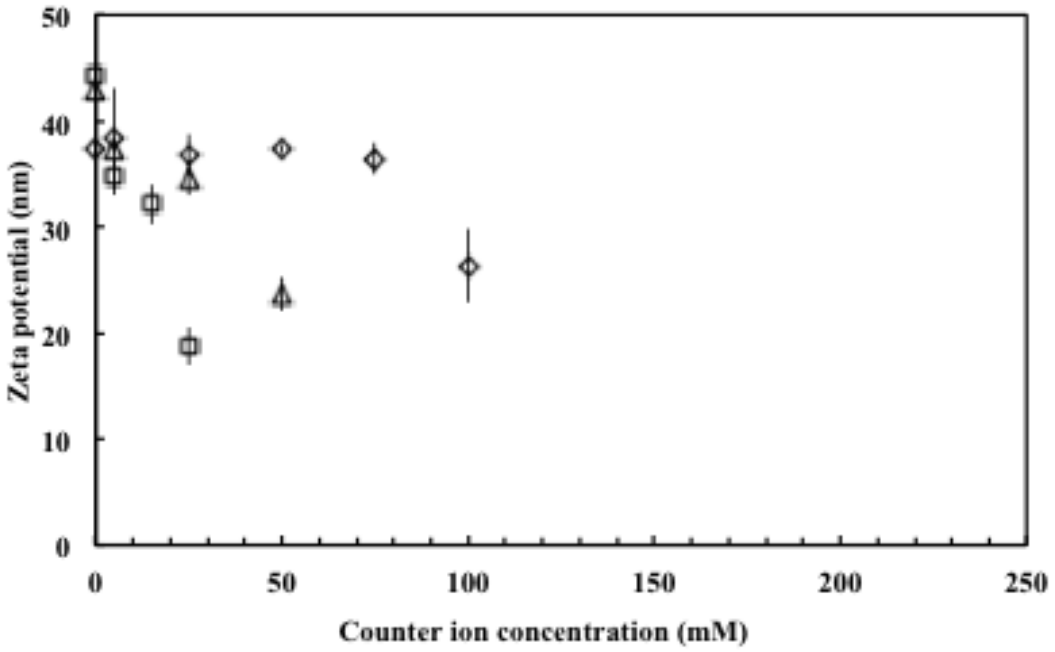

Figure 3.3 The hydrodynamic radius and zeta potential of positively charged PEI/SDS nanoparticle suspension as function of anion (counter ion) concentration at different SDS concentrations (a) 1.4 mM SDS (b) 4 mM SDS (c) 6 mM SDS. At each SDS concentration, three anions are compared: Cl^- (◇), SO_4^{2-} (△), PO_4^{3-} (□).In all the figures, last given points for each salt correspond to the PEI/SDS systems before the onset of macroscopic flocculation. The results show that for each SDS concentration, anion of higher valency cause higher level of PEI/SDS nanoparticle aggregation.

Figure 3.5 represents the effect of salts with the same anion valence but different hydration radius (ions in the Hofmeister series) on the hydrodynamic radius and zeta potential. We observe in Figure 3.5 (a), slightly larger increase interparticle size and zeta potential of the PEI/SDS nanoparticles in the presence of Cl^- when compared to NO_3^-. Similarly, SO_4^{2-} yields nanoparticles of larger size compared to HPO_4^{2-} at the same anion concentration (Figure 3.5 b (i)). Figure 3.6 summarizes the critical anion concentration beyond which coagulation occurs. These results from the plot indicate that the ability of small anions to induce instability of these PEI/SDS nanoparticles increases in the order $NO_3^- < Cl^- < HPO_4^{2-} < SO_4^{2-} < PO_4^{3-}$.

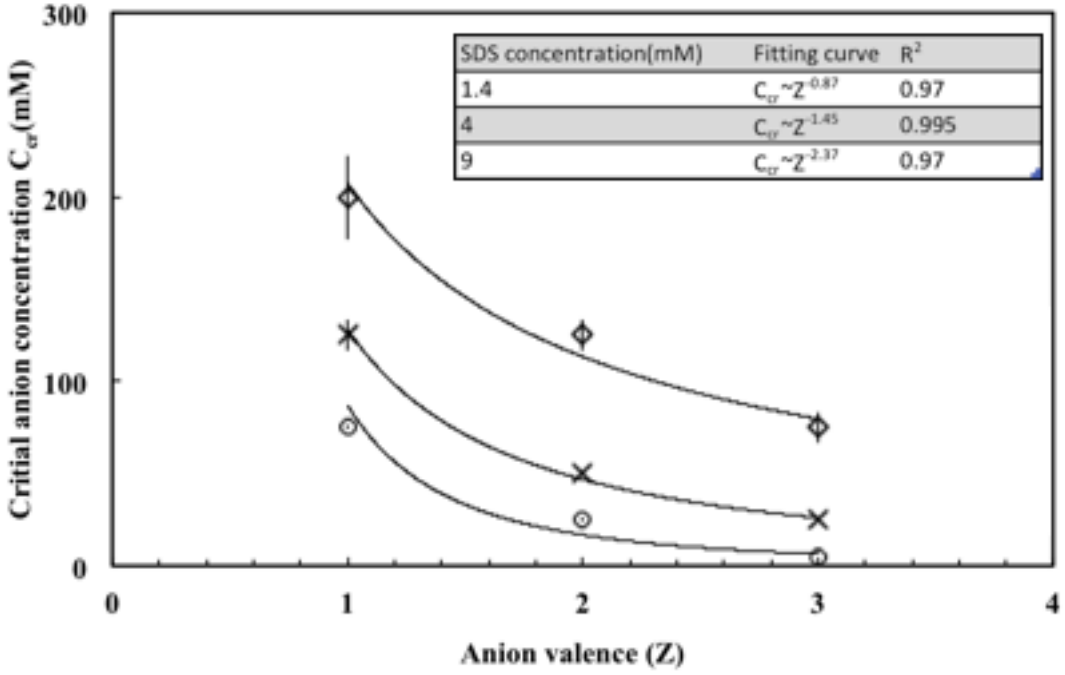

Figure 3.4 The critical anion concentration for each anion vs anion valence at different SDS concentration: 1.4 mM (◇), 4 mM (×), 9 mM (○). The critical anion concentration C_{cr} decreases with increasing valency of anion and increasing SDS concentration. The inset shows the power fitting results for each set of experimental data that can be rationalized with Shultz-Hardy rule: Z^{-a}.

a (i)

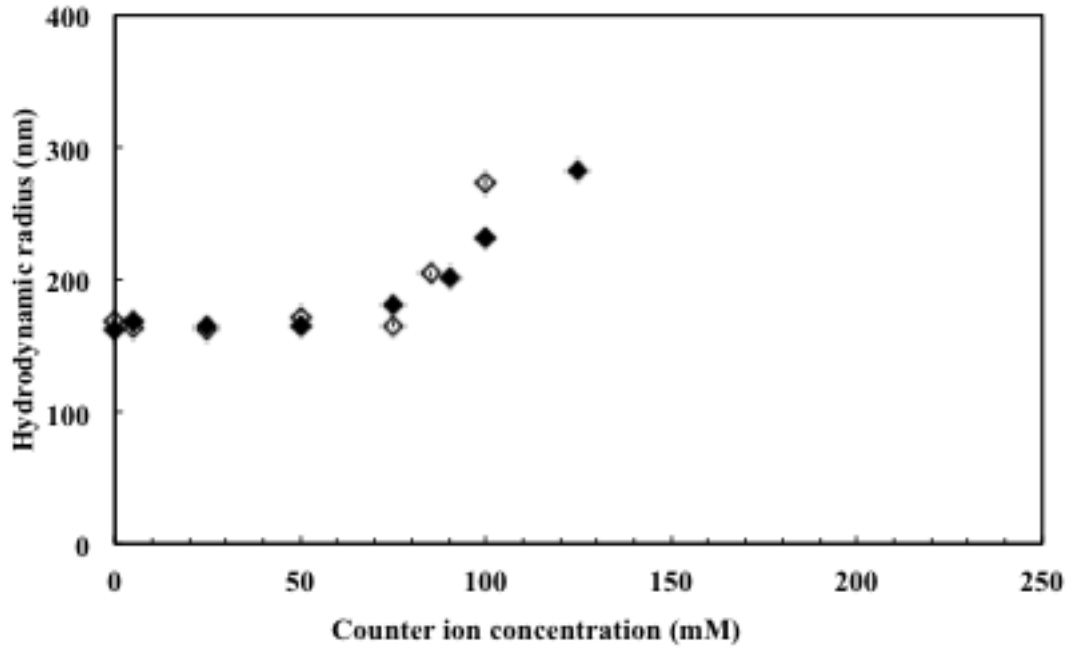
Hydrodynamic radius (nm)
400
300
200
100
0
0
50
100
150
200
250
Counter ion concentration (mM)

a (ii)

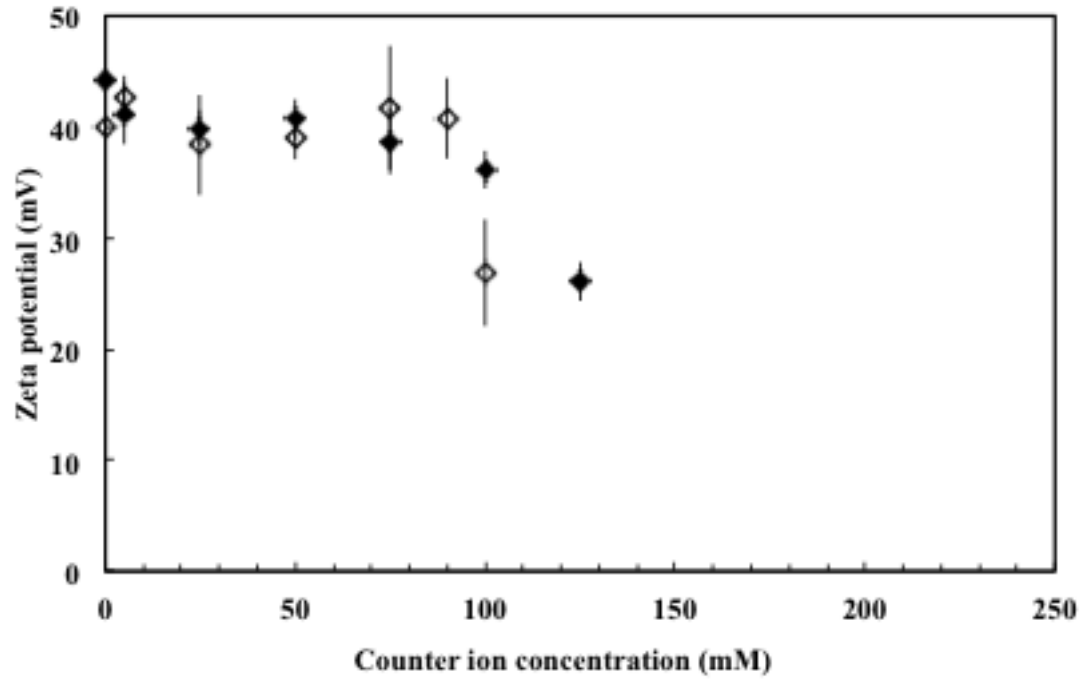
Zeta potential (mV)
50
40
30
20
10
0
0
50
100
150
200
250
Counter ion concentration (mM)

b (i)

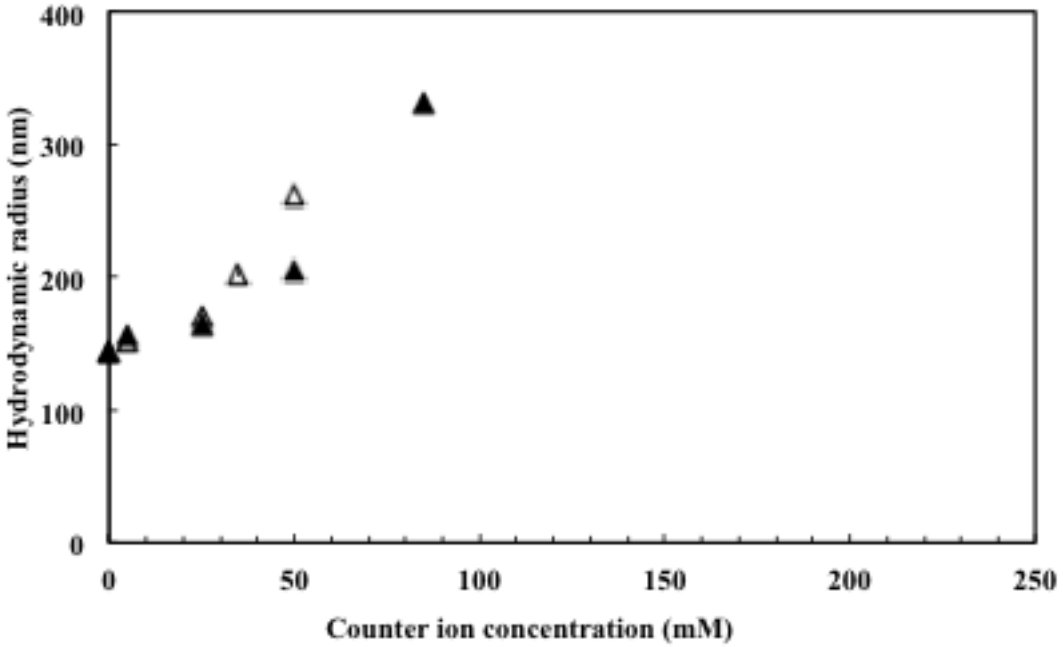

b (ii)

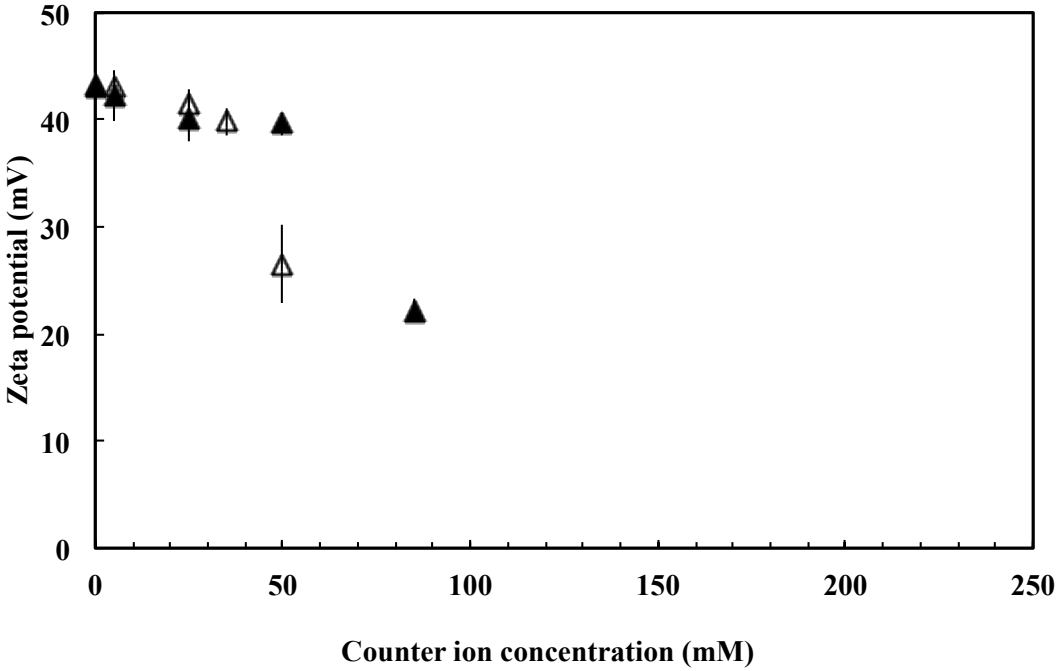

Figure 3.5 The hydrodynamic radius and zeta potential of positively charged PEI/SDS nanoparticle suspension as function of anion concentration at 4 mM SDS (a) monovalent anions (◇ Cl^- and◆ NO_3^-) (b) divalent ions (Δ SO_4^{2-} and ▲ HPO_4^{2-}). The results show that for the anions of same valence, the mismatch of water affinity between amine group of the PEI shell and the added anions results in weaker binding of anions onto PEI/SDS nanoparticles resulting in higher critical anion concentration.

3.4.3 Effect of Co-ions

In this experiment, we used salts with the same anion Cl^-, but different cations Na^+, Ca^{2+}, Mg^{2+} and Al^{3+} to analyze the contribution of cations to the stability of PEI/SDS nanoparticles in solution. In Figure 3.7 the hydrodynamic radius and zeta potential of PEI/SDS nanoparticles vs. Cl^- concentration are plotted for three different cations (Na^+, Ca^{2+} and Al^{3+}). We find that at low SDS concentration (1.4 mM, Figure 3.7 (a)), for Na salts, the particle size remains constant up to 75 mM [Cl^-], then increases from 153 nm to 239 nm at 200 mM [Cl^-],and precipitates upon further increase in [Cl^-]. The zeta potential at 200 mM [Cl^-] decreases below 20 mV. By contrast, the multivalent cations increase the stability of PEI/SDS nanoparticles against precipitation. For instance, while a small amount of [Cl^-] (150mM) is sufficient to dramatically increase the hydrodynamic radius to 220 nm in the case of NaCl, we found that for $CaCl_2$ and $AlCl_3$, higher Cl^- concentrations (>250mM) are required to obtain the same particles size. We find the critical Cl^-concentrationfor C_{cr} to be 500 mM for $CaCl_2$ and 1.2 M for $AlCl_3$ for our complex nanoparticle system.

The particle size of nanoparticles in the presence of different cations also depends on SDS concentration (Figure 3.7 (b), (c)). With an increase of SDS concentration, the particle size starts to increase at lower Cl^-concentration. Besides, the critical Cl^- concentration for various salts is found to be lower for higher SDS concentrations.

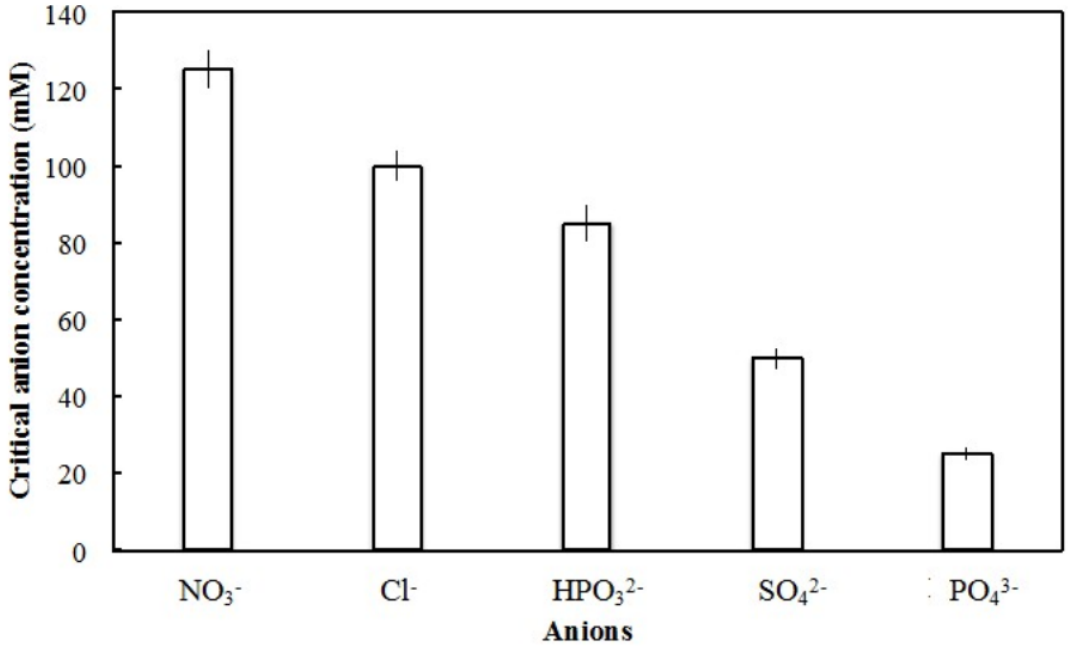

Figure 3.6 Concentrations of anion required to reach the hydrodynamic radius of 200 nm for PEI/SDS nanoparticles. The results show that the ability of anions to induce large macroscopic flocculation increase in the order of $NO_3^- < Cl^- < HPO_4^{2-} < SO_4^{2-} < PO_4^{3-}$. From the results for anions of different valence, it seem plausible to assume the electrostatic forces play a role in determining the order of ability of anions to induce precipitation; therefore, higher valent anions lead to more aggregations. But for same valent anions, the effect of anions to induce aggregations related to the specific ion pairing between anions and PEI; the trend follows the law of matching water affinity that is mainly due to solvation force.

Figure 3.8 shows the dependence of particle size and zeta potential on the concentration of $[Cl^-]$ for different monovalent and divalent cations. While different monovalent cations (Na^+, K^+) show very similar effects on both particle size and zeta potentials, for the two divalent cations (Ca^{2+}, Mg^{2+}), however, addition of Mg^{2+} causes a greater increase in the particle size when compared to Ca^{2+}. Figure 3.9 shows the concentration of each cation required to reach an arbitrarily chosen hydrodynamic radius of 200 nm. It is found that the ability of cations to improve stabilization of the nanoparticle system against flocculation follow the order of $Na^+ \approx K^+ < Ca^{2+} < Mg^{2+} < Al^{3+}$. Further, a comparison with Figure 3.6 reveals that overall anions have a larger influence on the particle size and zeta potential in our nanoparticle system, when compared with cations.

a(i)

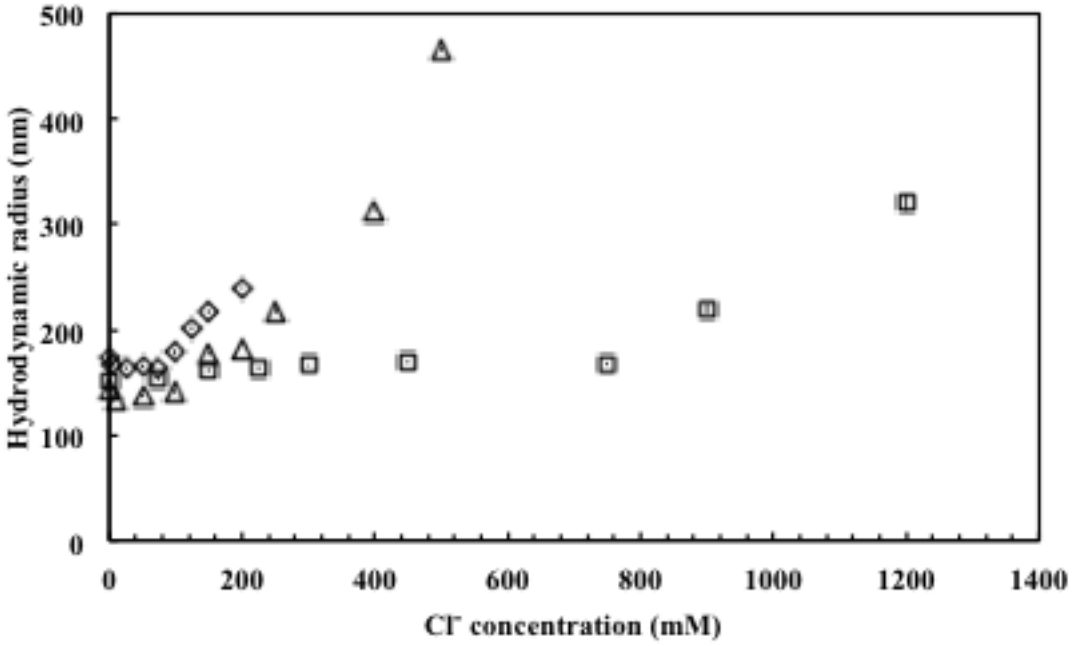
Hydrodynamic radius (nm)
0
100
200
300
400
500
0
200
400
600
800
1000
1200
1400
Cl⁻ concentration (mM)

a(ii)

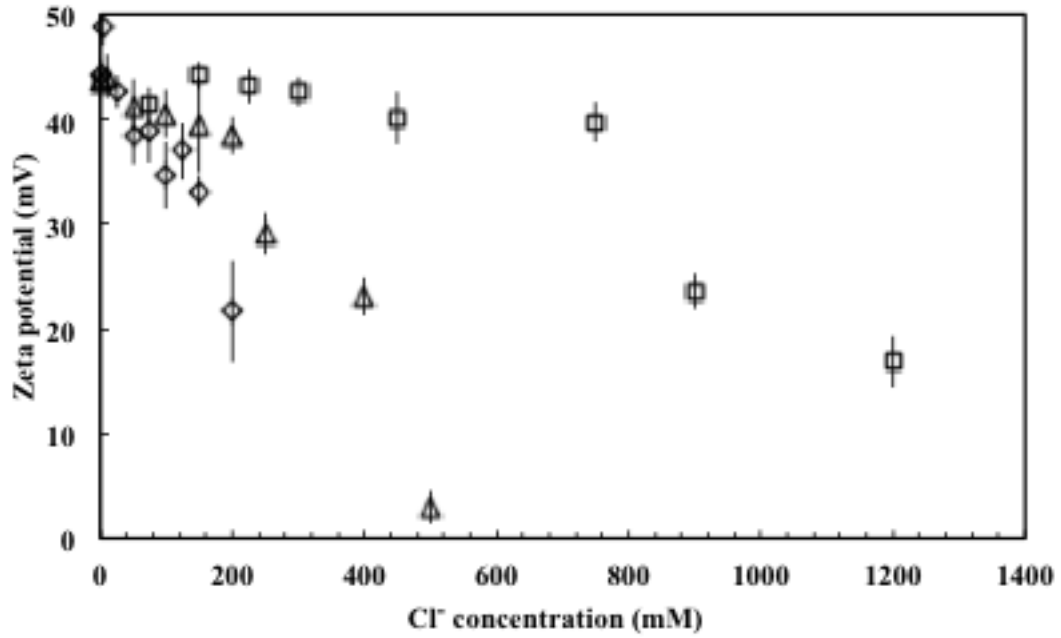
Zeta potential (mV)
0
10
20
30
40
50
0
200
400
600
800
1000
1200
1400
Cl⁻ concentration (mM)

b(i)

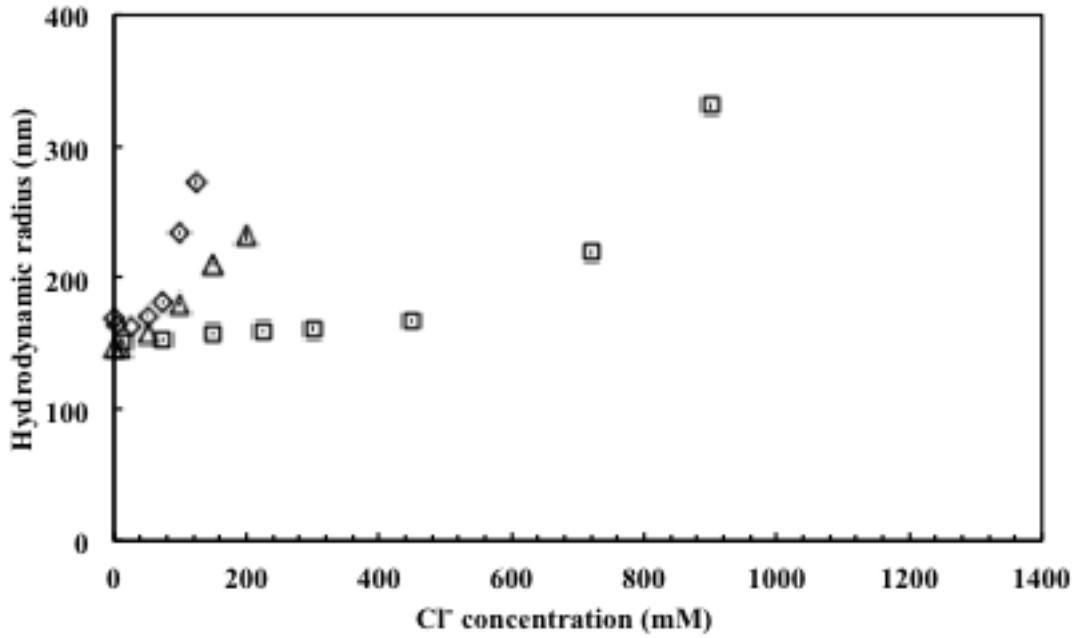
Hydrodynamic radius (nm)
0
100
200
300
400
0
200
400
600
800
1000
1200
1400
Cl⁻ concentration (mM)

b(ii)

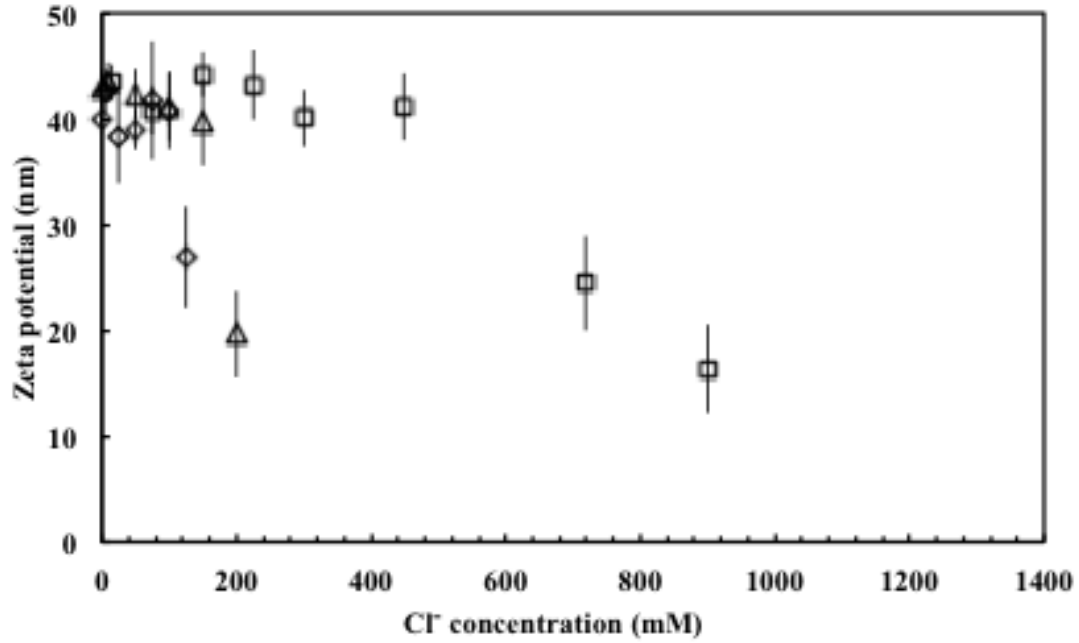
Zeta potential (nm)
0
10
20
30
40
50
0
200
400
600
800
1000
1200
1400
Cl⁻ concentration (mM)

c(i)

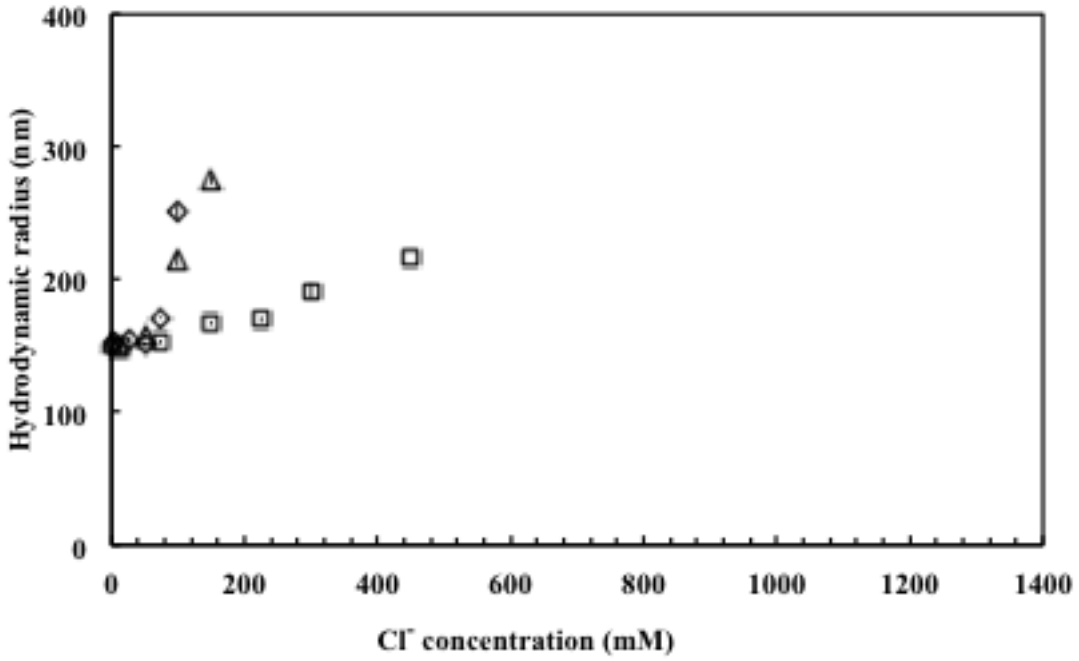

c(ii)

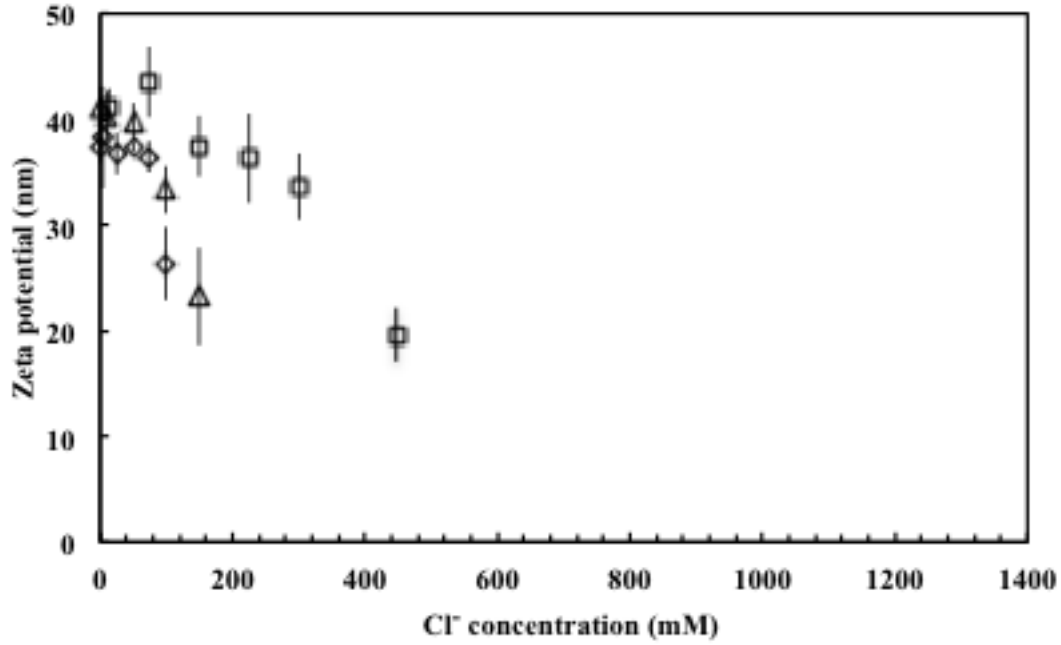

Figure 3.7 Effect of different cations (co-ions) on hydrodynamic radius and zeta potential of positively charged PEI/SDS nanoparticle suspension (a) SDS 1.4 mM(b) SDS 4 mM (c) SDS 6 mM. At each SDS concentration, three cations are compared: Na^{+}(◇), Ca^{2+} (△), Al^{3+} (□).Similar to Fig.1, last given points for each salt correspond to critical [Cl^{-}] concentration beyond which the precipitation starts to form. The results show that for each SDS concentration, cations of higher valence interact with PEI to form thicker protection shell and increase the value of critical [Cl^{-}] concentration.

a(i)

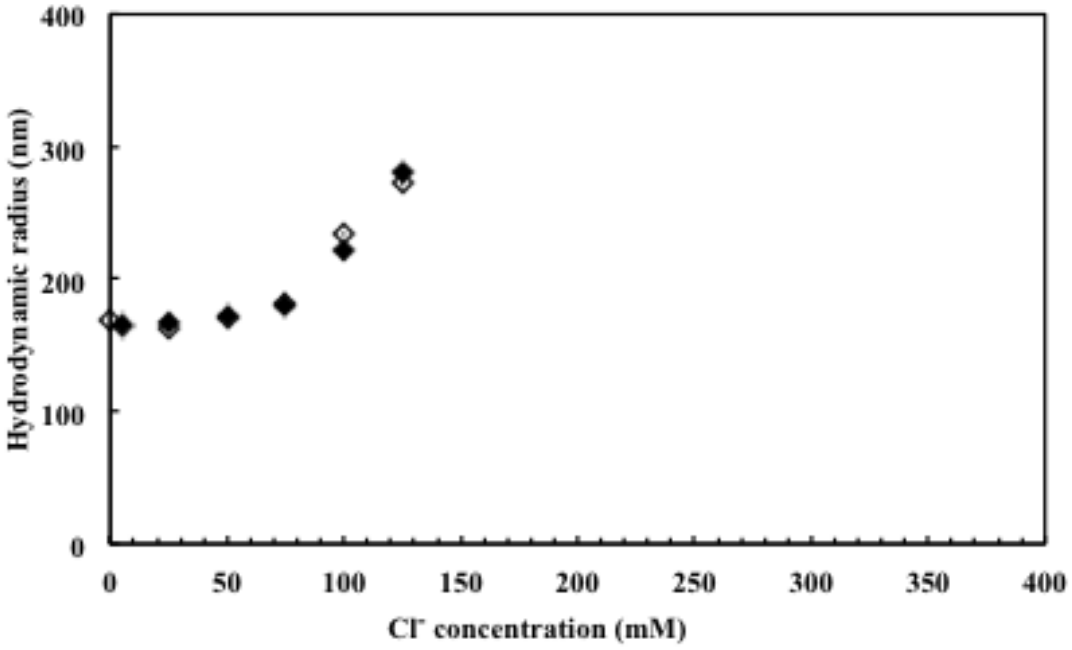
Hydrodynamic radius (nm)
0
100
200
300
400
0
50
100
150
200
250
300
350
400
Cl- concentration (mM)

a(ii)

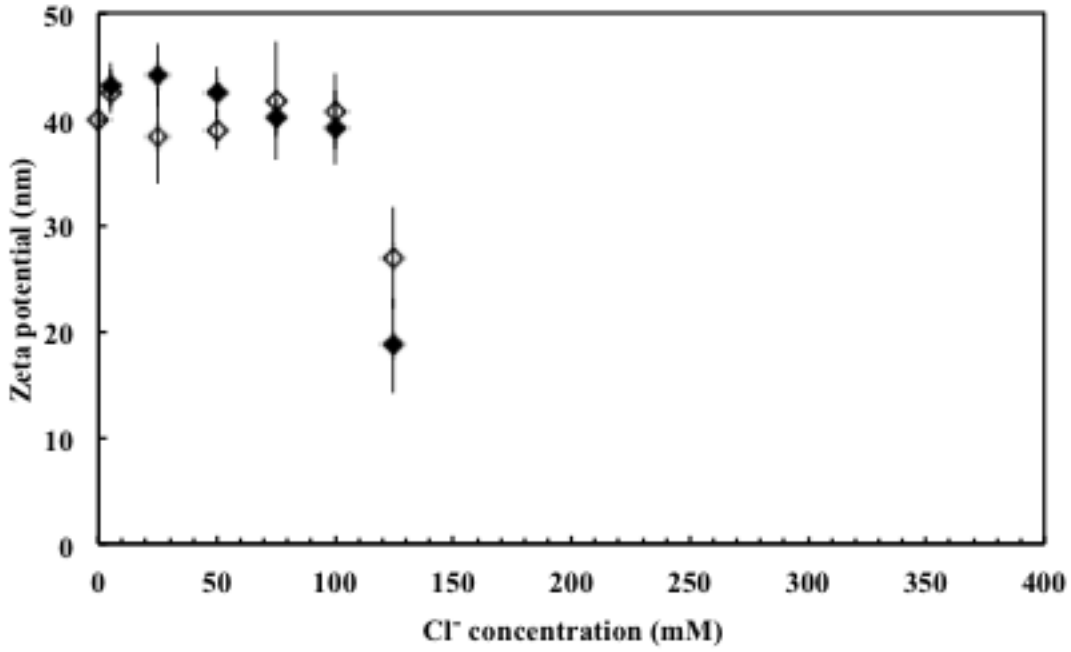
Zeta potential (nm)
0
10
20
30
40
50
0
50
100
150
200
250
300
350
400
Cl- concentration (mM)

b(i)

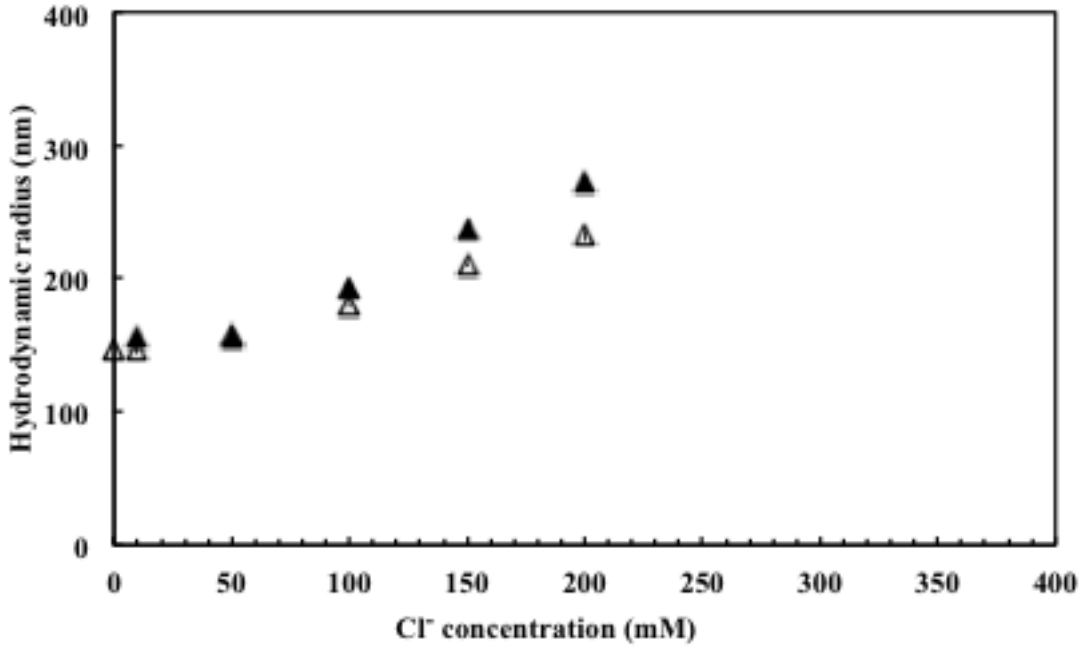

b(ii)

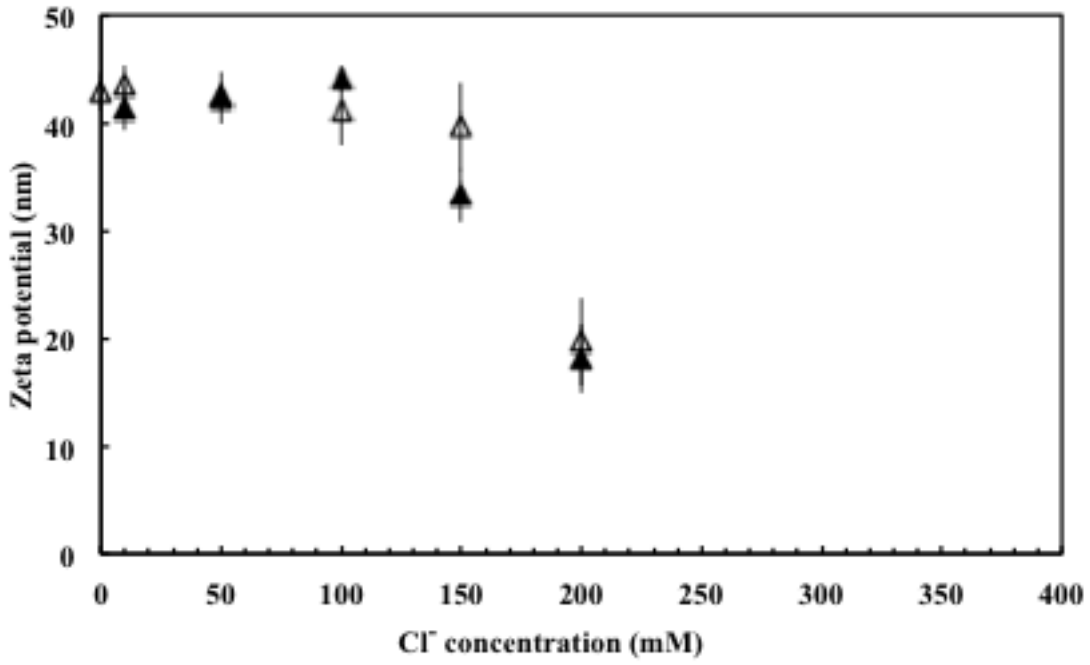

Figure 3.8 The hydrodynamic radius and zeta potential of positively charged PEI/SDS nanoparticle suspension as function of anion concentration at 4 mM SDS (a) monovalent cations(◇ Na^+ and ◆ K^+) (b) divalent cations (Δ Ca^{2+} and ▲ Mg^{2+}). The results show that for monovalent cations, the trend of particle size and zeta potential changes in a very similar way. For divalent cations, Mg^{2+} reduces the solubility of the aggregates more than Ca^{2+} mainly due to its high water affinity.

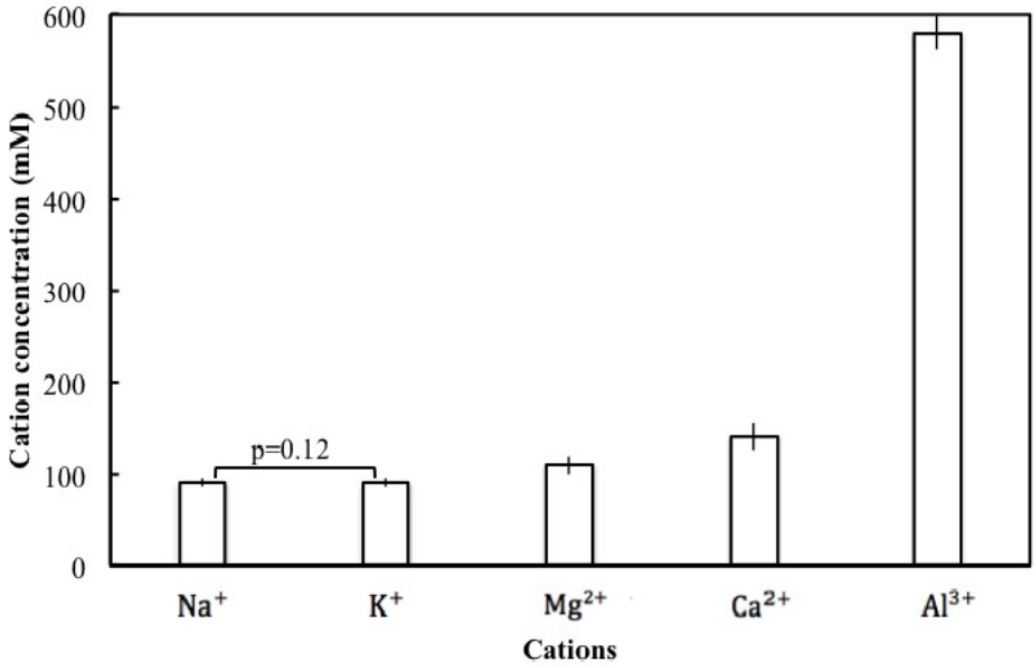

Figure 3.9 Concentrations of cation required to reach the hydrodynamic radius of 200 nm for PEI/SDS nanoparticles. The results show that the ability of cations to inhibit large macroscopic flocculation increase in the order of $Na^+ \cong K^+ < Mg^{2+} < Ca^{2+} < Al^{3+}$ .The overall effect of salts to induce aggregation is due to the increases of ionic strength. Cations of higher valence interact more with PEI and stabilize the system with thicker out shell. For same valentcations, the ions with higher water affinity induced more aggregation; the trend follows the law of matching water affinity that is mainly due to solvation force.

3.5 Discussion

Particle characterization: The results from Figure 3.2 indicate that the size and charge of the aqueous nanoparticle system is dominated by the self-assembly process and the resulting thermodynamic state of the nanoparticles. We find that while the size of the particles remains almost constant below a certain critical concentration, the particle zeta potential decreases with increasing SDS concentration, and increasing SDS to PEI ratio. This is primarily because the positive charge density on the PEI is compensated for by the negative charges on the entrapped SDS molecules. This net surface charge on the nanoparticles (> 40 mV, required for stable dispersions) provides long-term kinetic stability to the colloidal dispersion by preventing aggregation. Dautzenberg et al. [44] proposed that these particles exist as highly compact,

almost spherical particles with a charge neutralized core, surrounded by chains of the polyelectrolyte which are in excess. In our case, this would mean a charge neutralized core of PEI and SDS with a shell of the cationic PEI, which results in the net positive charge of our complexes, and prevents further aggregation. Beyond a critical concentration of the SDS, the total surface charge drops much below the zeta potential required to form stable dispersions (< 35 mV), and the system forms large aggregates (as indicated by the sudden doubling of particle size) that precipitate out of solution. Therefore, by adjusting the ratio of SDS and polyelectrolyte such that there is always an excess of polyelectrolyte, stability of the nanoparticles can be maintained for a longer time (our system is now stable for 6 months, while up to a year has been reported in some nanoparticles).

Salt effect: In many applications involving polyelectrolyte/surfactant nanoparticle systems, the ionic strength of the aqueous solution can vary. For example, during use as drug delivery vehicles, the particles are expected to encounter salt concentrations as high as 0.5 M. Similarly, applications in the oil industry can expose these nanoparticles to even higher salt concentrations. Therefore, an understanding of the interaction of salts with these polyelectrolyte/surfactant based complex nanoparticles is essential for designing stable systems. Here we report on the stability of PEI/SDS nano complexes in nine different electrolyte solutions with varying concentrations, valency, and hydration radius. To best of our knowledge, while the effect of salts on the formation of these nanoparticles has been studied extensively [12, 45][21, 46, 47], how salts would influence the stability of PEI/SDS nanoparticles in aqueous solutions, after their formation, and in the absence of any excess surfactants or polyelectrolytes has not been studied for different salts. What is currently known may be

summarized as follows: it has been reported that adding salts could alter the electrostatic as well as non-electrostatic interactions that control the binding of the oppositely charged surfactants and polyelectrolytes leading to different phases including formation of soluble mixtures, insoluble complexes or dissociation of the complex systems in the presence of excess polyelectrolyte or surfactants. For the PEI/SDS system the possible binding equilibrium between salt and the complex, was proposed to be the following:

$$\mathrm{PEIH^+DS^-} + \alpha\mathrm{A^-} \rightarrow \mathrm{PEIH^+ \cdot \alpha A^-} + \mathrm{DS^-_{free}}$$

$$\mathrm{DS^-_{free}} + \beta\mathrm{B^+} \rightarrow \beta\mathrm{B^+DS^-_{Micelle}}$$

Addition of salt was also shown to influence micellization equilibriums, or even the morphology of the particles in polyelectrolyte surfactant mixtures [18, 38].

We find that overall for our nanoparticle system without any excess components, the addition of salts causes an increase in particle size, a decrease in zeta potential and ultimately precipitation. However, under no conditions did we encounter dissociation of the nanoparticles into its component parts, indicating that the interactions of the formed nanoparticles are significantly different from PEI/SDS mixtures, or PEI/SDS nanoparticles in the presence of excess surfactants. Therefore, as discussed in detail below, we treat our nanoparticles as soft colloidal systems, and apply the well-known effects of salts on solid colloidal systems, to verify if these rules also apply to our soft systems.

Effect of anions and the Schultz-Hardy rule: As mentioned before, in our experiment, the PEI/SDS nanoparticles are positively charged. From a basic knowledge of intermolecular forces between colloidal particles, positive surface charge on these particles will cause an electric double layer to form [33]. The overlapping double layer between two particles results

in electrostatic repulsion, which in turn stabilizes the colloidal suspension. Upon addition of salts, anions (counterions for this charged system) will screen the positively charged particles and induce strong aggregation, ultimately leading to coagulation or flocculation. This aggregation occurs over a narrow concentration range.

As illustrated in Figure 3.3, for each anion studied, the PEI/SDS nanoparticle size increases with increase of anion concentrations and eventually precipitates out of solution at certain critical anion concentration. Considering the charge screening effect due to electrostatic interactions, at very low ion concentrations, the Debye screening length κ^{-1} in solution is large enough to cause repulsion between the charged colloids, keeping them stable in solution. As the salt concentration rises, Debye length κ^{-1}decreases due to screening effects of counterions ultimately resulting in aggregation and precipitation. The reduction of zeta potential at this salt concentration also indicates a decrease of electrostatic repulsion in our colloidal system. Additionally, our results show that multivalent counter ions are more prone to induce precipitation than the lower valent counter ions at the same ion concentration. This observation can be attributed to the fact that multivalent anions have a stronger screening effect and are bound more strongly to the polyelectrolytes due to their higher valence and greater charge per unit volume [41, 43]. The Schultz-Hardy rule, an empirical formula, dictates that the coagulation concentration scales as z^{-6} for a highly charged colloids (potential >150 mV). For weaker charged systems such as the nanoparticles being explored here, a weaker dependence on the valency (z^{-n}, n ~ 1.6-4.5) is expected.

Figure 3.4 shows that indeed the critical anion concentration C_{cr} scales as a power law of the anion valence. In fact, for the higher concentrations of nanoparticles (SDS concentration of 4

mM and 9 mM) the critical concentration agrees with that predicted by Shultz-Hardy rule (based only on long-range electrostatic forces) for weakly charged systems, although the exponent is found to be significantly lower for the low entrapped SDS concentrations [35]. This suggests that short-range forces such as solvation forces may also be important. To check the validity of short-range forces (that may cause specific ion pairing or dehydration)[30, 48, 49] on the stability of PEI/SDS nanoparticles, additional experiments were carried out using different anions of same valence but different sizes due to differences in hydration (so called Hofmeister salts). If the interparticle interactions in these systems are mainly related to long-range electrostatic forces, the particle size and onset of flocculation should depend only on the valence of ion, and not on the chemical nature of the ion. However, Figure 3.5 illustrates that anions of same valence yield differences in their effects on particle coagulation and precipitation. The critical anion concentration in the case of Cl^- is 100 mM, whereas it is 125 mM for NO_3^-. Similarly, the concentration of SO_4^{2-}beyond which precipitation occurs is significantly less (~50 mM) compared with HPO_4^{2-} (85 mM). In accordance with the observations by Hofmeister over a century ago, anions can cause aggregation of charged colloids in the following order; SO_4^{2-}>HPO_4^{2-}> acetate$^-$> citrate$^-$>Cl^->NO_3^-[48, 50]. A similar trend is observed in our nanoparticle system.

This observation can be further explained by the "Law of Matching Water Affinity". Collins [50] argued that if the solvation force dominates the ion binding between small ions and large macromolecules, the "Law of Matching Water Affinity" is important in regulating such binding. This law states that oppositely charged ions in solution will only form ion pairs when they have the same water affinity. According to Collin [48, 50], anions follow the order

NO_3^-<Cl^- < SO_4^{2-}< HPO_4^{2-} in the number of bound water molecules. NO_3^- and Cl^- are weakly hydrating with less than one water molecule; SO_4^{2-} is moderately hydrated with two water molecules, while HPO_4^{2-} is highly hydrated with four water molecules. At the same time, the positively charged amine group in PEI is bound to two water molecules on average [51].The "Law of Matching Water Affinity" dictates that SO_4^{2-} binds the strongest with the PEI shell when compared with HPO_4^{2-} and the monovalent anions due to mismatch of water affinity in these cases. As a result, SO_4^{2-} binds more firmly with the amine groups in the PEI chain, causing more efficient screening of positive charge on the aggregates. This hypothesis is supported by Figure 3.5, where we observe that 50 mM SO_4^{2-}causes the zeta potential to drop from around 40 mV to 25 mV. This neutralization of charge reduces the electrostatic repulsion between the nanoparticles, increasing their tendency to precipitate.

Effect of cations: To explore the role of cations on the stability of these nanoparticles, we measured the hydrodynamic radius change with [Cl^-] concentration for monovalent and multivalent cations, for three different SDS concentrations. Our results are summarized in Figure 3.7. We find that for each of the nanoparticle concentration studied, the multivalent cations show a stronger ability to eliminate precipitation formation; the critical Cl^- concentration for different cations follows the order Na^+<Ca^{2+}<Al^{3+}. Hayakawat et al. [52] suggested that cations of higher valency interferes more with polyelectrolyte/surfactant binding than the cations of lower valency. Contrary to this result, we found that Al^{3+} showed the most stabilizing effect on particle size and aggregation once the nanoparticles were formed, suggesting that the interactions with cations may be different. One possible explanation is that even though the PEI/SDS nanoparticles are positively charged, once the Debye layer is

screened, cations may diffuse into the nanoparticle system and interact with either the PEI or SDS or both. Sammalkorpi et al. [37] provided molecular dynamics simulation results showing that Ca^{2+} yields stronger salt bridges between charged SDS head groups while Na^{+} shows no specific binding to micelles and stay highly mobile on the micellar surface [53]. Our own results (see Figure 3.10) show that Ca^{2+} destabilizes pure SDS solutions at 25 mM, while up to 0.5 M concentration of Na^{+} does not. If indeed the cations were able to interact with the SDS in the nanoparticle core, we would expect that Na^{+} would lead to a more stable solution, which is contrary to our results. Further, if there is a weakening of the PEI/SDS bond due to competitive binding between the salt and SDS, then we would expect a dissociation of our nanoparticles. However, no dissociation is observed, even when 1.0 M concentration of salt was added to the precipitated mixture. Rather we observe an increase in size before precipitating that may be due to "swelling" of the nanoparticles. We hypothesize that this swelling is due to the diffusion of cations into the complex, and subsequent interactions with PEI. Since we have ruled out the interaction of cations with DS^{-} micelles, the different trends of increase in particle size due to addition of salts could be due to the indirect hydration effect of the cations with the hydrated PEI shells. Using NMR and light scattering studies, Dautzenberg et al. [44] showed that interactions between multivalent cations and positively charged polyelectrolyte could lead to a conformation change of polyelectrolyte complex, leading to the formation of thicker stabilizing shell. This thicker stabilizing shell would then protect the complex from further aggregation, leading to a more stable system. Figure 3.7 suggests that similar to the observation by Dautzenberg [44], in our system, the multivalent cations stabilize the nanoparticles by interacting with the PEI chains. Al^{3+}, with larger hydration radius possibly stabilizes the

nanoparticles more than the monovalent ions. To further prove this hypothesis, we recorded the effect of addition of a small concentration of Ca^{2+}(10 mM) followed by addition of Na^{+} to our nanoparticle system (shown in Figure 3.11). Surprisingly, even when a small amount of Ca^{2+} was added, the nanoparticles were able to resist coagulation at twice the original Na^{+} concentration. This implies that the larger Ca^{2+} blocks further interactions with Na^{+}, stabilizing the system. Additionally, Al^{3+} is acidic, and can lower the pH. A lower pH would cause an increase in the surface charge of the polyelectrolyte and further improve the resistance to aggregation [44].

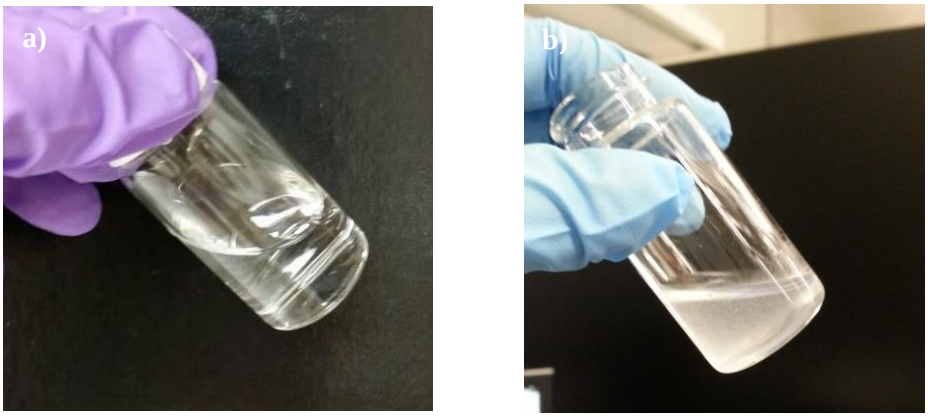

Figure 3.10 a) Clear solution of 3.8 mM SDS in the presence of 0.5 M NaCl b) Precipiates formed by 3.8 mM SDS with 25 mM $CaCl_2$

To further explore the role of the chemical nature of the cation on nanoparticle stabilization, we studied the effect of the addition of two monovalent and two divalent salts on nanoparticle stability. As seen in Fig.6, we do not observe a difference in critical Cl^{-} concentration for K^{+} and Na^{+}. However, the critical Cl^{-} concentration for $Ca^{2+}$was found to be higher than Mg^{2+}. Mg^{2+}shows a relative higher water affinity than Ca^{2+}, therefore Mg^{2+}can easily form hydrogen bonding with water molecules around the polyelectrolyte and cause “salting out” of the particles [50].

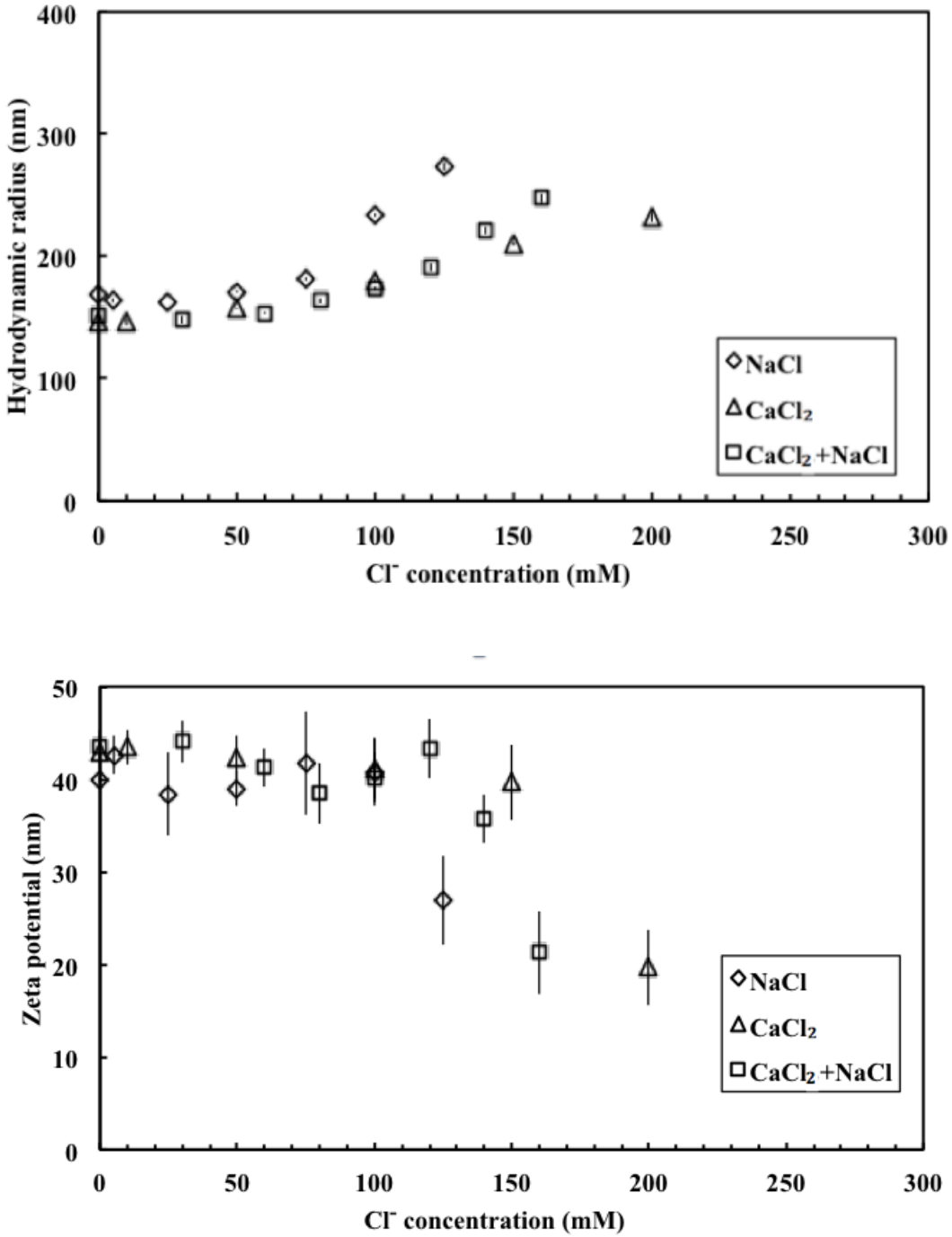

Figure 3.11 The hydrodynamic radius and zeta potential of positively charged PEI/SDS nanoparticle suspension as function of Cl^- concentration at 4 mM SDS; In the case of $CaCl_2$+NaCl represent the condition when 10 mM $CaCl_2$ is added into PEI/SDS suspension followed by addition of NaCl. The results show that the PEI/SDS nanoparticles are stabilized against further addition of NaCl by a small amount of $CaCl_2$ salts.

Finally, we find that the anions cause destabilization of the nanoparticle complex at concentrations that are significantly lower than the cations. This observation suggests that

anions play a more significant role than the cations to maintain the stability of this positively charged nanoparticle system. This establishes that while the primary effect of the addition of salts is due to electrostatic interactions with the charged colloids, secondary effects such as hydration effects and salvation forces also control the interactions of these colloidal particles with different salts.

3.6 Conclusions

In conclusion, the polyelectrolyte complex nanoparticle are formed as a result of self-assembly where the electrostatic charges between the components of the complex system undergo electrostatic interactions and minimize the energy barrier required for assembly. As a result they form stable nanoparticle dispersions in solution. We find that the nanoparticles can be influenced by addition of salts. We establish the validity of the Schultz-Hardy rule for higher concentrations of these refined nanoparticles. To the best of our knowledge, such an effect has not been described for polyelectrolyte surfactant mixtures, possibly because of the interactions of the ions with the individual oppositely charged components. In addition, we found that non-electrostatic hydration forces also control the stability of these nanoparticles. Anions with increased hydration radius induce instability of PEI/SDS nanoparticles and follow the order $NO_3^- < Cl^- < HPO_4^{2-} < SO_4^{2-} < PO_4^{3-}$, as expected for salts in the Hofmeister series that follow the "Law of Matching Water Affinity" [48, 50]. Further, unlike solid colloidal dispersions, cations also influence the stability of the nanoparticle system, possibly by causing reorganizing of the PEI shell. The cations follow the order $Na^+ \approx K^+ < Ca^{2+} < Mg^{2+} < Al^{3+}$. Moreover, the effects of salts on the free surfactant micelles do not hold in this system, suggesting that the encapsulated surfactant molecules are shielded from the effect of salts. In contrast, in case of

polyelectrolyte surfactant mixtures, the salts are found to interact with the individual components, thus altering the association behavior of the polyelectrolyte surfactant aggregates and often leading to dissociation of the aggregates at very high salt concentrations [14, 17, 18]. The refined nanoparticles do not dissociate, even at very high (~1 M) salt concentrations. Therefore, when considering the effect of salts on the stability of these refined polyelectrolyte surfactant nanoparticles after their formation, and in the absence of free excess components, interactions of the particles as a whole with both cations (co-ions) and anions (counter-ions) should be considered. In our system, in addition to electrostatic forces, we show that solvation forces also play a significant role. These refined nanoparticles can also be applied to protect encapsulated components from environmental effects in several commercial and biomedical applications.

References

[1] Y. V. Shulevich, T. H. Nguyen, D. S. Tutaev, A. V. Navrotskii, I. A. Novakov, Separation and Purification Technology 113 (2013) 18.

[2] C. Berkland, M. Cordova, J. T. Liang, G. P. Willhite, University Of Kansas, US 11/515,580, 2012.

[3] S. A. Agnihotri, N. N. Mallikarjuna, T. M. Aminabhavi, Journal of Controlled Release 100 (2004) 5.

[4] E. D. Goddard, Colloids and Surfaces 19 (1986) 301.

[5] S. Aidarova, A. Sharipova, J Krägel, R. Miller, Advances in Colloid and Interface Science 205 (2014) 87.

[6] A. F. Thnemann, M. Miller, H. Dautzenberg, J. F. Joanny, H. Lwen, Advances in Polymer Science 166 (2004) 113.

[7] L. Chiappisi, I. Hoffmann, M. Gradzielski, Soft Matter 9 (2013) 3896.

[8] N. A. Alhakamy, A. S. Nigatu, C. J. Berkland, J. D. Ramsey, Therapeutic Delivery 4 (2013) 741.

[9] A. Naderi, P. M. Claesson, M. Bergstrom, A. Dedinaite, Colloids and Surfaces A 253 (2005) 83.

[10] R. Me´sza´ros, L. Thompson, M. Bos, I. Varga, T. Gila´nyi, Langmuir 19 (2003) 609.

[11] K. Thalberg, B. Lindman, K. Bergfeldt, Langmuir 7 (1991) 2893.

[12] M. A. Winnik, S. M. Bystryak, C. Chassenieux, Langmuir 16 (2000) 4495.

[13] H. Dautzenberg, Macromolecules 30 (1997) 7810.

[14] T. Matsuda, M. Annak, Langmuir 24 (2008) 5707.

[15] C. Wang, K. C. Tam, Langmuir 18 (2002) 6484.

[16] K. Pojják, E.Bertalanits, R. Mészáros, Langmuir 27 (2011) 9139.

[17] X. Wang, Y.Li, J. Li, J. Wang, Y. Wang, Z. Guo, H. Yan, The Journal of Physical Chemistry B 109 (2005) 10807.

[18] S. V. Solomatin, T.K. Bronich, T. W. Bargar, A. Eisenberg, V. A. Kabanov, A. V. Kabanov, Langmuir 19 (2003) 8069.

[19] H. Dautzenberg, W. Jaeger, Macromolecular Chemistry and Physics 203 (2002) 2095.

[20] M. Y. Gorshkova, I.F. Volkova, V. A. Izumrudov, Polymer Science, Ser. A 52 (2010) 368.

[21] A. Mezei, Abraham, K. Pojják, R. Mészáros, Langmuir 25 (2009) 7304.

[22] K. Pojjak, E. Bertalanits, R. Meszaros, Langmuir27 (2011) 9139.

[23] Y. Yan, L.Li, H. Hoffmann, Journal of Physical Chemistry B 110 (2006) 1949.

[24] T. Reihs, M. Mészáros, K. Lunkwitz, Journal of Colloid and Interface Science 271 (2004) 69.

[25] M. Muller, T. Reihs, W. Ouyang, Langmuir 21 (2005) 465.

[26] Y Gao , L.T. Duc, A. Ali , B. Liang , J. Liang , P. Dhar, Langmuir 29 (2013) 3654.

[27] T. K. Sen, K.C. Khilar, Advances in Colloid and Interface Science 119 (2006) 71.

[28] S. I. Szilagyi, A. Sadeghpour, M. Borkovec, Langmuir 28 (2012) 6211.

[29] P. Sinha, I. Szilagyi, F. J. M. Ruiz-Cabello, P. Maroni, M. Borkovec, Journal of Physical Chemistry Letters 4 (2013) 648−652.

[30] J. Montes Ruiz-Cabello, Z. Csendes, P.Sinha, T. Oncsik, I. Szilagyi, P. Maroni, M. Borkovec, Journal of Physical Chemistry B 117 (2013) 11853.

[31] S. H. Behrens, D. I. Christl, R. Emmerzael, P. Schurtenberger, M. Borkovec, Langmuir 16 (2000) 2566.

[32] J. Lyklema, Journal of Colloid and Interface Science 392 (2013) 102.

[33] J. Israelachvili, Intermolecular and Surface Forces. Elsevier, San Diego, US, 2011.

[34] J. Hsu, Y.Kuo, Journal of Colloid and Interface Science 171 (1995) 254.

[35] G. Trefalt, I. Szilagyi, M. Borkovec, Journal of Colloid and Interface Science 406 (2013) 111.

[36] J. Hsu, Y.Kuo, Journal of Colloid and Interface Science 185 (1997) 530.

[37] M. Sammalkorpi, M. Karttunen, M. Haataja, Journal of Physical Chemistry B, 113 (2009) 5863.

[38] A. Dieh, P. S. Kuhn, Physical Review E 9 (2009) 011805.

[39] Y. Zhang, P. S. Cremer, Current Opinion in Chemical Biology 10 (2006) 658.

[40] Y. Roiter, O. Trotsenko, V. Tokarev, S. Minko, Journal of American Chemical Society 132 (2010) 13660.

[41] O. Trotsenko, Y. Roiter, S. Minko, Langmuir 28 (2012) 6037.

[42] W. J. Dressick, K. J. Wahl, N. D. Bassim, R. M. Stroud, D. Y. Petrovykh, Langmuir 28 (2012) 15831.

[43] A. V. Dobrynin, M. Rubinstein, Progress in Polymer Science 30 (2005) 1049.

[44] H. Dautzenberg, J.Kriz, Langmuir 19 (2003) 5204.

[45] J. Warr, D. M. Bloor, J. F. Holzwarth, E. Wyn-Jones, Langmuir 16 (2000) 3093.

[46] A. Mezei, R. Mészáros I. Varga, T. Gilányi, Langmuir 23 (2007) 4237.

[47] H. Wang, Y.Wang, H. Yan, Langmuir 22 (2006) 1526.

[48] K. D. Collins, Biophysical Chemistry 119 (2006) 271

[49] N. Vlachy, B. Jagoda-Cwiklik, R. Vácha, D. Touraud, P. Jungwirth, W. Kunz, Advances in

Colloid and Interface Science 146 (2009) 42.

[50] K. D. Collins, Methods 34 (2004) 300.

[51] E. M. Nelson. The Adsorption of DNA onto Unmodified Gold Nanoparticles. University of Rochester, Rochester, New York, 2008.

[52] K. Hayakawat, C.T.Kawt, Journal of Physical Chemistry B 87 (1983) 506.

[53] A. Renoncourt, N.Vlachy, P. Bauduin, M. Drechsler, D. Touraud, J. M. Verbavatz, M. Dubois, W. Kunz, B. W. Ninham, Langmuir 23 (2007) 2376.

[54] K. Pojják, E.Bertalanits, R. Mészáros, Langmuir 27 (2011) 9139.

4 Interface Induced Disassembly of a Refined Self-assembled Nanoparticle System

4.1 Abstract

We present a study of static and dynamic interfacial properties of self-assembled polyelectrolyte/surfactant nanoparticles (size 110-120 nm) at a fluid-fluid interface. Surface tension vs. time measurements of an aqueous solution of these nanoparticles show a concentration dependent biphasic adsorption to the air/water interface while interfacial microrheology data show a concentration dependent initial increase in the surface viscosity (up to 10^{-7} N m/s), followed by a sharp decrease (10^{-9} Nm/s). Direct visualization of the air-water interface shows disappearance of particles from the interface over time. Based on these observations we propose that the polyelectrolyte/surfactant nanoparticles at fluid/fluid interfaces exist in two states: initial accumulation of nanoparticles at the air/water interface, followed by interface induced disassembly of the accumulated nanoparticles into their components. The lack of change in particle size, charge and viscosity of the bulk aqueous solution of polyelectrolyte/surfactant nanoparticles with time indicates that this disintegration of the self-assembled nanoparticles is an interfacial phenomenon. Changes in energy encountered by these nanoparticles at the interface lead to instability of the self-assembled system and dissociation into its components. Such systems can be used for applications requiring directed delivery and triggered release of entrapped surfactants or macromolecules at fluid/fluid interfaces.

4.2 Introduction

Colloidal nanoparticles at fluid interfaces have been the subject of several research explorations in the past decade, primarily due to their increased use in industrial and biomedical applications [1-3]. While the formation of two-dimensional structures formed from microparticles is now

relatively well understood due to significant theoretical and experimental efforts in this area (as reviewed recently [4]), the adsorption of nanoparticles to fluid-fluid interfaces from a stable suspension and consequent inter-particle interactions at the interface are poorly understood. Understanding the behavior of nanoparticles at interfaces is also becoming important in biology, due to the closely related fields of self-assembly of biological macromolecules like proteins [5], viruses [6, 7], and nanoparticles [8] at biologically relevant interfaces. The adsorption and stability of nanoparticles (NPs) at interfaces is greatly influenced by interfacial phenomenon: thermal fluctuations, immersion depths and interfacial forces such as the line tension associated with NPs are believed to influence their stability to a greater degree. For example, activation energy associated with particle removal from the interface was shown to be 10^7 times the thermal energy for polystyrene microparticles adsorbed at the air/water interface [9], while for a nanoparticle system, thermodynamic models indicate that it may be as low as 10-100 times the thermal energy [1]. By manipulating the size [10], anisotropy or surface chemistry [3, 11-14] nanoparticles can absorb and form very stable self-assembled microstructures at fluid-fluid interfaces. Examples of nanoparticle disassociation, lack of adsorption, desorption or wettability alterations at the interface have also been reported [11, 13, 15, 16]. In order to successfully engineer potentially transformative technologies based on the adsorption and/or self-assembly of nanoparticles at interfaces, a better understanding of the interfacial behavior of nanoparticles at these fluid-fluid interfaces is required.

In this chapter, we report on the interfacial behavior of apolyethylenimine (PEI)/sodium dodecyl sulphate (SDS) nanoparticles adsorbing at an air/water interface. These nanoparticles form as a result of electrostatic interactions between the negatively charged surfactant and positively charged polyelectrolyte. They form stable colloidal systems in the bulk, leading to their use as

drug delivery vehicles for treatments that need limited toxicity to off-target tissue, such as delivery of anticancer drugs and vaccines or even viral gene therapy [17]. In spite of frequent encounters with hydrophobic interfaces, the behavior of these nanoparticle complexes at interfaces has not been explored in detail or exploited for industrial applications. On the other hand, self-assembly of mixtures of surfactants and polyelectrolytes at the air/water interface has received a lot of attention, particularly since polymers are added to several surfactant mixtures for applications in oil industry and consumer products like cosmetics, detergents, etc. [18-22] The primary goal was to study the adsorption dynamics, stability and possible interparticle interactions between polymer-based nanoparticles at the air/water interface. Using surface tension measurements of a nanoparticle system that forms a stable colloidal suspension, we probed the surfactant-like properties and short and long term stability of PEI/SDS nanoparticles at a fluid-fluid interface. We found that even though the major constituent of the nanoparticles is a hydrophilic polyelectrolyte with no tendencies to adsorb at the air/water interface, the nanoparticles with entrapped SDS showed surfactant properties that were either diminished (short time scale) or enhanced (longer times) when compared to free SDS. The surface tension measurements also indicate a two-step process occurring at the air/water interface, the characteristics of which are different from a mixture containing polyelectrolytes and surfactants of opposite charges accumulating at an air/water interface [23]. Direct visualization of the surface indicates initial presence of particles at the interface that disappear with time. We attribute the observed changes in the surface tension with time to a concentration and time dependent adsorption and interfacial energy induced disassociation of the nanoparticles at the air/water interface, and not a desorption of the nanoparticles from the interface.

To gain further insight into the interparticle interactions between the nanoparticles at the interface, we also measured the surface shear viscosity of this interface using an interfacial microrheometer. To the best of our knowledge, there are no measurements of the surface shear viscosity of these nanoparticles at the air/water interface, possibly due to the non-trivial nature of these measurements. The smaller the surface viscosity, the harder it is to decouple the response of the two-dimensional interfacial film from that of the three-dimensional subphase [24-27]. Using micrometer or nanometer sized probe particles, we and others have significantly increased the sensitivity of the system to shear stresses resulting from the interfacial film [26, 28-31]. This allowed us to measure very dilute films of free SDS with surface viscosities as low as 10^{-9} Nm/s. Our surface viscosity results indicate an initial increase in the surface viscosity of the system (up to 10^{-7} Nm/s), followed by two orders of magnitude reduction in the surface viscosity with time. These results also support the proposed initial formation of a nanoparticle film with higher resistance to shear, which undergoes molecular rearrangements into a less ordered system, possibly due to dissociation of the nanoparticles and release of the entrapped SDS.

Since the bulk solution of polyelectrolyte/surfactant nanoparticles is stable over several months, we attribute the observed changes at the interface to interfacial energy driven disassembly of the nanoparticles. This interfacial phenomenon may be used for triggered release of trapped surfactants at fluid-fluid or solid/fluid interfaces, particularly for applications related to enhanced oil recovery, delivery of healthy surfactants at the air/water interface in the lung to treat certain types of respiratory distress syndrome or delivery of entrapped enzymes for biosensor applications.

4.3 Materials and Methods

4.3.1 Chemicals

Surfactant sodium dodecyl sulphate, SDS, (MW: 288.38 g/mol) and branched polyelectrolyte polyethylenimine, PEI (MW: 25 kDa) were purchased from Sigma Aldridge and used without further purification. Water used in these experiments are obtained from a Millipore water purification system with initial pH = 7.0. All other chemicals used in this study were purchased from Fisher Scientific, including methylene blue, sodium tetraborate, methylene chloride, nickel sulphate ($NiSO_4 \cdot 6H_2O$), boric acid (H_3BO_3), nickel chloride ($NiCl_2 \cdot 6H_2O$), nitric acid, acetone, sodium hydroxide (NaOH) and Whatman Anodisc alumina filter (25 mm diameter with polypropylene support rings and 0.02 μm pores).

4.3.2 Methods

Nanoparticle synthesis: The PEI/SDS mixtures were prepared following the same procedure as described in previous work [32]. The positively charged PEI/SDS nanoparticles were prepared by mixing and constantly stirring 0.25% PEI and 26.6 mM SDS stock solutions in a weight ratio of 3:1. After mixing for 5 minutes, excess surfactants and PEI not bound to the nanoparticles were eliminated by repeated centrifugation and replacement of supernatant with water (typically at 15000 rpm for 1.5 hours). The nanoparticles were collected and resuspended with Millipore water after removal of the supernatant. The final concentration of entrapped surfactant (SDS) in the PEI/SDS nanoparticles was calculated from the entrapment efficiency from UV absorbance at 650 nm as described in the reference [22]. The absorbance of PEI solution at the same wavelength was not observed so that we are sure PEI had no effect on the measurement of SDS concentration during the entrapment efficiency test. The initial stock nanoparticle solution with SDS entrapped concentration of 30 mM was then diluted to different concentrations by Millipore water.

Adsorption Isotherms: The dynamics of nanoparticle adsorption to the air-water interface was recorded by a Wilhelmy plate sensor, which is part of the KSV-NIMA Langmuir trough purchased from Biolin Scientific. To initiate each experiment, a well-mixed solution of the nanoparticles (volume 3 ml) was added to a small petri-dish. A wet calibrated filter paper flag was dipped into this solution and used as a probe to monitor changes in the surface pressure due to adsorption of surface-active material. The surface tension (γ) was determined from the surface pressure (π) measurement using the following relationship: $\gamma = 72.2 - \pi$. Each experiment was run for a maximum of 20 hours at 22 $\pm$2 ℃. In some cases, data accumulation was stopped earlier if the saturation pressure for pure SDS was reached. The concentration range of nanoparticles used was such that the final total concentration of SDS in the system ranged from 0.4 mM to 10 mM (note: critical micelle concentration of pure SDS is ~ 8.31 mM).

Active Interfacial Microrheology: Precise monitoring of the changes in the viscosity of the interface due to adsorbing nanoparticles was possible due to a custom designed interfacial microrheometer system, described in details elsewhere [29]. Briefly, reorientation of magnetic nanorods (l =3~6 μm, d=300 nm) placed at the air/colloidal dispersion interface due to an externally applied magnetic field was recorded under varying bulk concentrations as shown in the schematic (Figure 4.1). The magnetic nanorods were synthesized by first depositing Nickel into alumina templates by electrochemical deposition and then releasing the nanorods by dissolving the template in sodium hydroxide. The Ni nanorods released from the alumina templates were thoroughly washed in acetone, isopropanol and chloroform to be free of organic impurities, and finally dispersed in water and stored at room temperature when not in use. Magnetic fields (2 —3 Gauss) were generated through homebuilt electromagnetic coils. Before initiating each experiment, the nanorod solution was sonicated for around 40 minutes to break up

any nanoparticle aggregates, and then carefully placed at the air/nanoparticle solution interface in a small petri-dish. A permanent magnet is placed on top for a minute to ensure that all nanorods are retained at the surface. The reorientation of the magnetic rods due to the applied field is visualized with a LEICA Inverted Microscope coupled to a fast camera (Andor Luca) and the digitized images of the motion recorded and stored for further analysis using the Andor capture software. The reorientations of the nanorods were recorded every 10-20 minutes for a maximum of 8 hours at 22 $\pm$2°C. To ensure detection of any heterogeneity at the interface, the interface was scanned often and the motion of nanorods located at different positions was imaged. The inherent drift of the interface also ensured that the data points for surface viscosity were a representation of any heterogeneity in the system. However, it must be noted that this drift has no influence on the nanorod orientation.

Analysis of rod motion: The orientation of a magnetic nanorod (length *l*, magnetic moment *m*) due to an externally applied magnetic field, **H,** can be described by the angle, φ(t), between the long axis of the rod and the direction of the applied field [29] (see Figure 4.1). For a purely viscous medium, the rod responds to changes in the direction of **H** as:

$$\mu_0 mH\sin\varphi = f_r \eta_w l^3 \frac{d\varphi}{dt} \qquad (4.1)$$

the solution to which is: $\tan\left(\frac{\varphi}{2}\right) = \exp\left(-\frac{t}{\tau}\right)$ (4.2)

The relaxation time, $\tau = f_r \eta_w l^3 / \mu_0 mH$, depends on f_r, the dimensionless drag coefficient of the rod, which is a sum of the bulk (f_w) and surface (f_s) drag: $f_r = f_w + f_s$. The rod angle φ(t) is obtained for each experiment using a particle tracking program written in Matlab, and φ(t) plotted vs. t to obtain f_r. The bulk drag, f_w, is constant and taken to be half that of the drag on a rod of diameter *d* and length *l* (*l*/*d* = 10) rotating in a viscous fluid: $f_w = \frac{p}{6\left[\ln\left(2l/d - 0.8\right)\right]}$ [26].

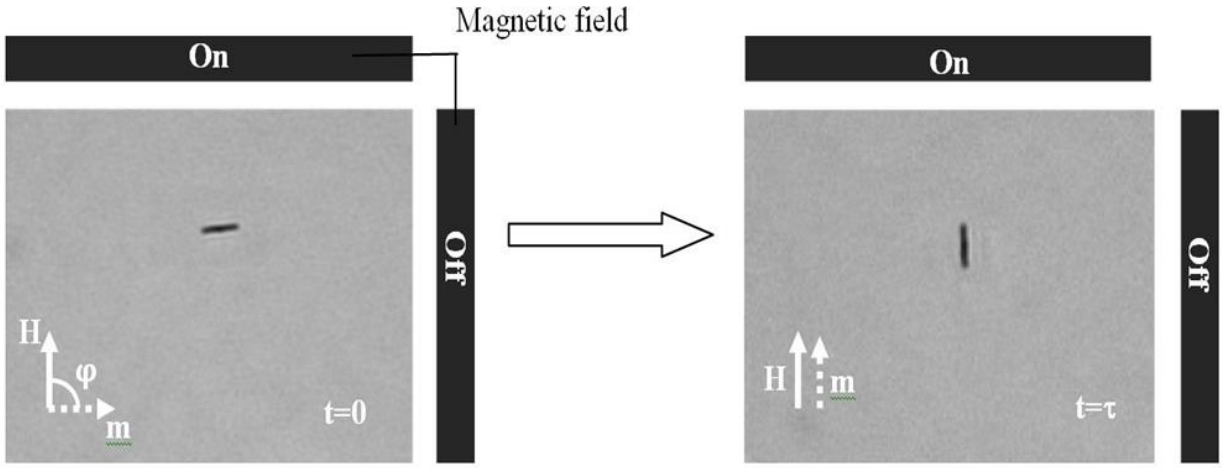

Figure 4.1 The schematic of the interfacial nanorod rheometer set-up. A set of perpendicular coils is used to apply magnetic fields. A Nickel nanorod (black rod) placed at the air/water interface will re-orient itself due to the applied magnetic field, the time taken for which is related to the viscosity.

We find that even for dilute films of pure SDS, with viscosities = 10 nNs/m, $f_r >> f_w$. However, for all values of surface viscosity less than 1 nN s/m, this is no longer true, and the rod motion may be dominated by the bulk stresses. Therefore, for this study surface viscosity values below 1 nN s/m may be regarded as below the detection limit of this system.

Bulk viscosity measurements: A digital cone-and-plate viscometer (DVII+ Pro, CP-40 0.8° cone, Brookfield Engineering, Middleboro, MA) was used to characterize the bulk viscosity of the resuspended nanoparticle solution with different entrapped SDS concentrations. The temperature was controlled at 25℃. 0.6 ml sample was used for the measurements at a shear rate of 60 rpm. The torque was greater than 10% to ensure accuracy of the data.

4.4 Results

4.4.1 Adsorption of nanoparticles to the air/water interface

Figure 4.2 (a), (surface tension vs. time measurements of PEI/SDS nanoparticles with different concentration of total SDS in the system), demonstrates that the dynamics of adsorption of nanoparticles at the interface shows a concentration dependent biphasic behavior (red, green and

purple curves). The value of the surface tension reached during the first stage is directly proportional to the concentration of the total SDS molecules entrapped in the nanoparticles, but is always lower than that for the same concentration of free SDS (see Figure 4.2 (b) for more details). The length of the first plateau region (referred to as Stage 1 in this chapter, see Figure 4.2 (a)) is inversely proportional to the concentration of the total entrapped SDS in solution, and completely disappears close the CMC of pure SDS (blue curve). At the same time, we found this biphasic behavior to be absent at very low concentrations of SDS (< 1mM, black curve). At the end of the second stage, for all concentrations of nanoparticles above 1 mM, the surface tension of the air/water interface reached an equilibrium value that corresponds to the saturation value achieved by free SDS molecules beyond CMC (35 mN/m). Figure 4.2 (b) represents the surface tension attained by the nanoparticle system at the end of the first (open squares) and second stages (solid circles) as a function of total SDS concentration and is compared with the equilibrium surface tension of free SDS molecules (open diamonds). The nanoparticles with entrapped SDS reach the same minimum surface tension at a much lower concentration of SDS (1.6 mM vs. 8.0 mM for pure SDS) at the end of the second stage in their adsorption process (solid circles). This is in contrast with the surface tension achieved at the end of the first stage (open squares), which is lower than that of free SDS (open diamonds). The inset shows that the polyelectrolyte solution without SDS cannot lower the surface tension between air/water significantly for many orders of stock concentration of PEI.

(a)

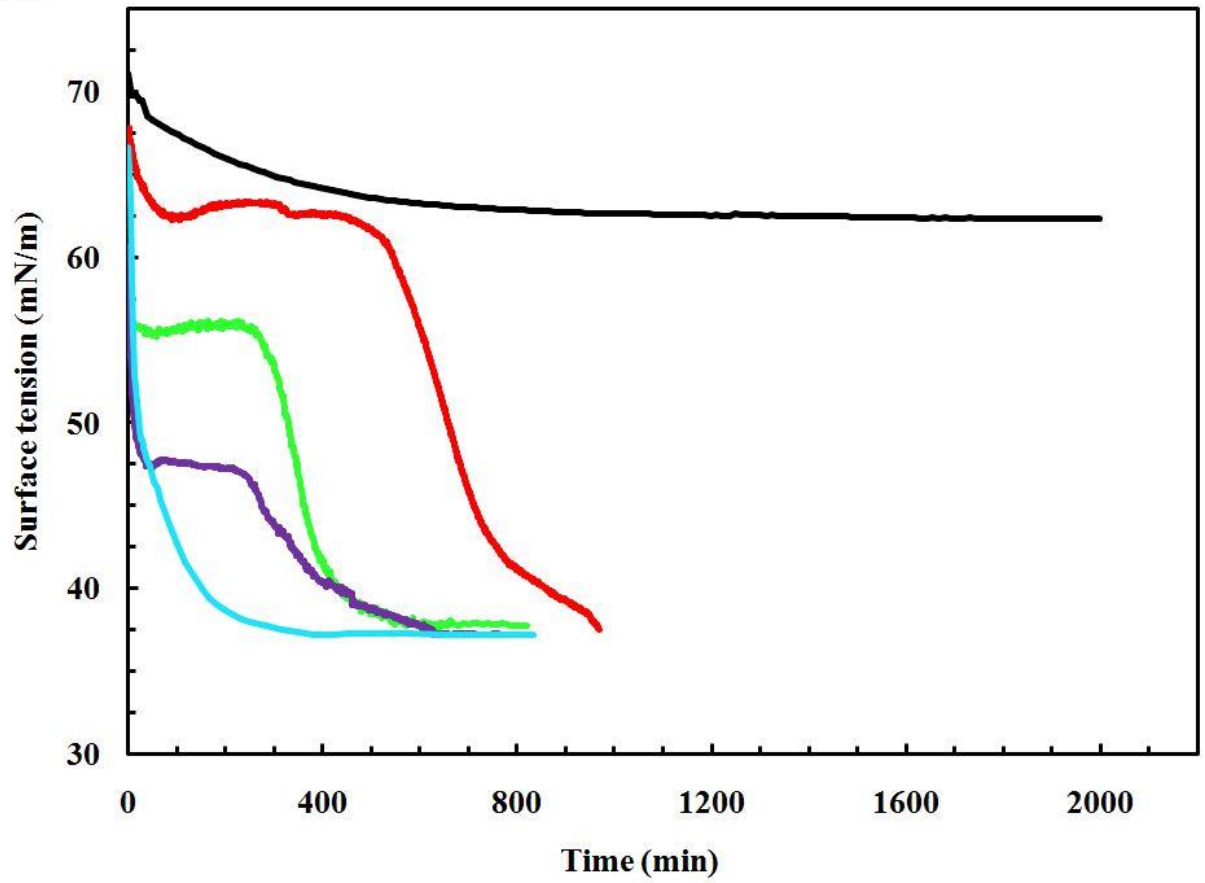
70
60
50
40
30
Surface tension (mN/m)
0
400
800
1200
1600
2000
Time (min)

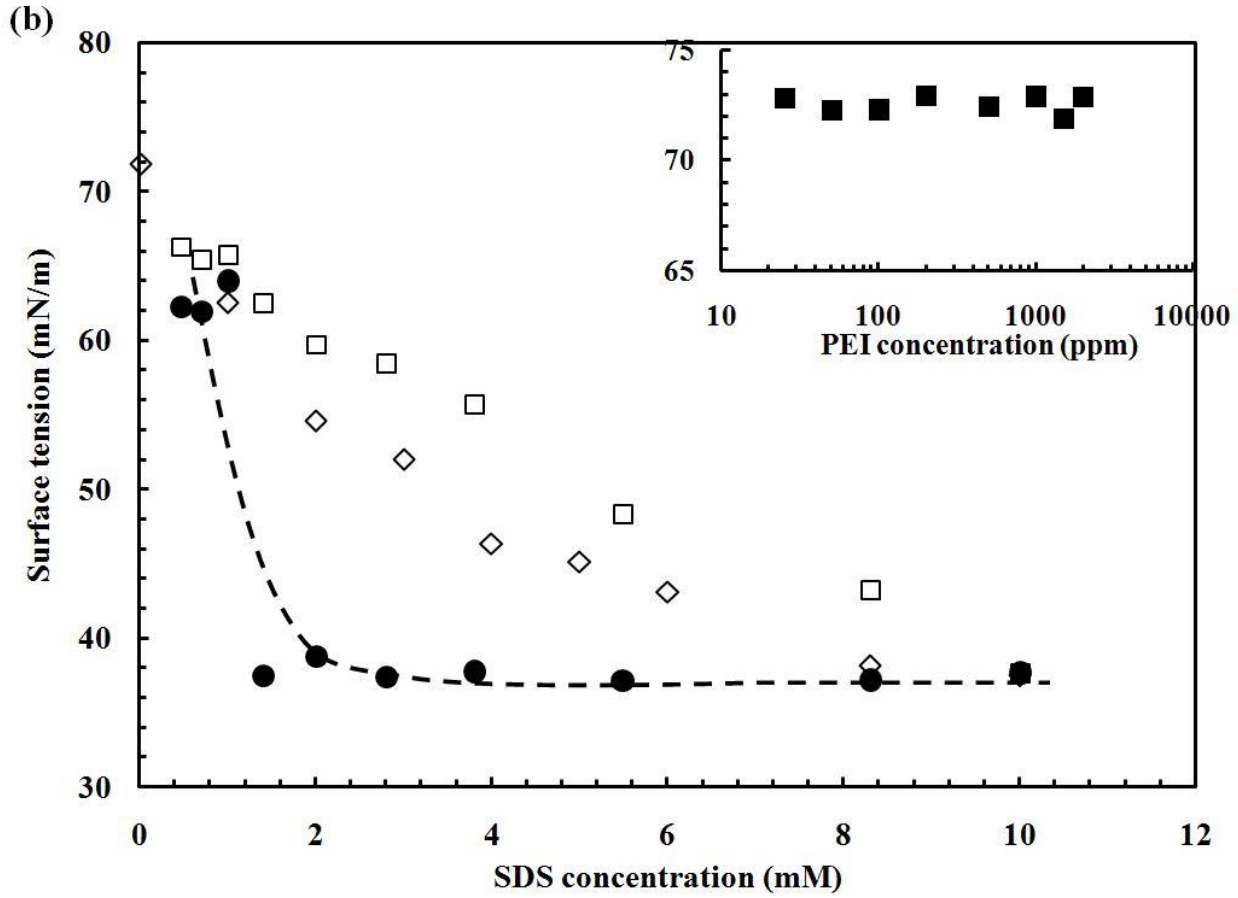

Figure 4.2 (a) Surface Tension vs. time for various different concentrations of total entrapped surfacatant SDS, 1 mM (black), 1.4 mM (red), 3.8 mM (green), 6 mM (purple), 8 mM (blue). We find a biphasic decrease of surface tension vs. time for several intermediate concentrations of entrapped surfactant.The final saturation concentration reached for all concentrations above 1.0 mM corresponds to the minimum surface tension achieved by pure SDS beyond the critical micelle concentration. (b) Equilibrium Surface tension vs. SDS concentration for free SDS solution (◇), nanoparticle solution at the end of the first stage (●), nanoparticle solution at end of second stage (□). We find that the nanoparticles show decreased surfactant properties at short times, but increased surfactant properties at long times. Inset shows that the polyelectrolyte complex without SDS is hydrophilic and cannot lower the surface tension. (Note: the CMC for SDS solution is 8.31 mM)

4.4.2 Viscosity of nanoparticles at the air/water interface

Figure 4.3 (a) shows the surface viscosity of the nanoparticles with different amounts of entrapped SDS. For all concentrations above 1 mM, we find that the surface viscosity shows an initial increase in viscosity with time. However, a peak in the viscosity value is observed, beyond which the surface viscosity begins to drop. The inset to the figure shows the early stages of the change in surface viscosity, and the dotted lines indicate that the time required to reach a peak in surface viscosity depends inversely on the concentration of total entrapped SDS. During the course of each experiment, we find that the final viscosity of the interface drops to ~ 1 nNs/m or lower. Interestingly, for the nanoparticle solution with net SDS concentration below 1mM, we find that the surface viscosity always remains close to the detection limit of our system, indicating that at this lowest concentration no significant surface viscosity can be detected for the duration of the experimental study. Figure 4.3 (b) shows that in comparison to the entrapped system, the surface viscosity of free SDS remains relatively stable for over 300 minutes. Additionally, there is no measureable surface viscosity for the polyelectrolyte solution without any SDS. In a control experiment (Figure 4.3 (c)) that measures the bulk viscosity of the nanoparticle solution as a function of time, no change in the viscosity is observed and the viscosity is found to be similar to that of pure water. Figure 4.3 (d) shows the surface viscosity of free SDS as a function of concentration. Our results show that SDS itself forms a dilute system at the interface, with values of surface viscosity above CMC= 20-30 nN·s/m.

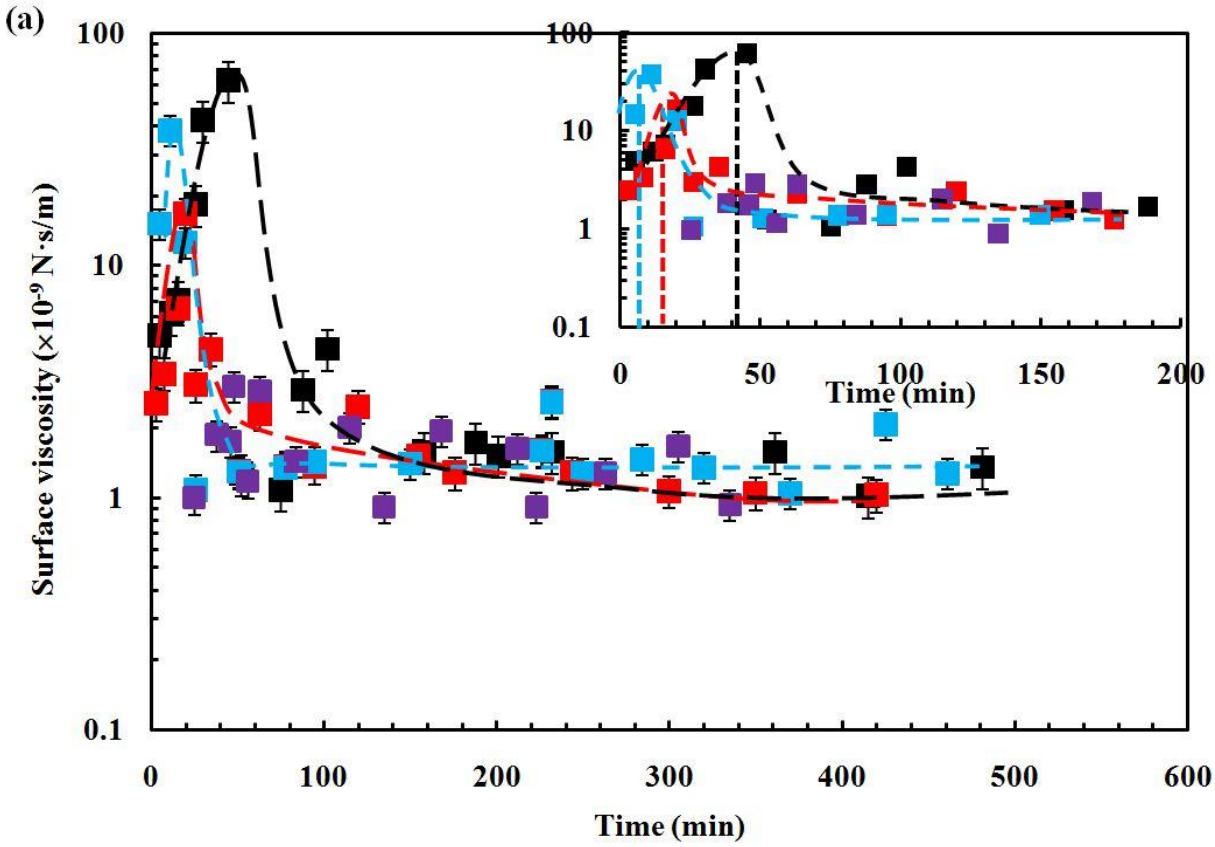
(a)
Surface viscosity (×10⁻⁹ N·s/m)
Time (min)
100
10
1
0.1
0
100
200
300
400
500
600
50
150

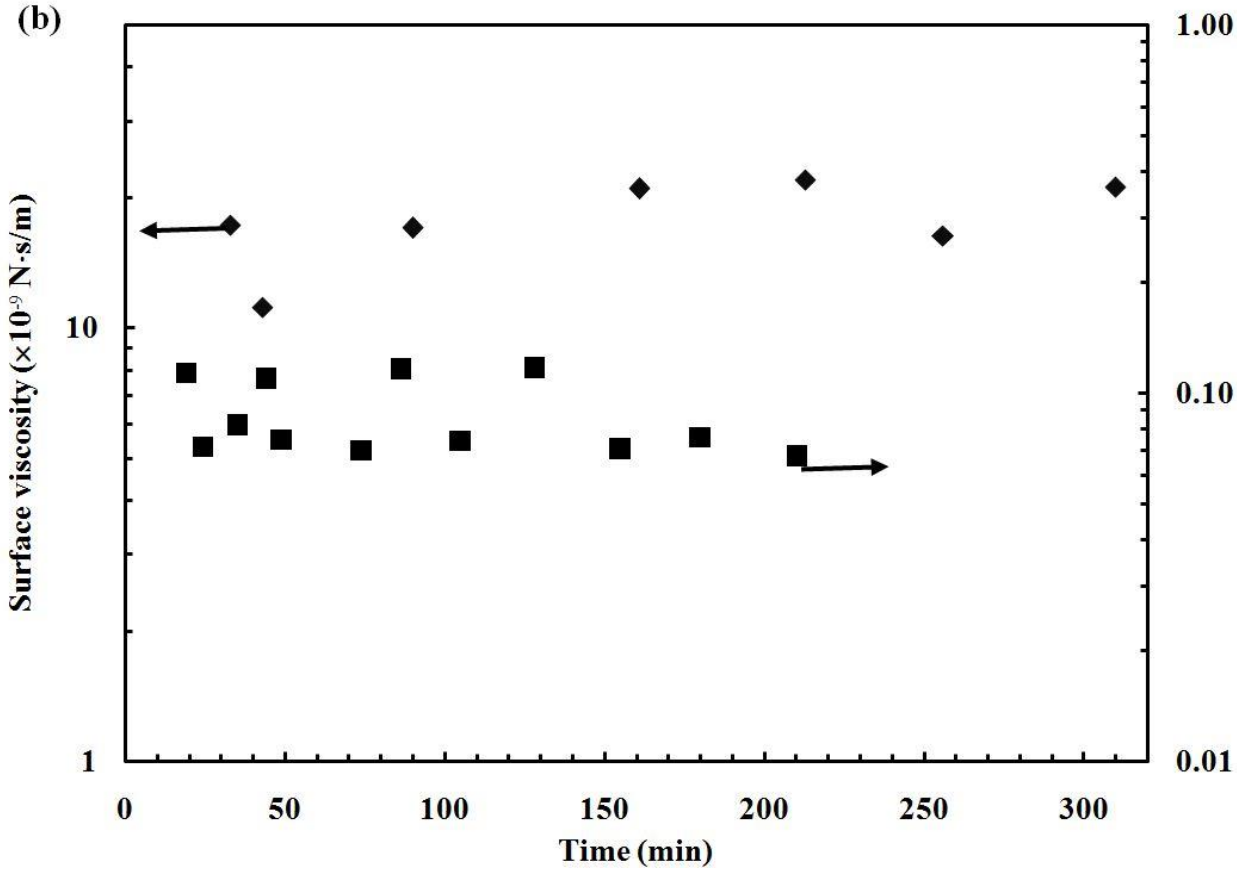
(b)
Surface viscosity (×10⁻⁹ N·s/m)
Time (min)
1.00
0.10
0.01
10
1
0
50
100
150
200
250
300

(c)

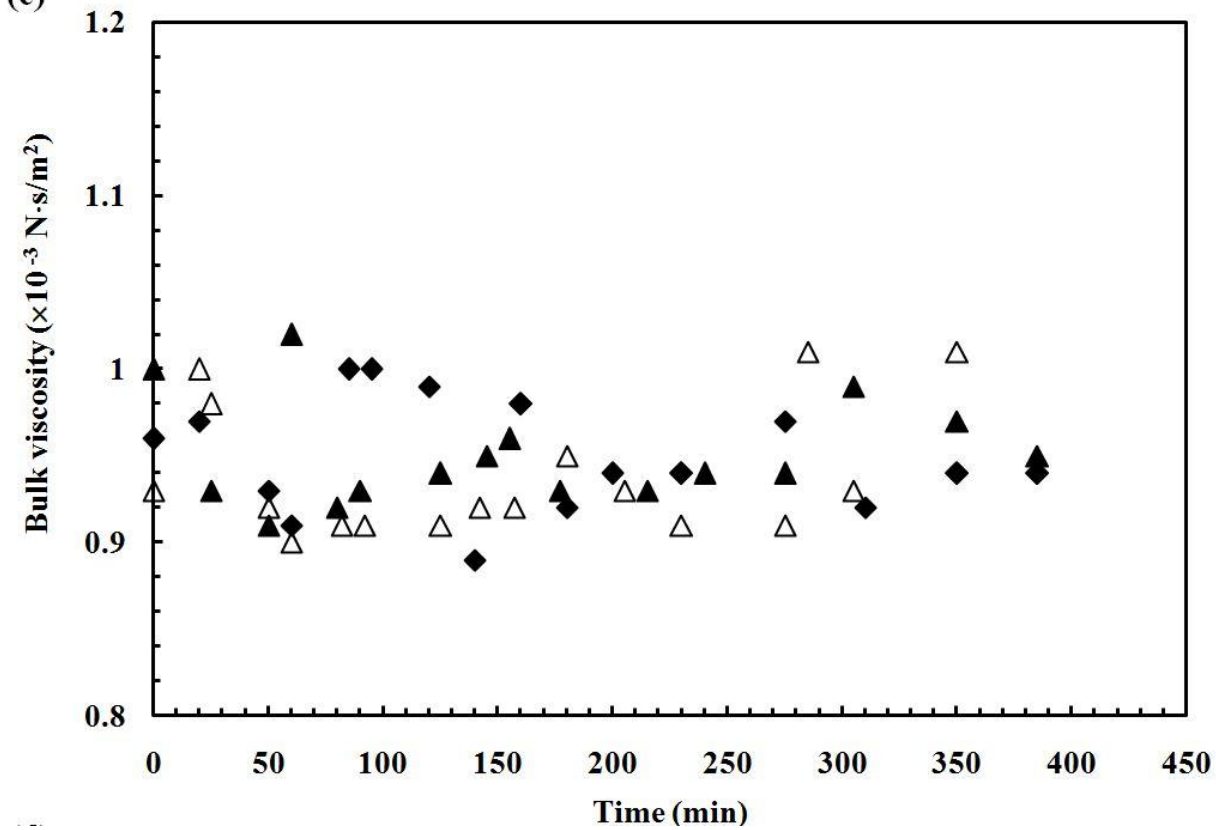
1.2
1.1
1
0.9
0.8
Bulk viscosity (×10 -3 N·s/m2)
0
50
100
150
200
250
300
350
400
450
Time (min)

(d)

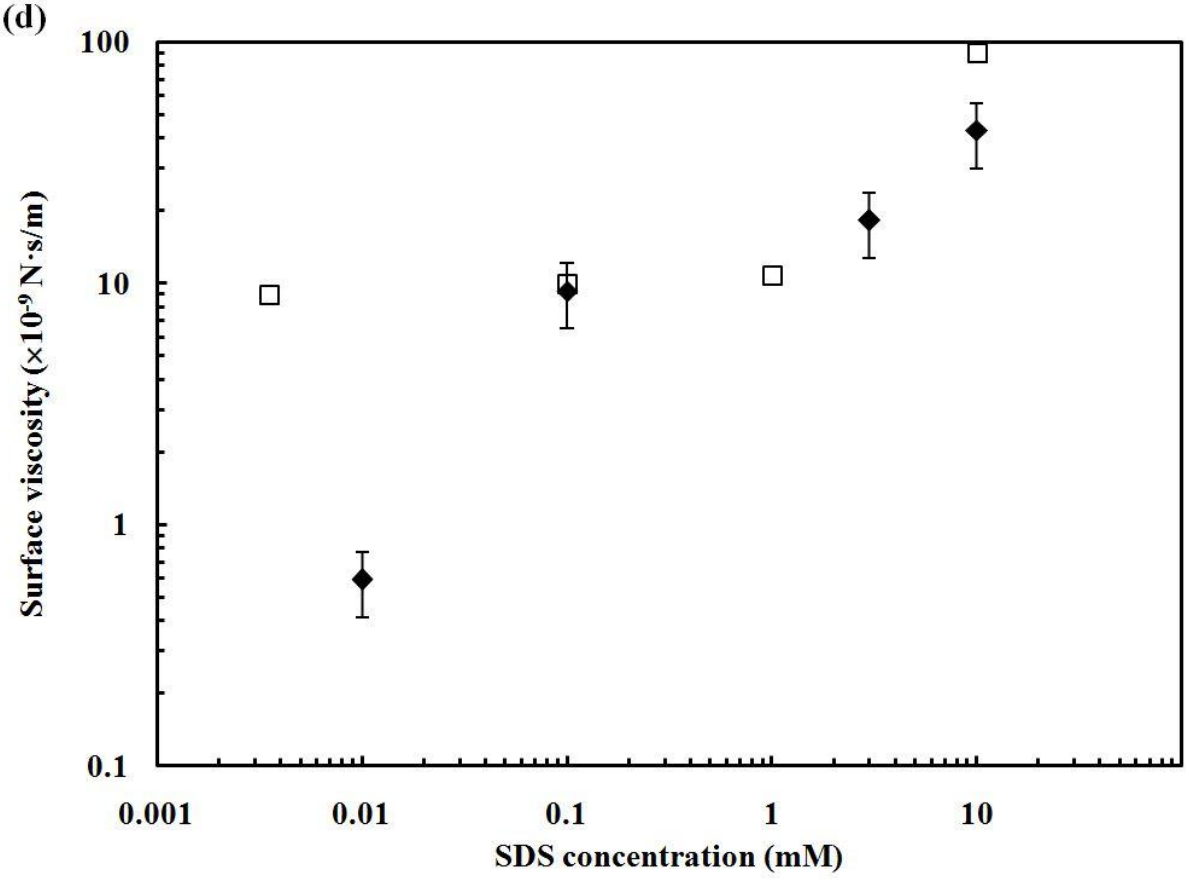
100
10
1
0.1
Surface viscosity (×10-9 N·s/m)
0.001
0.01
0.1
1
10
SDS concentration (mM)

Figure 4.3 (a) Surface viscosity vs. time for different concentrations of total entrapped surfacatant SDS, 1.0 mM (purple), 3.8 mM (black), 6 mM (red), 8 mM (blue). We find that for concentrations above 1 mM, the surface viscosity reaches a maximum value at short times (possibly due to the initial accumulation of nanoparticles at the interface). However, the disassembly of the nanoparticles causes the surface viscosity to drop by orders of magnitude. Inset shows the time dependence of surface viscosity at shorter time scales. For concentrations below 1.0 mM, no change in surface viscosity was detected.(b) Surface viscosity vs time for SDS solution (◆) and PEI solution (■)shows surface viscosity of free SDS molecules remains steady at longer times, while the PEI solution without SDS does not contribute to the surface viscosity at all. (c) Bulk viscosity of nanoparticle solution as a function of time for the stock concentrations 1 mM (◆), 3.8 mM (△), 8 mM (▲) shows no significant change in the bulk viscosity with time. The viscosity is similar to that of pure water indicating that the significant changes in surface viscosity with time are a surface induced phenomenon. (d) Surface viscosity of pure SDS shows a concentration dependence of surface viscosity. Closed diamonds (◆) correspond to current measurements obtained by analyzing the active reorientation of Nickel nanorods, while open squares are values reported before by some of us by analyzing thermal rotation of nanorods [43]. (Note: the CMC for SDS solution is 8.31 mM)

In order to facilitate measurement of the surface viscosity of the nanoparticles at the air/water interface, the interface was visualized under a microscope in transmission mode as shown in Figure 4.4. The results show that initially bright white specks (possibly nanoparticles) were observable at the interface. However, with time these dots disappear from the field of view.

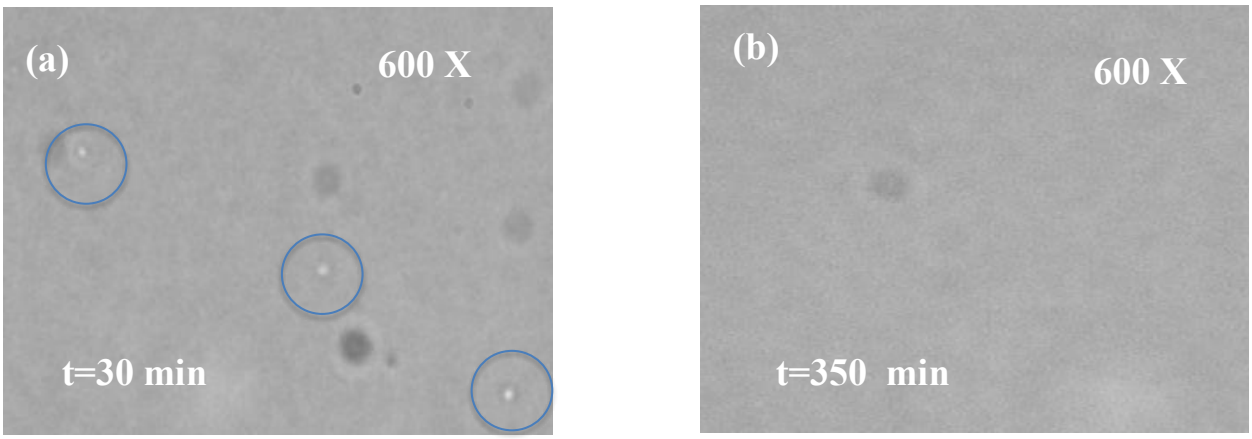

Figure 4.4 Visualization of nanoparticles at short time (a) vs. long time (b) by microscope.

4.4.3 Salt effect on nanoparticle adsorption

In order to characterize the effect of salt on the surface behavior of nanoparticles, the surface tension measurements were taken in the presence of 25 mM NaCl or 25 mM $CaCl_2$ in Figure 4.5. The surface tension results for nanoparticles with addition of salts are quite different from that in water solution: for both investigated salts, the two-step adsorption is absent and the rate of change in surface tension decreases upon addition of salts. Comparing to NaCl, the addition of $CaCl_2$ leads to a more rapid decrease of surface tension. The surface tension in the presence of $CaCl_2$ attains steady values within one hours at lower SDS concentrations; At concentration higher than 1.4 mM, the equilibration of surface tension occurs in 30 minutes. A similar fast adsorption is observed in the presence of NaCl, however, it takes longer time to reach the steady state of surface tension, generally up to several hours. The surface tension isotherms at equilibrium shown in Figure 4.6 allow further comparison between the effects of NaCl and $CaCl_2$ on adsorption of nanoparticles. In pure water solution, the surface tension at very low SDS concentration remains 65 mM/m. Whereas the surface tension at same SDS concentration (<0.3 mM) reduces to 47 mN/m with addition of salts. Further, the critical SDS concentration at which the surface tension reaches 34 mN/m reduces from 1.4 mM in pure water to 0.7mM in 25 mM

salt solution.

(a)

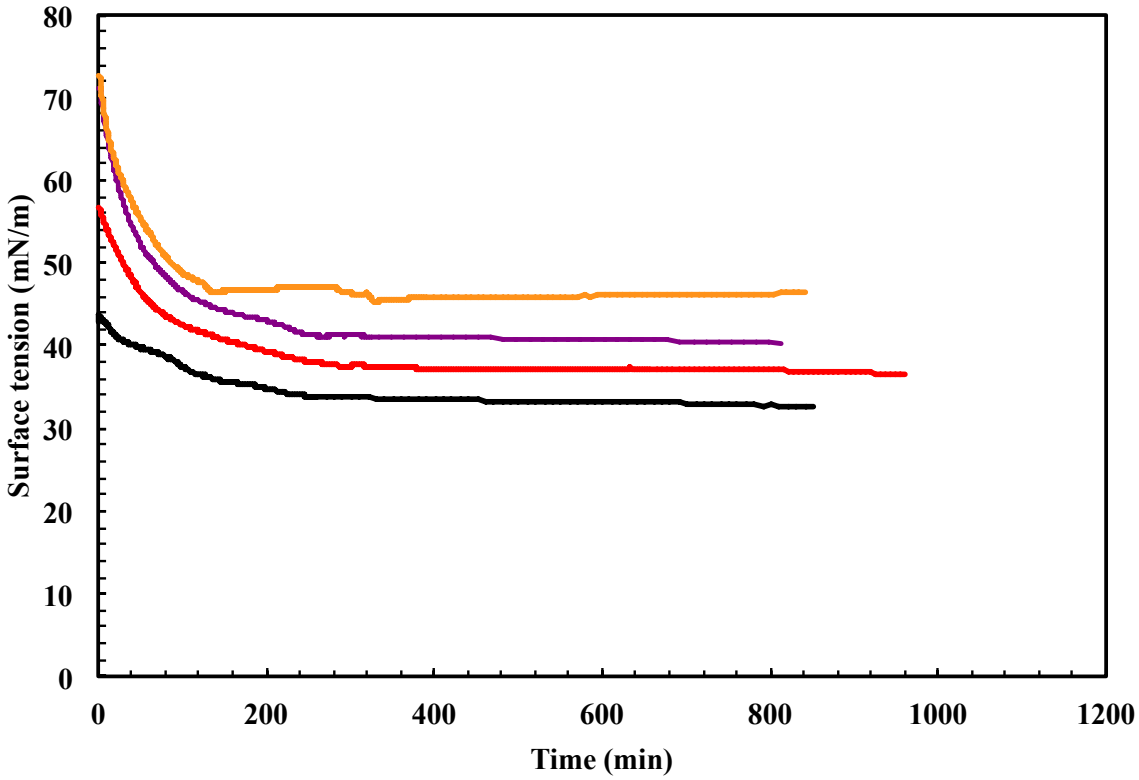

(b)

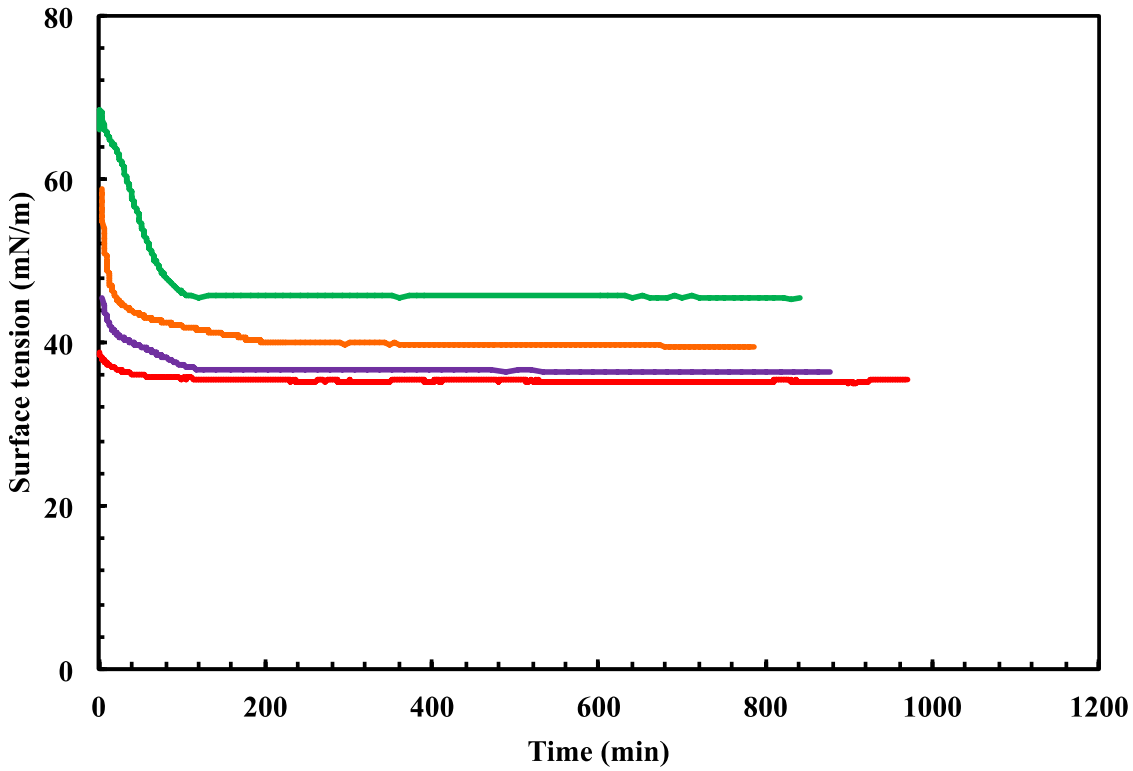

Figure 4.5 Surface tension vs. time for different concentrations of entrapped surfacatant SDS in presence of salts (a) NaCl (b) $CaCl_2$ SDS concentration:0.03 mM (green), 0.3 mM (orange), 0.7 mM (purple), 1.4 mM (red), 2.8 mM (black). With addition of salts, we observe one-step instead of two-step adsorption at certain range of SDS concentrations. The surface tension decreases more rapidly when compared to the results in absence of salts.

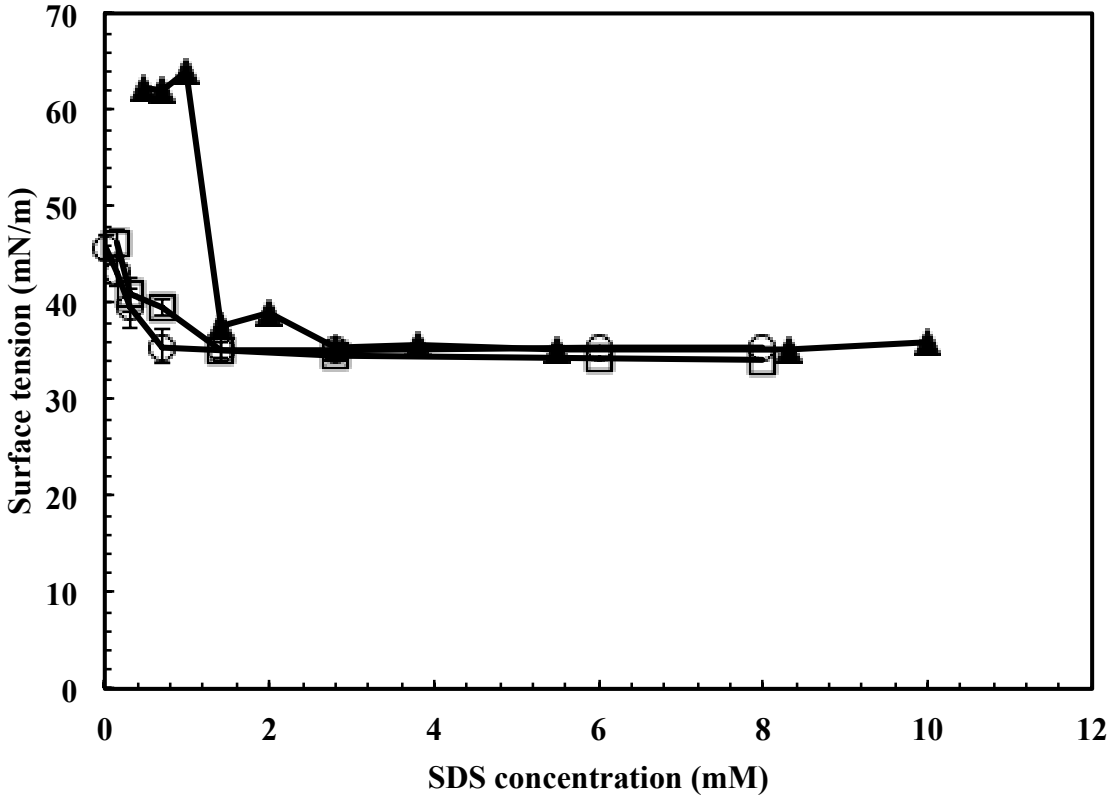

Figure 4.6 Comparison of surface tension isotherms at equilibrium state (> 12 hour) with and without salts (▲ no salt; □ 25 mM NaCl; ○ 25 mM $CaCl_2$). The equilibrium state of surface tension is reached at lower critical SDS concentration with added salts and the value of critical SDS concentration decreases with increasing ionic strength. This indicates the adsorption rate of PEI/SDS nanoparticles at air/water interface is accelerated in the presence of salt mainly due to reduced electrostatic barrier during first-step adsorption

4.5 Discussions

Nanoparticles at interfaces may be exploited for various applications involving nanotechnology. Yet, the behavior of nanoparticles at fluid-fluid interfaces is still poorly understood. In this chapter, we discuss the surfactant properties, dynamics of adsorption, stability and interparticle interactions of polyelectrolyte-based nanoparticles at a model fluid/fluid interface (air/water). These nanoparticle systems form very stable bulk colloidal suspensions; although recent research suggests that these nanoparticles are often trapped in a non-equilibrium energy minimum in the bulk system [33]. Figure 4.7 presents a schematic representation of a possible explanation for the dynamics of nanoparticle adsorption at the air/water interface, showing an initial accumulation of the nanoparticles at the interface, followed by interface induced disassociation of the nanoparticles accumulated at the air/water interface, even when the nanoparticles in the bulk system remain stable. To the best of our knowledge, this is the first demonstration of interfacial energy induced disassembly of self-assembled nanoparticles trapped in a non-equilibrium energy minimum. Below we discuss our results in more details.

Adsorption dynamics: The surface tension measurements as a function of time of our nanoparticle dispersions show a SDS concentration dependent biphasic behavior. We hypothesize that this biphasic adsorption curve is a result of rapid adsorption of the nanoparticles to the air/water interface followed by a slower disassembly, possibly due to altered energetics at the interface. Our results indicate that the air/water interface offers a thermodynamic equilibrium for the nanoparticles (possibly due to the presence of entrapped surfactant with a high equilibrium surface tension), causing the particles to adsorb at the air/water interface and attain a saturation surface pressure (first stage). However, it must be noted that Figure 4.2 (b) indicates that the surface tension attained by the PEI/SDS nanoparticles at the end of the first stage is more

than that of free SDS at the same concentration. This indicates that the nanoparticles have a lower tendency to adsorb to the interface, when compared to free SDS, but much higher tendency when compared to the polyelectrolyte mixture (Figure 4.2 (b) inset).

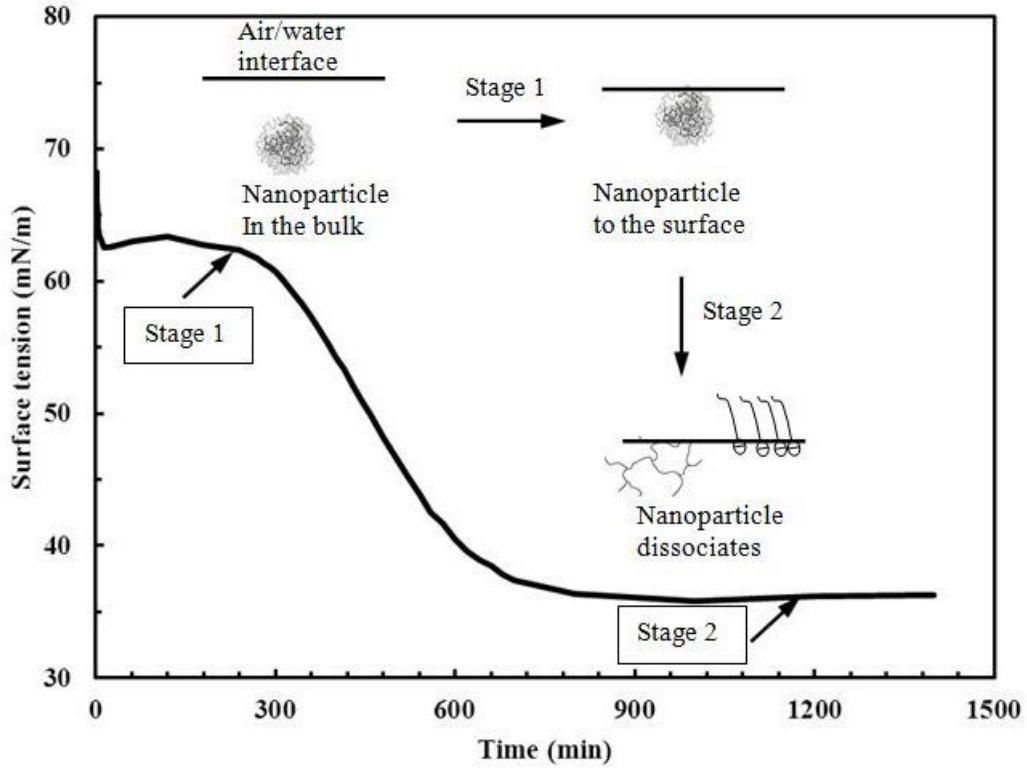

Figure 4.7 Schematic of a possible mechanism of nanoparticle adsorption and interface induced release of entrapped surfactant. The first plateau corresponds to adsorption of self-assembled nanoparticles at the air/water interface. However, with time, the nanoparticles undergo disassembly into its components, and the final surface tension reached corresponds to the saturation surface tension of free SDS for concentrations higher than the CMC of SDS.

Zasadzinski and collaborators [34, 35] have previously shown that the change in surfactant concentration at the air/water interface, $^{d\Gamma}/_{dt}$ may be described by theories of colloidal stability:

$$\frac{d\Gamma}{dt} = C_0 \left(\frac{D_{eff}}{\pi t}\right)^{1/2} \exp(-V_{max}/k_B T) \qquad (4.3)$$

Where C_0 is the bulk surfactant concentration, D_{eff} is the effective diffusivity of the surfactants, V_{max} is the maximum effective height of the potential energy barrier that needs to be overcome, k_B is the Boltzman constant and T is the temperature. Treating the nanoparticles as large surfactant aggregates, V_{max} for our system may be described as

$$V_{max} = (E_i - E_b) + \Pi\Delta A + E_{elect} \qquad (4.4)$$

where $(E_i - E_b)$ is the energy difference between the particles at the interface, and the particles in the bulk system, that drives the adsorption of the particles in the first stage. However, the electrostatic energy of the interface E_{elect}, due to the accumulation of charged nanoparticles, opposes further adsorption of the charged nanoparticles. $\Pi\Delta A$, associated with the energy required to remove the currently adsorbed nanoparticles to make room for more nanoparticles to adsorb also opposes further particles adsorption, resulting in the first saturation plateau. Note that analogous to a typical surfactant, the PEI/SDS nanoparticles demonstrate a concentration dependent increase in the saturation surface tension (Figure 4.2) during this first stage.

The second decrease in surface tension is explained by a possible disassembly of the nanoparticles at the interface into its component parts since the second plateau in surface tension corresponds to the equilibrium surface tension γ_{eq} for free SDS concentrations greater than its CMC. This disassembly is also evidenced by direct visualization of the interface, as well as a sharp decrease in the surface shear viscosity at the interface (discussed later). We believe that the interfacial energy is responsible for this behavior. It has been recently proven that, the nanoparticles in the bulk system are trapped in different non-equilibrium energy minima leading to its kinetic stability [36]. However, the nanoparticles at the air/water interface can be removed from this non-equilibrium energy minimum towards a more thermodynamically stable state with time due to the energies associated with the interface (Equation 4.4), which causes the self-

assembled nanoparticles system to disassemble into its component parts. Increased accumulation of the nanoparticles to the interface increases the kinetics of the disassembly process, which explains why the length of the first saturation plateau is inversely proportional to the net concentration of SDS in the system, and completely disappears when the net SDS concentration of the nanoparticle solution matches the CMC of free SDS. This hypothesis is also supported by our observation that a second stage is not observed at concentrations below 1 mM; the net change in energy is not sufficient to disassemble the stable self-assembled system.

It must be noted that a similar two step process was previously reported for the dynamic surface tension of a mixtures of surfactant and polyelectrolyte of opposite charges [23]. However, in case of the polyelectrolyte/surfactant mixture, the equilibrium surface tension reached during the first plateau was equal to the equilibrium surface tension of the surfactant alone. Therefore, the first step was attributed to adsorption of free monomeric surfactant, followed by the adsorption of polyelectrolytes. This behavior is in sharp contrast with the interfacial behavior of our nanoparticle system, where the surface tension reached at the end of the first stage is always less than that of the free surfactant, while the equilibrium surface tension reached at the end of the second stage is always the same and corresponds with the saturation surface tension of free SDS.

Surface viscosity: Measurement of the interfacial rheological properties is exquisitely related to changes in the interfacial arrangement of molecules [37]. Our results indicate that the surface viscosity due to the presence of nanoparticles at the air/water interface is not only a function of the concentration of entrapped SDS but also time. The initial increase in surface viscosity as a function of time, for concentrations above 1 mM in Figure 4.3 (a) is attributed to the initial accumulation of nanoparticles at the interface that causes an increased resistance to shear. The peaks in surface viscosity correspond with the start of the second decrease in surface tension.

This is possibly due to disassociation of the nanoparticles at the interface, which causes a decrease in the resistance to shear. With time, up to two orders of magnitude decrease in the surface viscosity is observed. It is also noted that the final surface viscosity of the system does not correspond to the surface viscosity of a free SDS solution measured at the same concentration, but rather corresponds to the negligible surface shear viscosity of PEI mixture at the same concentration (Figure 4.3 (c)). This suggests that the net concentration of free SDS accumulated at the interface due to dissociation of the nanoparticles is significantly less than the concentration of free SDS required to reach the same saturation concentration. This observation is in direct conflict with surface shear and dilatational rheology measurements of a mixture of oppositely charged polymer-surfactant complex by Monteux et al., who showed the existence of a maximum in elasticity for a polymer-surfactant ratio of 1:1 [38] and the shear moduli were found to be independent of time. This again demonstrates that the behavior of polyelectrolyte-based nanoparticles is significantly different from interfacial properties of polyelectrolyte surfactant mixtures. The difference in the polymer system itself may also contribute to the negligible surface viscosity measured. Additionally, it must also be noted that for the nanoparticle solution containing 1 mM SDS, the surface viscosity is found to be negligible, indicating that not enough nanoparticles are able to accumulate at the interface. This is possibly why a second stage is not observed in this system.

Direct visualization of the interface also provides evidence of disappearance of the nanoparticles with time. Since the surface tension continues to decrease at a constant surface area, this disappearance cannot be attributed to desorption of nanoparticles from the interface, as has been reported recently for ligand-capped gold nanoparticles [39]. Instead, we believe that this can be explained by a disassembly of the self-assembled nanoparticle system into its components that

form a more fluid interface than the adsorbed nanoparticles, as noted in the schematic in Figure 4.7. However, the components are retained close to the interface after dissociation due to interactions between the SDS and the PEI. Desorption of the PEI already present at the interface would lead to an increase in surface tension, which is contradictory to our observation of a further decrease in surface tension. Therefore, these nanoparticles can also be used as a way to deliver hydrophilic polyelectrolytes (or peptides) to hydrophobic interfaces. The lack of change in particle size, charge and viscosity of the bulk system also indicates that this disintegration of the self-assembled nanoparticles is an interfacial phenomenon.

Salt effect: The surface tension measurement has proved the presence of kinetically-trapped nonequilibrium in adsorption layers which experienced two-step process. It has been reported that in the polyelectrolyte/surfactant mixtures, ionic strength has a profound effect on the adsorption kinetics; the addition of salts may result in acceleration of kinetic change in surface properties [40, 41]. Zhang et al. found addition of NaCl and $CaCl_2$ at narrow range of concentrations has similar impact on the surface layer formation by screen the internal interactions between surfactant head groups [41]. However, in our case, the surfactants mostly bind with polyelectrolyte and are shielded from environment, the salt cannot interact directly with surfactant micelles. An alternative explanation for this observation can be as follows: In pure water, the charged nanoparticles experienced two-step adsorption – diffusion from bulk to the surface and surface-induced release; the addition of salt causes increase of ionic strength in the solution, leading to the shielding of electrostatic interactions in the system and reducing the adsorption barrier, consequently, the first diffusion step occurs to fast to be resolved by Wihelmy plate method [40, 42]. Further, it should be noted that $CaCl_2$ has stronger effect on reducing the surface tension than NaCl, although the overall trend of the adsorption with added NaCl and

$CaCl_2$, is broadly similar. This is in agreement with the expectation that at the same salt concentration, the ionic strengths $CaCl_2$ are 3 times higher than NaCl, thus, the shielding effect is more stronger resulting in a larger number of nanoparticles adsorbed on the surface.

4.6 Conclusion

The interfacial behavior of nanoparticles at fluid-fluid interfaces is an interesting area of research that still remains poorly explored. However, in this chapter we have presented how interfacial phenomenon can increase the entropic energy of this system, causing the self-assembled system to undergo dissociation triggered by their adsorption and particle- particle interactions at a hydrophobic interface. This disassembly allows the release of the entrapped surfactant molecule at the interface, demonstrates excellent surfactant-like properties, and also works as a viscosity reducer at the air/water interface. Such kinetic adsorption can be tuned by ionic strength in the solution, addition of salts shields the adsorption barrier for initial diffusion process and help the system reach equilibrium much faster. Therefore, we propose to use such nanoparticle systems for targeted delivery of entrapped molecules at hydrophobic interfaces in a wide range of applications including altering the wettability of porous media for enhanced oil recovery applications in petroleum engineering, or delivery of drugs at the air/water interface in the lung.

References

[1] F. Bresme, M. Oettel, Journal of Physics: Condensed Matter 19 (2007).

[2] P. A. Kralchevsky, K. Nagayama, Advances in Colloid and Interface Science 85 (2000) 145.

[3] V. Garbin, J. C. Crocker, K. J. Stebe, Journal of Colloid and Interface Science 387 (2012) 1.

[4] M. Oettel, S. Dietrich, Langmuir 24 (2008) 1425.

[5] Z. Z. Liao, J. W. Lampe, P. S. Ayyaswamy, D. M. Eckmann, I. J. Dmochowski, Langmuir 27 (2011) 12775.

[6] J. B. He, Z. W. Niu, R. Tangirala, J. Y. Wan, X. Y. Wei, G. Kaur, Q. Wang, G. Jutz, A. Boker, B. Lee, S.V. Pingali, P. Thiyagarajan, T. Emrick, T.P. Russell, Langmuir 25 (2009) 4979.

[7] G. Kaur, J. B. He, J. Xu, S. V. Pingali, G. Jutz, A. Boker, Z. W. Niu, T. Li, D. Rawlinson, T. Emrick, B. Lee, P. Thiyagarajan, T.P. Russell, Q. Wang, Langmuir 25 (2009) 5168.

[8] P. R. Leroueil, S. Hong, A. Mecke, J. R. Baker, B. G. Orr, M. M. Banaszak, Accounts of Chemical Research 40 (2007) 335.

[9] P. Pieranski, Physical Review Letters 45 (1980) 569.

[10] Y. Lin, H. Skaff, T. Emrick, A. D. Dinsmore, T. P. Russell, Science 299 (2003) 226.

[11] T. S. Horozov, B. P. Binks, R. Aveyard, J. H. Clint, Colloids and Surfaces A 282 (2006) 377.

[12] J. R. Heath, C. M. Knobler, D. V. Leff, The Journal of Physical Chemistry B 101 (1997) 189.

[13] J. Faraudo, F. Bresme, The Journal of Chemical Physics 118 (2003) 6518.

[14] N. J. Alvarez, S. L. Anna, T. Saigal, R. D. Tilton, L. M. Walker, Langmuir 28 (2012) 8052.

[15] F. Bresme, N. Quirke, Physical Review Letters 80 (1998) 3791.

[16] K. Vegso, P. Siffalovic, E. Majkova, M. Jergel, M. Benkovicova, T. Kocsis, M. Weis, S. Luby, K. Nygard, O. Konovalov, Langmuir 28 (2012) 10409.

[17] S. M. Hartig, R. R. Greene, J. DasGupta, G. Carlesso, M. M. Dikov, A. Prokop, J. M. Davidson, Pharmaceutical Research 24 (2007) 2353.

[18] J. Penfold, D.J.F. Taylor, R.K. Thomas, I. Tucker, L. J. Thompson, Langmuir 19 (2003) 7740.

[19] J. Penfold, I. Tucker, R. K. Thomas, J. Zhang, Langmuir 21 (2005) 10061.

[20] D.J.F. Taylor, R. K. Thomas, J. D. Hines, K. Humphreys, J. Penfold, Langmuir 18 (2002) 9783.

[21] I. M. Tucker, J. T. Petkov, C. Jones, J. Penfold, R. K. Thomas, S. E. Rogers, A. E. Terry, R. K. Heenan, I. Grillo, Langmuir 28 (2012) 14974.

[22] C. D. Bain, P. M. Claesson, D. Langevin, R. Meszaros, T. Nylander, C. Stubenrauch, S. Titmuss, R. von Klitzing, Advances in Colloid and Interface Science 155 (2010) 32.

[23] H.A. Ritacco, J. Busch, Langmuir 20 (2004) 3648.

[24] P .G. Saffman, M. Delbruck, Proceedings of the National Academy of Sciences USA 72 (1975) 3111.

[25] T. M. Fischer, P. Dhar, P. Heinig, Journal of Fluid Mechanics 558 (2006) 451.

[26] V. Prasad, S. A. Koehler, E. R. Weeks, Physical Review Letters 97 (2006) 176001.

[27] M. H. Lee, D. H. Reich, K. J. Stebe, R. L. Leheny, Langmuir 26 (2010) 2650.

[28] S. Q. Choi, S. Steltenkamp, J. A. Zasadzinski, T. M. Squires, Nature Communications 2 (2011) 312.

[29] P. Dhar, Y. Y. Cao, T. M. Fischer, J. A. Zasadzinski, Physical Review Letters 104 (2010) 016001.

[30] K. Kim, S. Q. Choi, J. A. Zasadzinski, T. M. Squires, Soft Matter 7 (2011) 7782.

[31] F. Ortega, H. Ritacco, R. G. Rubio, Current Opinion in Colloid & Interface 15 (2010) 237.

[32] Y. Gao , L.T. Duc, A. Ali , B. Liang , J. Liang , P. Dhar Langmuir 29 (2013) 3654.

[33] A. Naderi, P. M. Claesson, M. Bergstrom, A. Dedinaite, Colloids and Surfaces A 253 (2005) 83.

[34] J. A. Zasadzinski, T. F. Alig, C. Alonso, J. Bernardino de la Serna, J. Perez-Gil, H.W. Taeusch, Biophysical Journal 89 (2005) 1621.

[35] J. A. Zasadzinski, P. C. Stenger, I. Shieh, P. Dhar, Biochimica et Biophysica Acta 1798 (2010) 801.

[36] K. Pojjak, E. Bertalanits, R. Meszaros, Langmuir 27 (2011) 9139.

[37] G. G. Fuller, J. Vermant, Annual Review of Chemical and Biomolecular Engineering 3 (2012) 519.

[38] C. Monteux, G. G. Fuller, V. Bergeron, Journal of Physical Chemistry B 108 (2004) 16473.

[39] V. Garbin, J. C. Crocker, K. J. Stebe, Langmuir 28 (2012) 1663.

[40] V. V. Lyadinskayaa, R. A. Campbellb, I. Vargac, S. Y. Lind, G. Loglioe, R. Millerf, B.A. Noskova, Colloids and Surfaces A: Physicochemical and Engineering Aspects (2014).

[41] X.L. Zhang, D.J.F Taylor, R.K. Thomas, J. Penfold, Journal of Colloid and Interface Science 356 (2011) 656.

[42] A. A. Mikhailovskaya, B. A. Noskov, S.Y. Lin, G. Loglio, R. Miller, Journal of Physical Chemistry B 115 (2011) 9971.

[43] P. Dhar, T.M. Fischer, Y. Wang, T.E. Mallouk, W.F. Paxton, A. Sen, Nano Letters 6 (2006) 66.

5 Distinctive Adsorption Behaviors of Refined Self-assembled Nanoparticles on Solid Substrates

5.1 Abstract

The adsorption behavior of refined polyethylenimine(PEI)/sodium dodecyl sulfate (SDS) nanoparticle on solid substrates were investigated by means of quartz crystal microbalance with dissipation (QCM-D) and atomic force microscopy(AFM) techniques. In particular, two substrates were used, silicon dioxide (SiO_2) and gold (Au). The results from real-time measurements of frequency and dissipation shifts showed two distinct adsorption behavior: 1) nanoparticle adsorption on two surfaces show distinct trend, the two-step adsorption was only observed on Au; 2) The equilibrium for each measurement were reached after a long time of aging, and at the equilibrium, the adsorption amount on Au was always higher than that on SiO_2. The dissipation change ΔD vs frequency change Δf plots together with rheological properties change calculated from Voigt model revealed differences between Au and SiO_2 in conformation and structure of the adsorbed layer of PEI/SDS nanoparticles during adsorption process. It is found that the nanoparticles were initially built up on the surface without any restructuring on both substrates. During the time of aging, the configuration on Au surface changed significantly and eventually formed relatively rigid and thick film. Such change was also confirmed by AFM images which showed the individual nanoparticles started to formed large aggregates on the surface during the time of aging. In contrast, the adsorbed film on SiO_2 did not have much change during aging. We inferred the different adsorption behavior on Au and SiO_2 was due to the different flexibility of adsorbed layer between neutral charged Au and negatively charged SiO_2. Loosely binding between nanoparticles and Au surface allowed rearrangement and migration of the adsorbed nanoparticles. However, the SiO_2 with negative charge had stronger

electrostatic attraction with the positively charged nanoparticles, leading to tight binding of nanoparticles on the surface, it was then hard for the nanoparticles to rearrange themselves on the surface.

5.2 Introduction

The increasing interest of using polyelectrolyte and oppositely charged surfactant system in extensive applications, such as food related delivery system, flocculation, detergent, oil recovery, corrosion control, water purification, provided a driving force for the fundamental studies of such system. For example, coadsorption of polyelectrolyte and surfactant is used for steel corrosion inhibition [1]. Polyelectrolyte and surfactant attaching to the solid substrates encapsulate nutrients/drugs and release them under different triggers for food delivery (T, pH, I) [2]. The retention of polyelectrolyte and surfactant applied in enhanced oil recovery in porous media may change the wettability of rock surface [3]. Since a lot of these phenomena occurring at liquid/solid interface are determined by the adsorption properties of the polyelectrolyte and surfactant complexes, it is important to have a better understanding about mechanisms of interfacial interaction between polyelectrolyte/surfactant system and the solid substrate so as to gain valuable insight into the interfacial behavior of such system and improve the control for functionalized surfaces.

In contrast to extensive research work on the mixtures of polyelectrolyte and surfactant in bulk solution [4-9], the detailed investigation of the interfacial behavior of such system on liquid/solid interface has not been fully explored even though there still are some data available on this subject [10-13]. Up to now, most of the related studies focused on polyelectrolyte/surfactant mixtures, which contains not only polyelectrolyte/surfactant nanoparticles but also free surfactant or polyelectrolyte. It was found that the polyelectrolyte/ surfactant aggregates could

adsorb on both oppositely and likely charged surfaces [14]. In general, these observations are the consequences of electrostatic and hydrophobic interactions, sometimes the solvency effects also play a role in adsorption of the mixtures [15, 16]. The interaction between polyelectrolyte/surfactant complexes at the liquid-solid interface is strongly influenced by a number of factors: bulk properties of the complexes being adsorbed (charge, size), the environment of the aqueous phase (pH and ionic strength) and the nature of the structural groups on the solid surface (surface charge, hydrophobicity) [15, 17].

For example, it was found that the bulk properties of the polyelectrolyte and surfactant system could affect the interface behavior: the adsorbed mass starts to increase above the critical aggregation concentration (cac) of the surfactant [18, 19] and the maximum surface adsorption is close to the phase separation region (charge neutralization point) [10]. Such behavior show a strong correlation between the bulk properties of the complexes and interfacial properties [18, 20]. Additionally, it is reported that the adsorption of such complexes onto the substrates can be promoted by increasing the surfactant chain length mainly due to the enhanced hydrophobic interactions [21]. When the mixture containing excess surfactant is diluted with water, mass adorbed on the surface may increase due to precipitation of the complexes [15, 18, 22].

On the other hand, ionic strength has strong effects on the adsorption behavior of polyelectrolyte/surfactant complexes by interfering with the interaction between complexes as well as altering the charge density on the substrates. In the first case regarding to the interactions between the adsorbed and adsorbing complexes, Lundin et al [23] found the addition of salt contributes to the reduced electrostatic barrier between the bounding and coming complexes (the complexes which has not bound to but close to the surface) by screening effect, therefore resulting in an increase of adsorption at the solid substrate. In the second case related to the

surface property change, for the hydrophilic silica substrates which contain an oxide layer with silanol groups, the ionization of the surface group increases with pH and ionic strength [24]. At pH value of 3-5, the silica is weakly negatively charged. With increasing pH and ionic strength, the degree of ionization of the silanol groups increases and charge density of silica rises. Researchers have found that decrease of salt concentration lowers the adsorption of polyelectrolyte complexes due to the loss of charge density on silica surfaces [11, 16]. Unlike silica, the nature of gold substrate is more complex. It cannot simply be classified as either hydrophilic or hydrophobic surface. The gold is hydrophilic only in vacuum, whereas under ambient conditions, a trace amount of organics physisorption can turn the surface into hydrophobic permanently [25]. Besides, gold is slightly negatively charged in water at ambient pH and the " image charge effects" can facilitate the adsorption. Such an effect can be explained as follows: the mobility of electrons in the gold is high, resulting in the negatively charges come very close to the charged groups of the adsorbed complexes, therefore sometimes we expect a stronger binding of the charged group to gold than on negatively charged surface (e.g. mica)[26]. Also, the hydrophobicity of the substrates has a great influence on the adsorption of polyelectrolyte and surfactant at the surface. For example, at hydrophobic interface, the mixed polyelectrolyte and surfactant can form a surface layer with surfactant concentration below the critical aggregation concentration (cac), whereas concentration of surfactant above cac are required to form a surface layer at hydrophilic interface [15].

In previous studies, the effect of free components in polyelectrolyte/surfactant mixtures on adsorption of the polyelectrolyte/surfactant nanoparticles has mostly been ignored. However, Muller's group has pointed out that excessive free polyelectrolyte or surfactant in the mixture might keep the charged nanoparticles from adsorption onto the substrate [16, 27]. Therefore,

interfacial behavior of polyelectrolyte/surfactant nanoparticles free of unbound polyelectrolyte and surfactant after centrifugation are expected to be different from polyelectrolyte/surfactant mixtures in previous studies. Inspired by these research, we characterized the adsorption and desorption behavior of PEI/SDS nanoparticle after centrifugation by applying quartz crystal microbalance-dissipation (QCM-D) technique. An advantage of the QCM-D technique is that it cannot only monitor the hydrated adsorbed mass change during adsorption, but also provide us with insight into the viscoelastic behavior of the adsorbed materials [28]. It was found that the conformation and reversibility of the adsorbed layer is similar to other polyelectrolyte and surfactant mixtures, no ordered PEI/SDS complexes form on the surface [29, 30]. To our best knowledge, no research has been done on adsorption of refined PEI/SDS nanoparticles on solid substrates.

The aim of our work are as follows: 1) show the long-term adsorption behavior of pure PEI/SDS nanoparticles on solid substrates (centrifugation is applied to eliminate the interruption from free polycations and small counterions); 2) investigate the influences of surface properties on the adsorption behavior of PEI/SDS nanoparticles, two different substrates are used: gold and silicon dioxide; 3) clarify the salt effects on the adsorption behavior of PEI/SDS nanoparticles on these substrates.

5.3 Experimental

Experimental Protocols: The QCM-D sensors used were gold-Au (QXS 301) and silicon dioxide -SiO_2 (QXS 303) (Biolin Scientific/Q-Sense, Sweden). The different sensor surfaces were cleaned according to standard protocols provided by Biolin Scientific/Q-Sense. The gold sensor surfaces were treated with 99.9% ethanol and sonicated for 10 min. SiO_2 sensors were treated in a solution of 2% sodium dodecyl sulfate (SDS) solution for 30 min at room temperature. All the

sensors were rinsed with Mill-pore water, dried with nitrogen gas and then left in UV chamber for 10 min and used immediately after this glow discharge treatment.

All measurements in this paper were conducted at 25° C. The nanoparticle stock solution was prepared by the same procedure as described in the Reference [31]. Then it was diluted with Millipore water to the desired concentrations. The prepared solutions were stirred with vortex before each test. In order to study the effect of salt on the adsorption of PEI/SDS nanoparticles, the nanoparticle solution were mixed with salt solution to produce nanoparticle solutions with 25 mM of added salts. The pH of solution was controlled at 7. For each set of experiment, the background solution at the same pH was run to establish a horizontal baseline. Afterwards, the nanoparticle solution was pumped at 0.1 mL/min for 15 minutes and then stopped. At the end of each adsorption, the cell was washed with the background solution to determine reversibility of nanoparticle adsorption.

QCM-D Data Analysis: If the adsorbed film is rigid and thin enough, say ΔD is very close to zero ($\Delta D \times 10^6 > 10\ \Delta f$) [32-34]. The adsorbed mass is proportional to the frequency change Δf, which is demonstrated by the Sauerbrey equation:

$$\Delta m = -\frac{C\Delta f}{n} \qquad (5.1)$$

Where the constant C is equal to 17.8 ng cm^{-2} Hz^{-1}, Δ m is the adsorbed mass, n is the overtone number.

If the film is more viscoelastic in which D values are relatively large, the film thickness has to be modeled with Voigt model, which is built-in in the Q Tool software [32-34]. From the modeling data, the values for the film thickness, shear elastic modulus, and shear viscosity can be obtained.

$$\frac{\Delta f}{f} = -\frac{d_s \rho_s}{d_Q \rho_Q}\left[1 - \eta_l \rho_l \frac{(\eta_s/\rho_s)\omega}{\mu_s^2 + \omega^2 \eta_s^2}\right] \qquad (5.2)$$

$$\Delta D = -\frac{1}{d_Q \rho_Q}\left[\eta_l \rho_l \frac{(d_s \mu_s)\omega^2}{\mu_s^2 + \omega^2 \eta_s^2}\right] \quad (5.3)$$

$$G' = \mu \quad (5.4)$$

$$G'' = 2\pi n f \quad (5.5)$$

In these equations, d is thickness, ω is density, and the subscripts Q, s, and l represent quartz crystal, adsorbed film, and bulk solution respectively. The mass sensitivity is about ~1.0 ng/cm^2 [35].

AFM: The conformation change of adsorbed PEI/SDS nanoparticles were measured with tapping mode atomic force microscopy (Nanoscope III, Multimode SPM, Veeco Inc.). Substrates used for the measurements were the same Au and SiO_2 sensors that we used for QCM-D. They were immersed in the PEI/SDS nanoparticle solutions at pH=7 for 2 hours and overnight respectively. Afterwards, the surfaces were washed with Millipore water at the same pH, and dried with nitrogen gas. Antimony doped silicon cantilevers with a resonant frequency of 300 kHz were used for AFM imaging, and the experiments were operated in air at room temperature. For each sample, the images were taken using a scan speed of 0.500 Hz and generated by taking 512 samples per line. Other parameters were adjusted for each image to give the clearest picture. Images were taken at several locations to make sure the typical topology was captured.

5.4 Results

5.4.1 Adsorption kinetics of SDS, PEI solutions on different surfaces

Figure 5.1 includes the raw data from QCM-D measurements in order to illustrate differences in the adsorption between SDS and PEI solutions on Au surface. Figure 5.1 (a) and (b) show the frequency and dissipation changes as a function of time respectively. For SDS, the frequency

decreases instantly as it adsorbs on the substrate, then levels off at a plateau value around - 4 Hz, the adsorption equilibrium is attained within 3-5 min. During the adsorption process, the change in dissipation is about 0.35×10^{-6}. When the SDS solution is replaced by H_2O, the frequency returns back to 0 Hz. In order to look into more details about the adsorption process, we plotted frequency vs dissipation in Figure 5.1 (c). We can see that during the adsorption process, the frequency decreases while dissipation increases, the slope of ΔD vs. Δf is approximately 0.09. During desorption, the curve almost overlaps with adsorption curve.

In contrast, partially positively charged PEI shows a completely different adsorption behavior. First, the adsorption of PEI gives a larger decrease in frequency, and the frequency reaches a stable value at longer time scale than SDS. Second, when the adsorbed PEI is rinsed with H_2O, the frequency shows a slight increase but never returns back to zero even after 2 hour of rinsing. Moreover, the ΔD vs. Δf curve in Figure 5.1(c) for PEI differ largely from that for SDS. The curve for PEI can be separated into three distinguishable regions: In region I, a decrease of 3 Hz in frequency with only 0.2-0.3$\times 10^{-6}$ change in dissipation is observed, the slope for $\Delta D \times 10^6$ vs Δf is about 0.1. Then frequency decreases up to -10 Hz as dissipation increases to 3.2×10^{-6}, the slope of the ΔD vs. Δf curve increases to 0.3 in region II. Eventually the dissipation flattened out whereas frequency continued to decrease in region III.

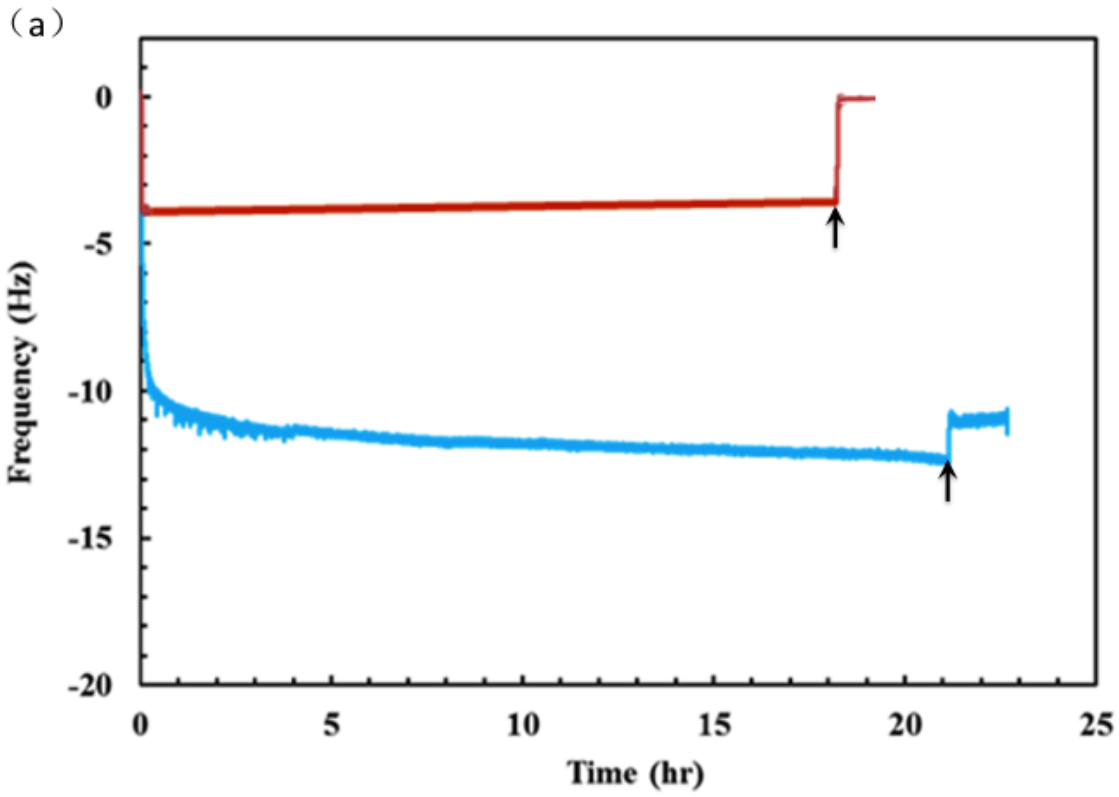
(a)
0
-5
-10
-15
-20
Frequency (Hz)
0
5
10
15
20
25
Time (hr)

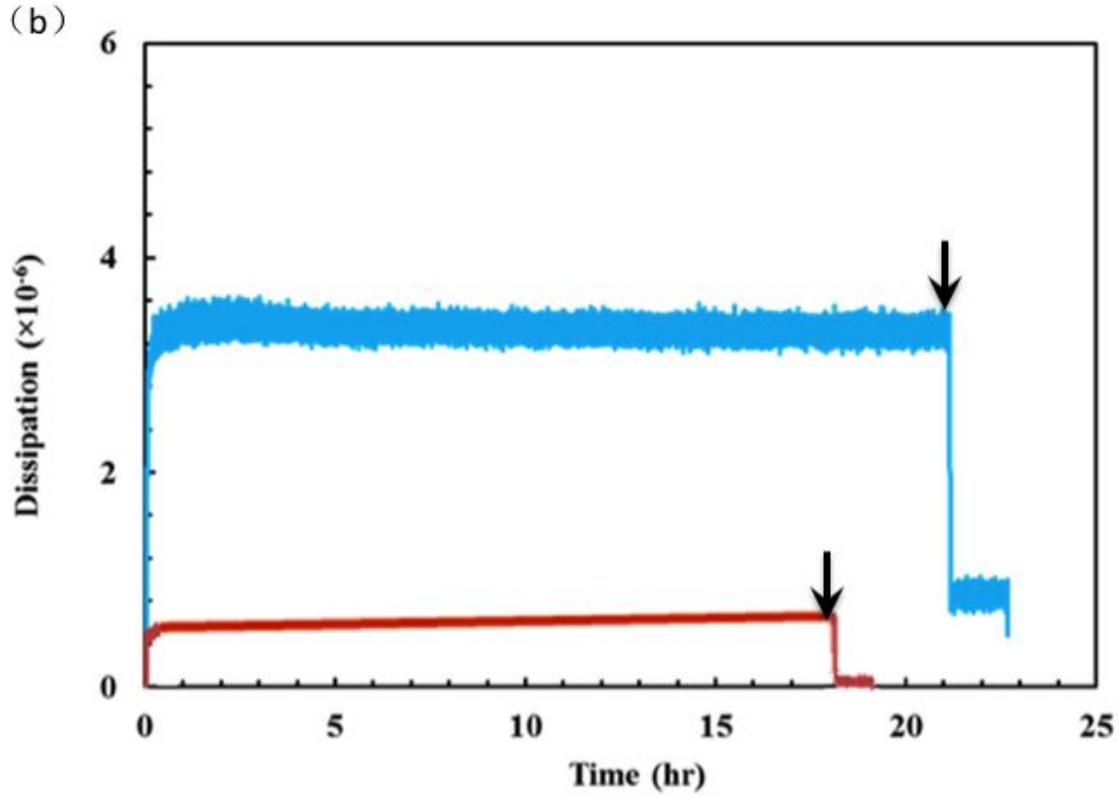
(b)
6
4
2
0
Dissipation (×10-6)
0
5
10
15
20
25
Time (hr)

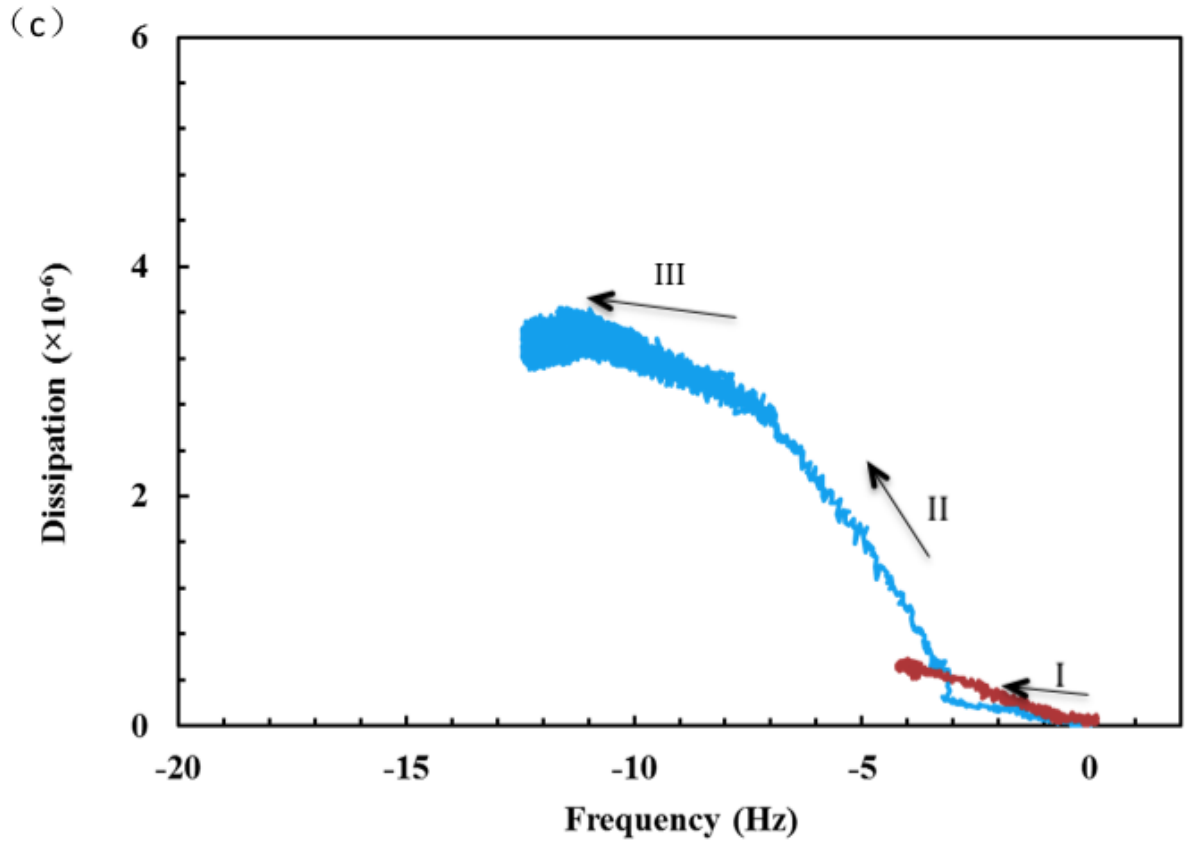

Figure 5.1 QCM-D experimental results for comparison of the adsorption between PEI and SDS on Au surface. a) Frequency change (Δf) vs time b) Dissipation ΔD vs time c) ΔD vs Δf for the 5th overtone. The blue color represents the results for PEI, red color for SDS. The arrows in (a) and (b) indicate the starting point for water rinse. The SDS adsorbed on the surface is more rigid than PEI. PEI requires longer time to reach the equilibrium.

Adsorption kinetics of SDS and PEI on SiO_2 surface is shown in Figure 5.2. When compared to the adsorption on Au, the responses of frequency and dissipation to adsorption of PEI or SDS solutions on SiO_2 surface are slightly different. For SDS solution, during adsorption, the frequency shift becomes smaller on SiO_2 than that on Au, and almost no change in dissipation is observed on SiO_2. For PEI solution, the frequency change is more on SiO_2 than that on Au, and the changes in dissipation is about 4×10^{-6}. During desorption, SDS is readily removed from the SiO_2 surface, but small change in frequency for PEI is observed by subsequent rinsing with H_2O.

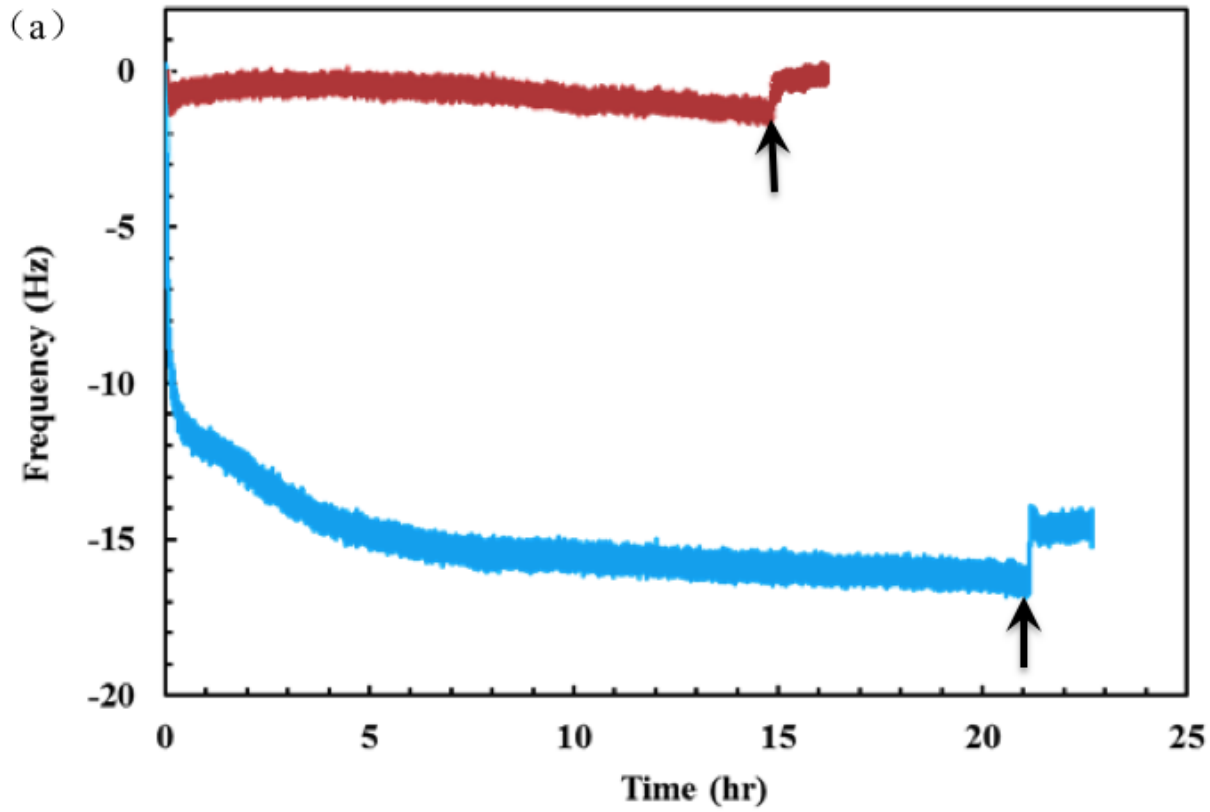
(a)
0
-5
-10
-15
-20
Frequency (Hz)
0
5
10
15
20
25
Time (hr)

（b）

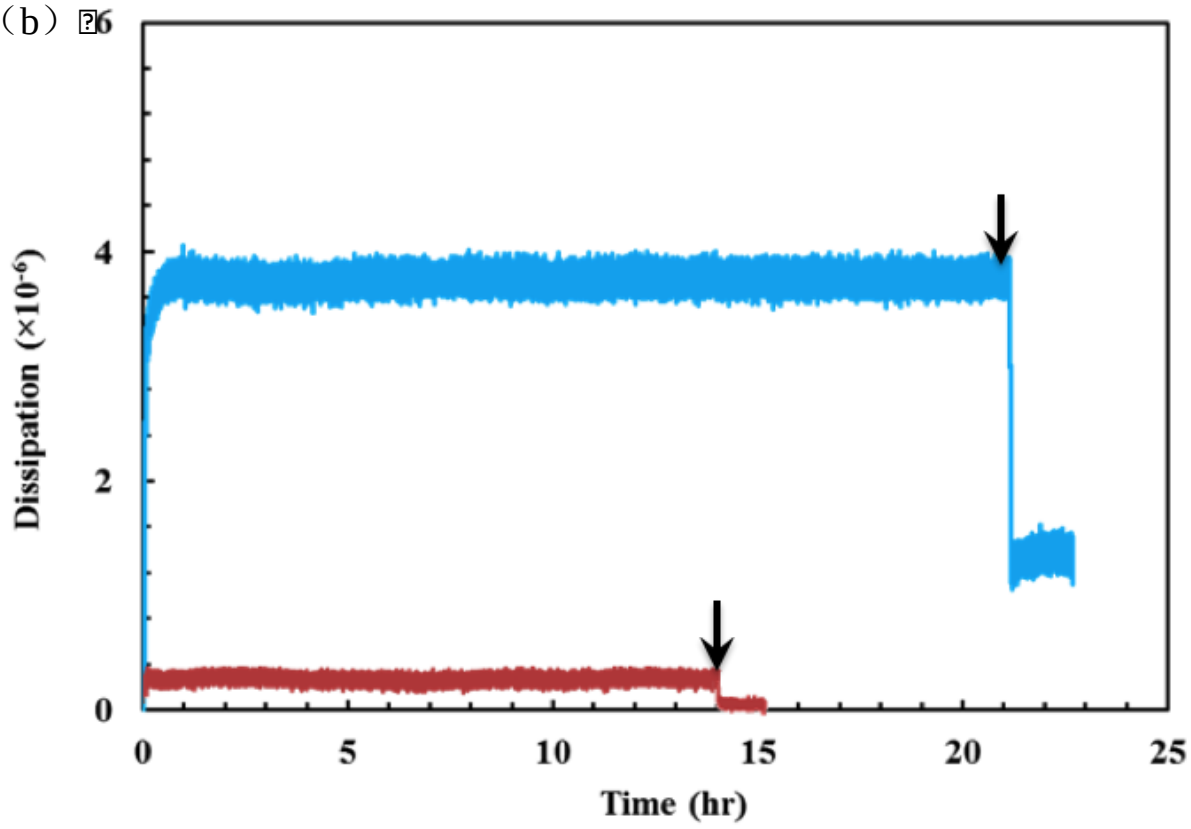
Dissipation (×10-6)
0
2
4
0
5
10
15
20
25
Time (hr)

(c)

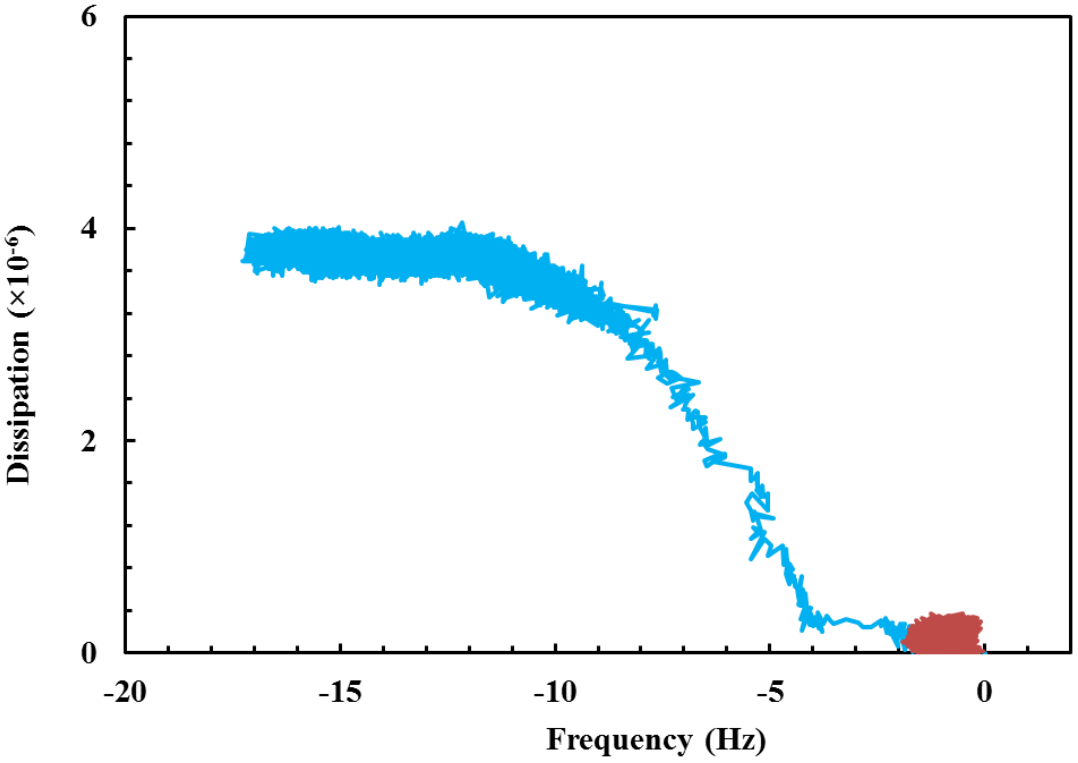
Dissipation (×10-6)
0
2
4
6
-20
-15
-10
-5
0
Frequency (Hz)

Figure 5.2 QCM-D experimental results for comparison of the adsorption between PEI and SDS on SiO_2 surface. a) Frequency change (Δf) vs time b) Dissipation changes (ΔD) vs time c) ΔD vs Δf for the 5th overtone. The blue color represents the results for PEI, red color for SDS. The arrows in (a) and (b) indicate the starting point for water rinse. SDS has no adsorption on SiO_2, whereas PEI has more adsorption on SiO_2

5.4.2 Sauerbrey equation and Voigt model of adsorbed SDS and PEI

We calculated adsorbed mass for both SDS and PEI on different surfaces by both Voigt model and Sauerbrey equation with the fifth overtone (25 MHz). The results of adsorbed mass for both SDS and PEI on different surfaces are shown in Table 1. We find that the Sauerbrey equation gives a very good estimate for SDS whereas the adsorbed layers formed by PEI does not follow the Sauerbrey equation. The change of dissipation for SDS is very small during adsorption/desorption. Additionally, the differences in frequency and dissipation after being normalized with different overtones are negligible. Therefore it is reasonable to calculate the adsorbed SDS with Equation (5.1). However, the dissipation change for PEI is relatively large and the differences of frequency at different overtones are significant, the adsorbed PEI cannot be taken as a simple elastic rigid layer, the viscoelasticity needs to be considered. In Table 1, the mass of SDS adsorbed on Au surfaces is about 0.14 mg/m^2 and it is negligible on SiO_2. For PEI, the adsorbed mass is 20 mg/m^2 on Au and 17.5 SiO_2 mg/m^2 respectively. If we assume the density of adsorbed layer is $1g/cm^3$, the corresponding thickness of PEI is about 20 nm on Au and 17.5 nm on SiO_2.

Table 5.1 Adsorbed mass and thickness of PEI and SDS on Au and SiO_2 surfaces

	Au		SiO_2	
	Mass (mg/m^2)	AFM Thickness (nm)	Mass (mg/m^2)	AFM Thickness (nm)
3.8 mM SDS	0.14	-	0.03	-
2000 ppmPEI	17.5	-	20.0	-
3.8 mM NP (short term)	42.5	15	47.5	15
3.8 mM NP	55	28	37.0	18

(long term)				

5.4.3 Adsorption kinetics of PEI/SDS nanoparticle on different surfaces

Figure 5.3 (a) and (b) show the dynamic frequency and dissipation changes induced by adsorption PEI/SDS nanoparticles on Au. Adsorption results of the PEI and SDS solution on Au are also included as a reference. When compared to the frequency change for pure SDS or PEI solution, a significant increase of frequency for adsorbed nanoparticles is observed. Moreover, the PEI/SDS nanoparticles exhibit a complicated two-stage adsorption behavior, similar to PEI solution. The frequency decreases rapidly to the first plateau, then followed by a slower secondary decrease. At the same time, no dissipation change is observed with further decrease of frequency. The stable value of Δf at each plateau depends on the bulk concentration and the equilibrium of adsorption is reached in a shorter time at higher nanoparticle concentration. After dilution with H_2O for approximate 2 hours, only a small amount of adsorbed materials are removed.

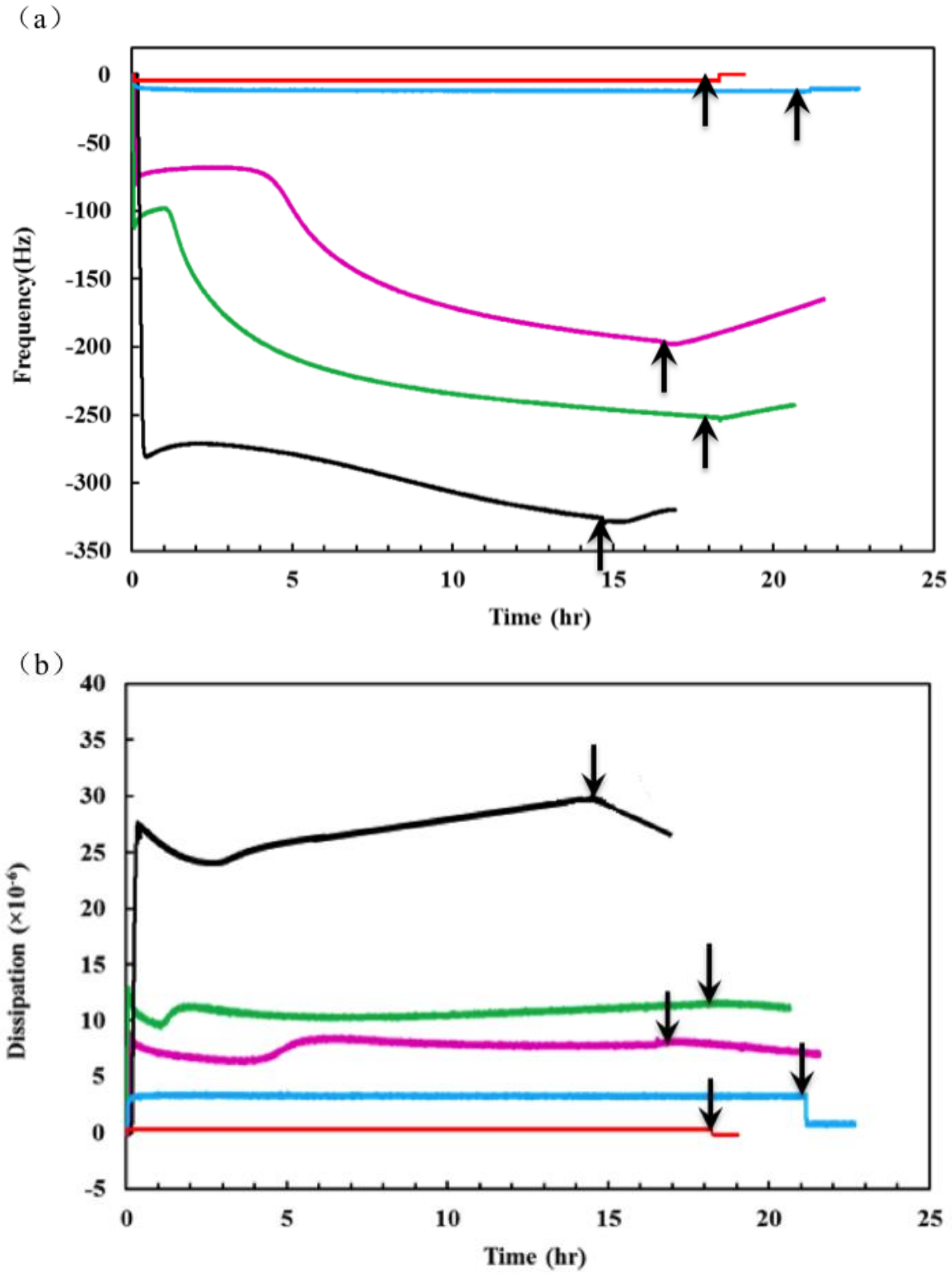

Figure 5.3 QCM-D experimental results for the adsorption of PEI/SDS nanoparticle on Au surface. The data of PEI and SDS solution are included as references. The blue color represents the results for PEI, red color for SDS, violet color for 1.4 mM SDS in PEI/SDS nanoparticle, green color for 3.8 mM SDS in the nanoparticle, black for 6 mM SDS in the nanoparticles. The arrows in (a) and (b) indicate the starting

point for water rinse. a) Frequency change (Δf) vs time b) Dissipation change (ΔD) vs time for the 5th overtone. Obviously, the two-step adsorption is observed on Au surface as an indication of complicated adsorption kinetics. The plateau value for Δf decreases with increase of SDS concentration

Figure 5.4 (a) and (b) show the frequency and dissipation variation upon adsorption of nanoparticle solution on SiO_2 as a function of time. We observed different patterns of adsorption behavior on SiO_2 from that on Au. The two-stage adsorption disappeared on SiO_2; instead, the adsorption of nanoparticle on SiO_2 begins with a sharp decrease in the frequency shift accompanied with a large maximum in the dissipation, followed by slow relaxation on the surface. Again, the adsorption of nanoparticles increases with bulk concentration of nanoparticles.

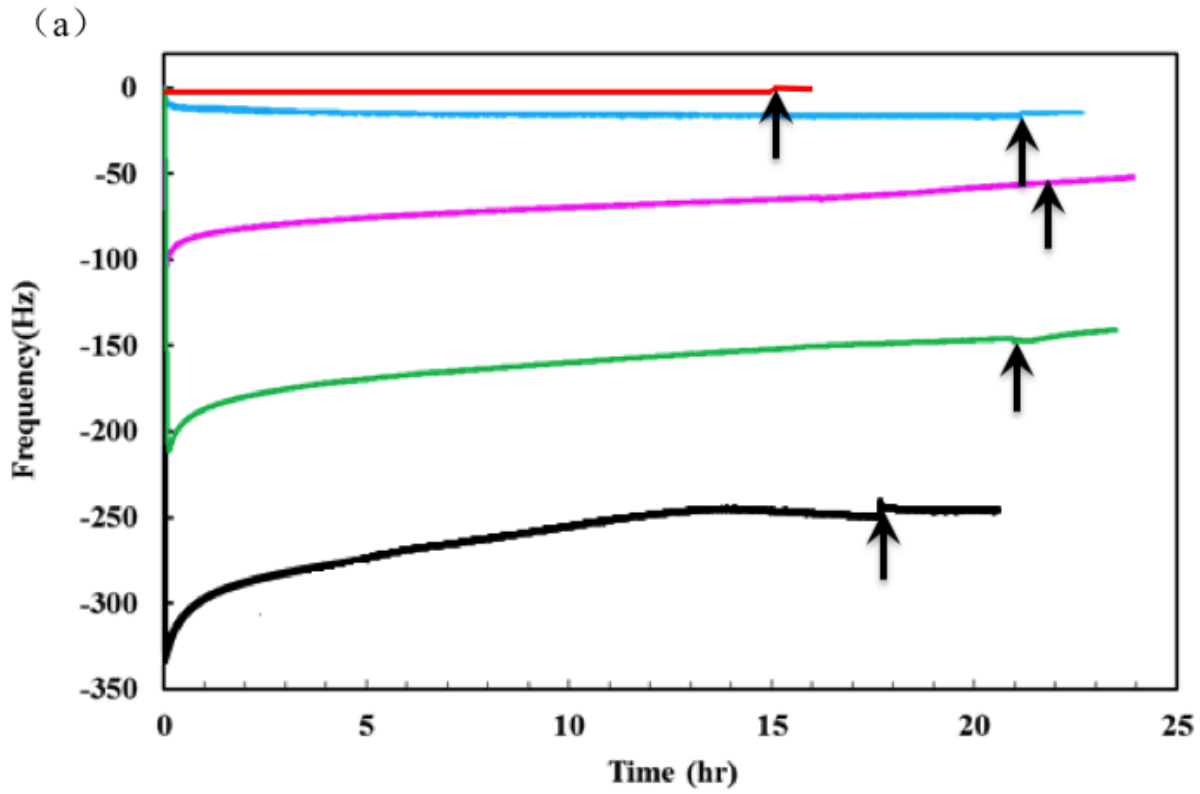

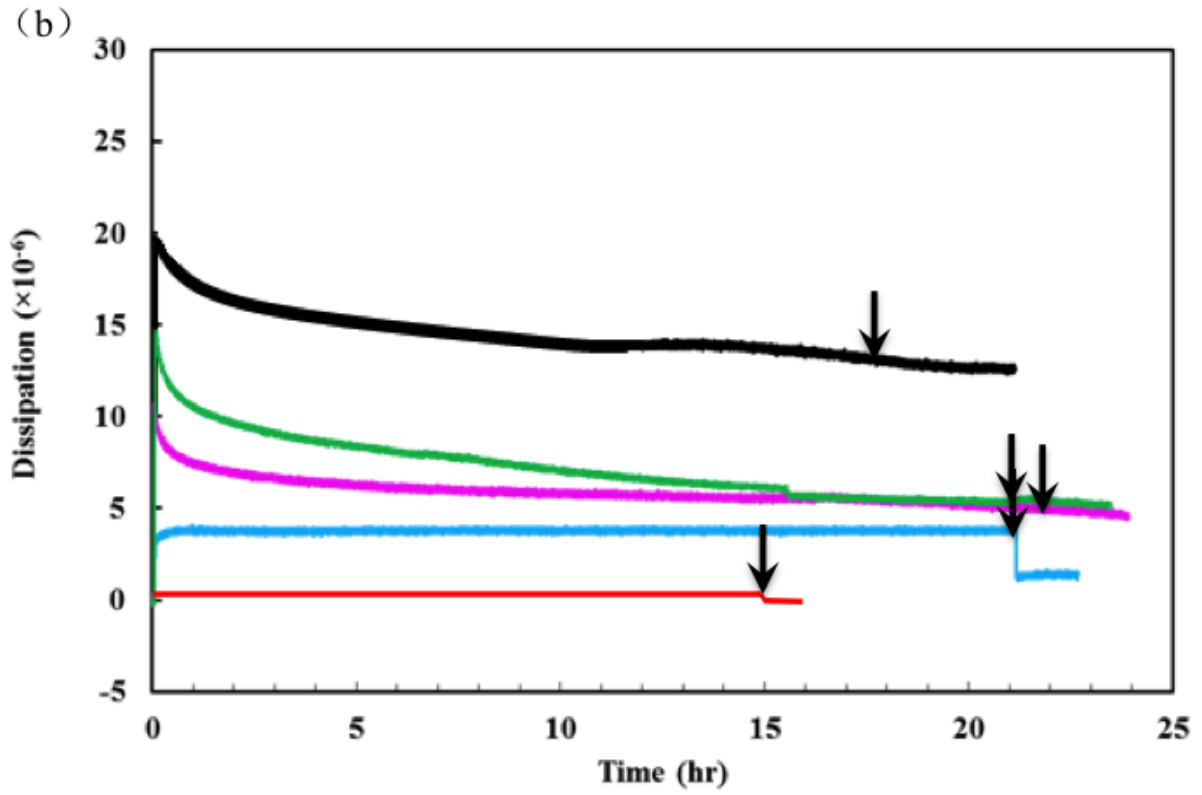

Figure 5.4 QCM-D experimental results for the adsorption of PEI/SDS nanoparticle on SiO_2 surface. The data of PEI and SDS solution are included as references. The blue color represents the results for PEI, red color for SDS, violet color for 1.4 mM SDS in PEI/SDS nanoparticle, green color for 3.8 mM SDS in the nanoparticle, black for 6 mM SDS in the nanoparticles. The arrows in (a) and (b) indicate the starting point for water rinse. a) Frequency change Δf vs. time b) Dissipation change ΔD vs. time for the 5th overtone. A clear plateau during PEI/SDS nanoparticle adsorption is observed on SiO_2 surface suggesting a completely difference adsorption mechanism on SiO_2 from Au surface.

In order to further characterize the formation of adsorbed layer and compare the differences in adsorption behavior between Au and SiO_2, the dissipation change vs. frequency change is plotted in Figure 5.5 and the curve for the PEI/SDS nanoparticle at 3.8 mM is chosen as an example. The curve for SiO_2 can be simply divided into two regions, labeled as 1' and 2'. In region 1', Δf drops almost linearly from 0 to -200 Hz with ΔD from 0 to 14×10^{-6}. Then the curve reverts its direction in region 2', an increase of Δf as well as a decrease of ΔD is observed. At shorter times (<2 hours), similar trend is observed on Au in region 1 and 2, but with time, the direction of curve continues to change; eventually it reaches a plateau in which the Δf continues to decrease while the dissipation levels off in region 3. Moreover, the relaxation represented by the change

from region 1' to 2' on SiO_2 is larger than that from region 1 to 2 on Au. We collect the slope of ΔD vs Δf curve for different concentrations at region 1 on Au, region 1' on SiO_2, and compare its value with that in region 3 on Au as well as region 2' on SiO_2 in Table 2. It is found that as the adsorption continues, the $\Delta D/\Delta f$ ratio decreases on Au surface while no change is seen on SiO_2. When compared with the slope of $\Delta D/\Delta f$ for PEI, the values for nanoparticles on both surfaces are smaller.

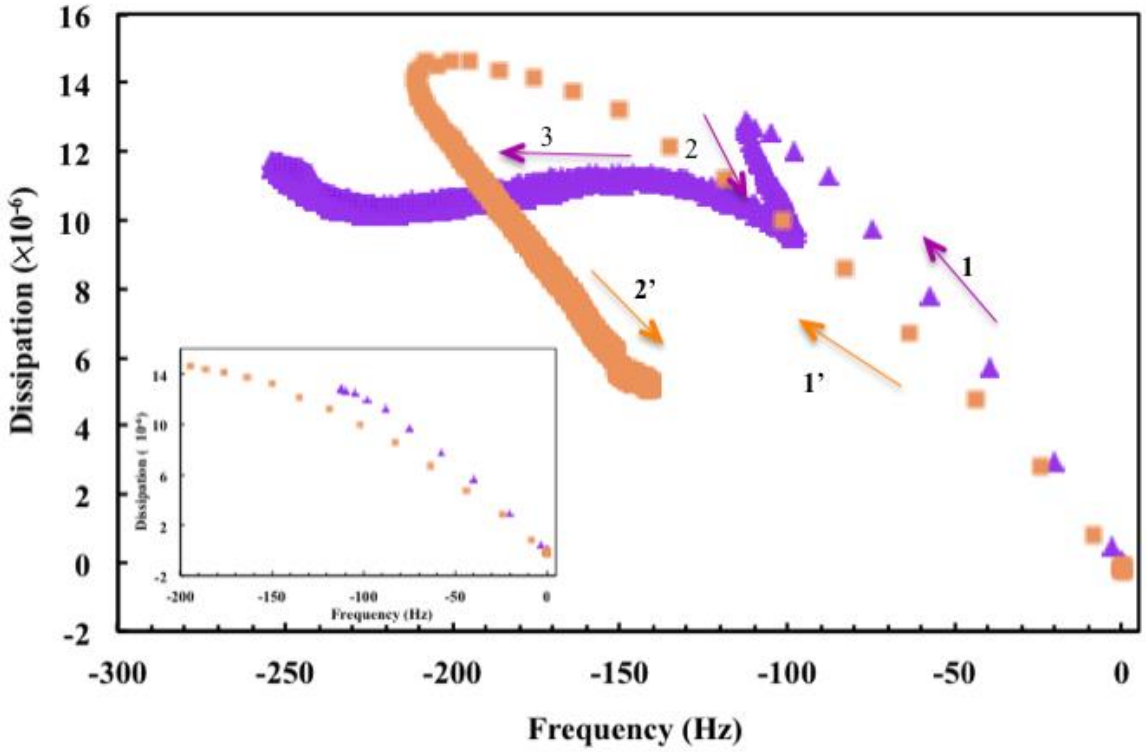

Figure 5.5 Comparison of dissipation ΔD vs. frequency Δf curves for PEI/SDS nanoparticles between Au and SiO_2 surfaces at 3.8 mM SDS concentration. Purple curve is the result on Au, orange curve is on SiO_2 Number on the curves represent different regions during adsorption. The inset shows the plot of the ΔD vs. Δf curves at shorter time (within 10 minutes).

Table 5.2 Comparison of $\Delta D/\ \Delta f$ for PEI, PEI/SDS nanoparticles on Au and SiO_2 surfaces between first plateau and second plateau

	Au		SiO_2	
$\Delta D/\ \Delta f$	Region 1	Region 3	Region 1'	Region 2'
PEI	0.27		0.23	
1.4 mM	0.08	0.04	0.07	0.062
3.8 mM	0.10	0.05	0.056	0.053
6 mM	0.07	0.09	0.055	0.052

5.4.4 Voigt modeling of adsorbed PEI/SDS nanoparticles

The measured data of Δf and ΔD at different overtones ranging from 3rd to 11th were fitted using the Voigt model. By using this model, we calculated the thickness as well as the viscoelastic properties (viscosity, shear modulus) of the adsorbed films. The viscoelastic properties together with the thickness data allow us to have a better understanding of the different adsorption behavior on two different surfaces. Figure 5.6 (a–c) compare adsorbed mass of the PEI/SDS nanoparticles between SiO_2 and Au surfaces at three different concentrations (1.4 mM, 3.8 mM and 6 mM). The thickness change corresponding to the adsorbed mass is given in Figure 5.7. The viscosity and shear moduli obtained from the modeling at the early stage (1-2hr after injection of nanoparticle solution) and at the end of adsorption (approximately 20- 22 hr after injection of nanoparticle solution) are compared in Figure 5.9 and 5.10. In Figure 5.6 and 5.7, we can see that the trend of mass adsorption and thickness change are quite similar on both surfaces at the early times of adsorption. However, at the end of adsorption, for each of the sensors, the nanoparticles attained larger amount of adsorbed mass and thickness on Au surface when compared to SiO_2 surface. As seen in Figure 5.8, this discrepancy between these two surfaces becomes stronger as the concentration increases. Also, significant differences of shear moduli and viscosity between the initial and second stage were found on Au but not on SiO_2.

（a）

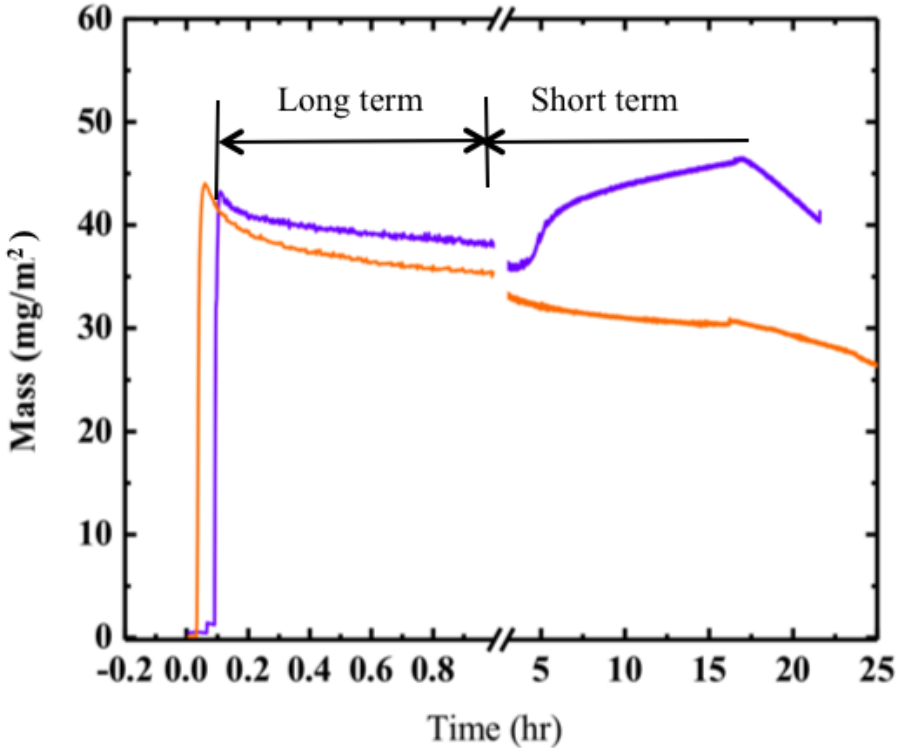
Long term
Short term
Mass (mg/m^2)
Time (hr)
60
50
40
30
20
10
0
-0.2 0.0 0.2 0.4 0.6 0.8
5
10
15
20
25

（b）

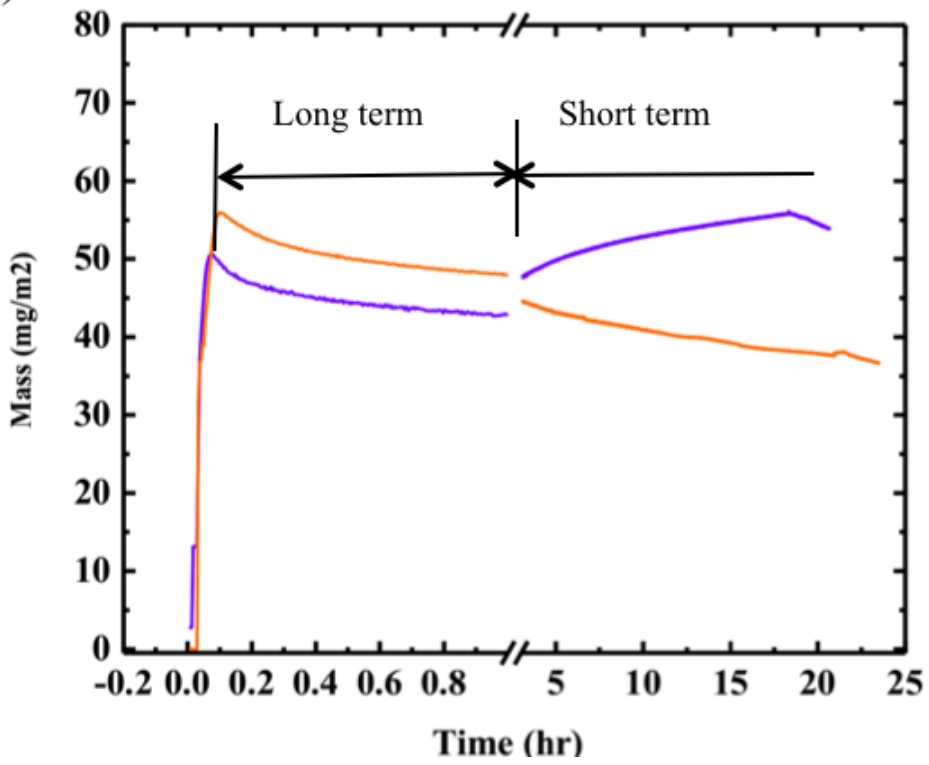
Long term
Short term
Mass (mg/m2)
Time (hr)
80
70
60
50
40
30
20
10
0
-0.2 0.0 0.2 0.4 0.6 0.8
5
10
15
20
25

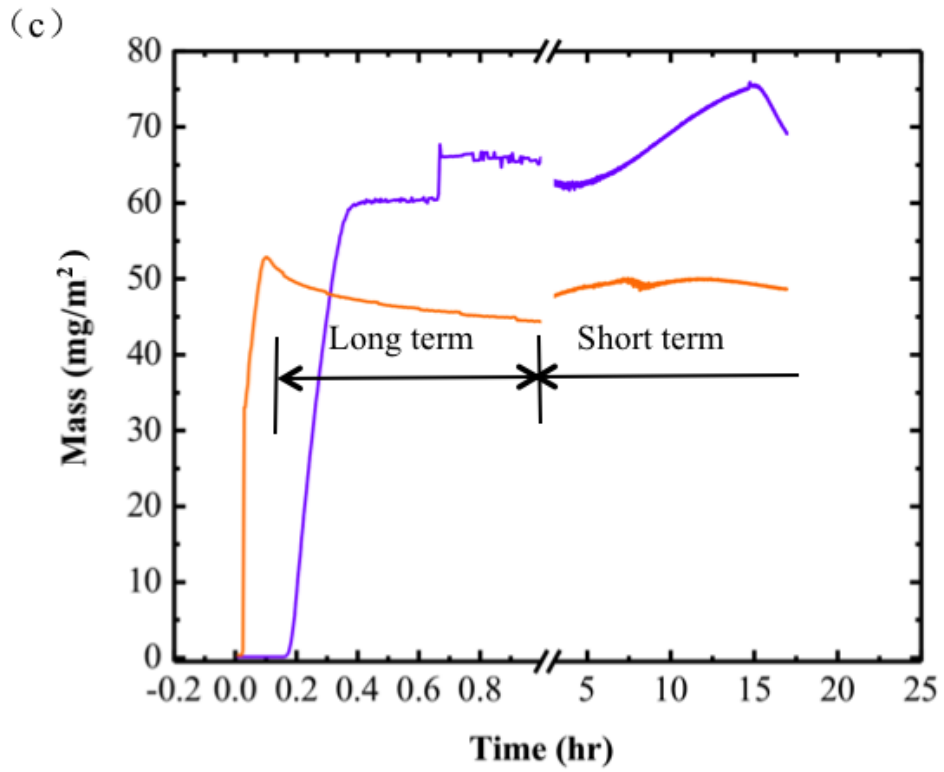

Figure 5.6 Comparison of Voigt modeling results of the adsorbed mass between Au and SiO_2 surface at different nanoparticle concentrations. a) 1.4 mM b) 3.8 mM c) 6 mM. The purple color represent the results on Au, the orange color is on SiO_2. In the first 1-2 hrs of adsorption, the mass is quite close on both surfaces. After long time of aging, the adsorbed mass on Au eventually exceeds that on SiO_2

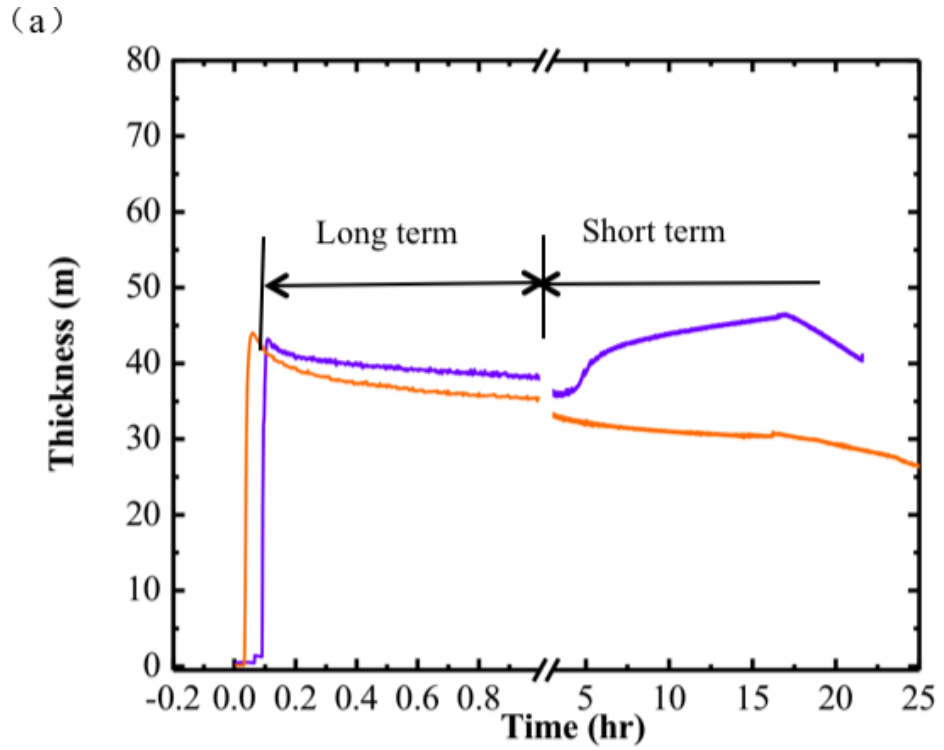

（b）

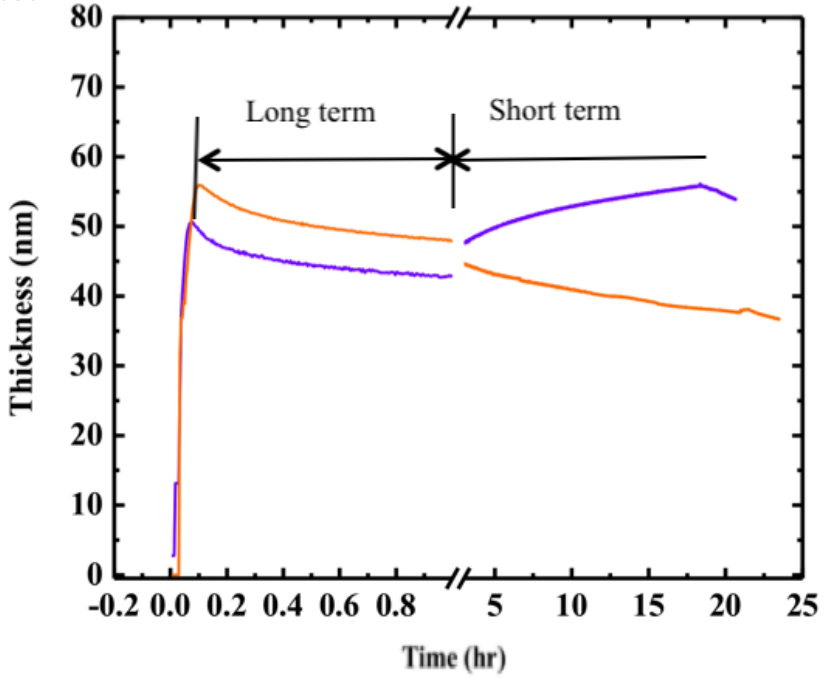
Long term
Short term
Thickness (nm)
Time (hr)
80
70
60
50
40
30
20
10
0
-0.2 0.0 0.2 0.4 0.6 0.8
5
10
15
20
25

（c）

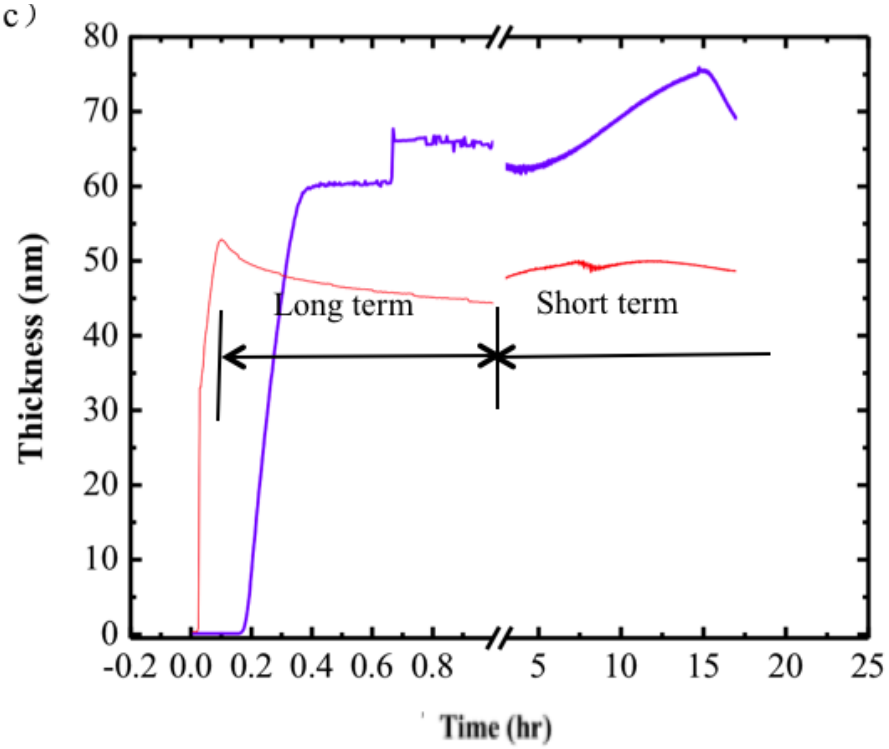
Long term
Short term
Thickness (nm)
Time (hr)
80
70
60
50
40
30
20
10
0
-0.2 0.0 0.2 0.4 0.6 0.8
5
10
15
20
25

Figure 5.7 Comparison of Voigt modeling results of the thickness of adsorbed layer between Au and SiO_2 surface at different nanoparticle concentrations. a) 1.4 mM b) 3.8 mM c) 6 mM. The purple color represent the results on Au, the orange color is on SiO_2. In the first 1-2 hrs of adsorption, the mass is quite close on both surfaces. After long time of aging, the adsorbed mass on Au eventually exceeds that on SiO_2

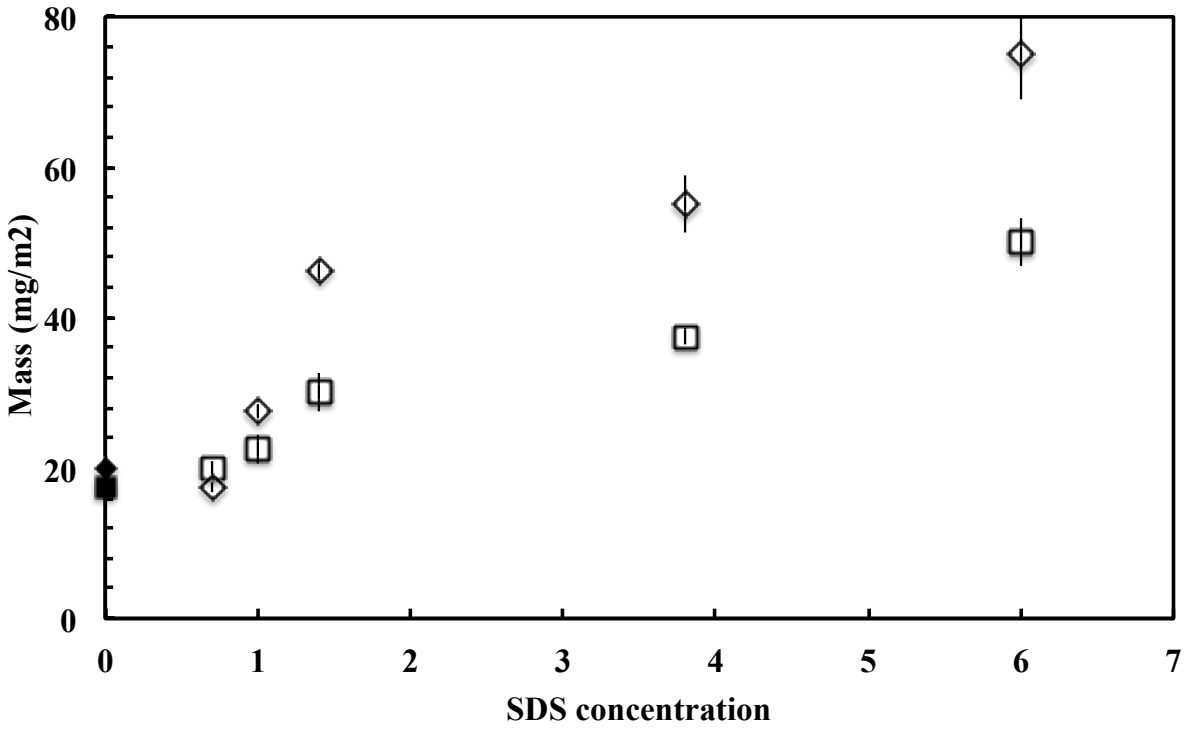

Figure 5.8 Comparison of adsorption isotherms for PEI/SDS nanoparticle onto different surface: Au ◇ vs. SiO_2 ■ . ◆ is the adsorbed mass of PEI on Au, ■ is the adsorbed mass of PEI on SiO_2. The adsorbed mass increases with SDS concentration; the amount of adsorbed mass is always larger than that on SiO2, and such difference becomes more significant with increase of SDS concentration.

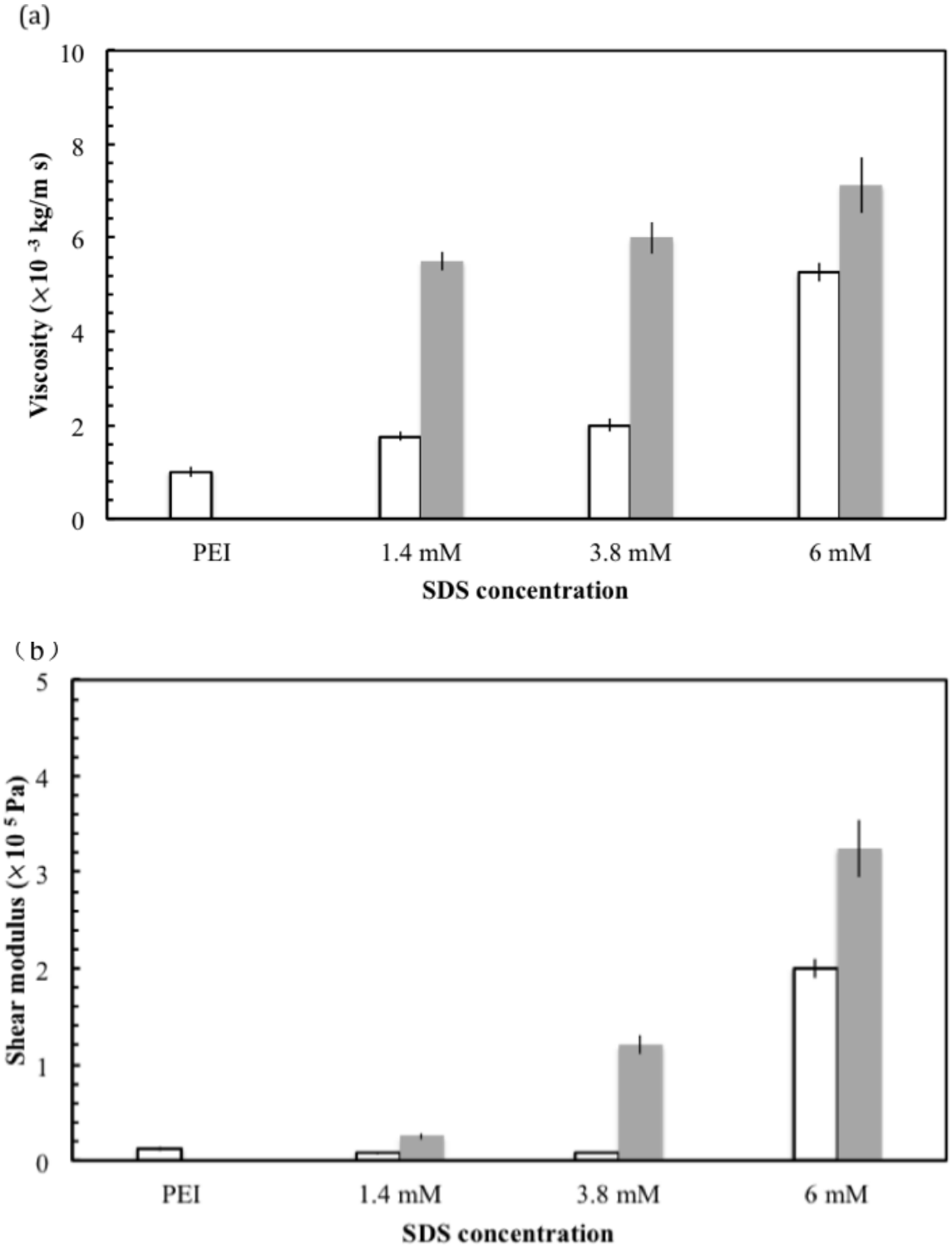

Figure 5.9 Results of viscoelastic properties from Voigt modeling for the adsorbed PEI/SDS nanoparticles on Au, (a) shear viscosity (b) shear modulus. The white columns represent the data after 1-2 hours adsorption, the grey columns represent the data after 20-22 hours of aging. The results show the nanoparticles have higher values of shear viscosity and shear modulus when comparing to PEI. After a long time of aging, both shear viscosity and shear modulus increase indicating a more rigid layer is formed

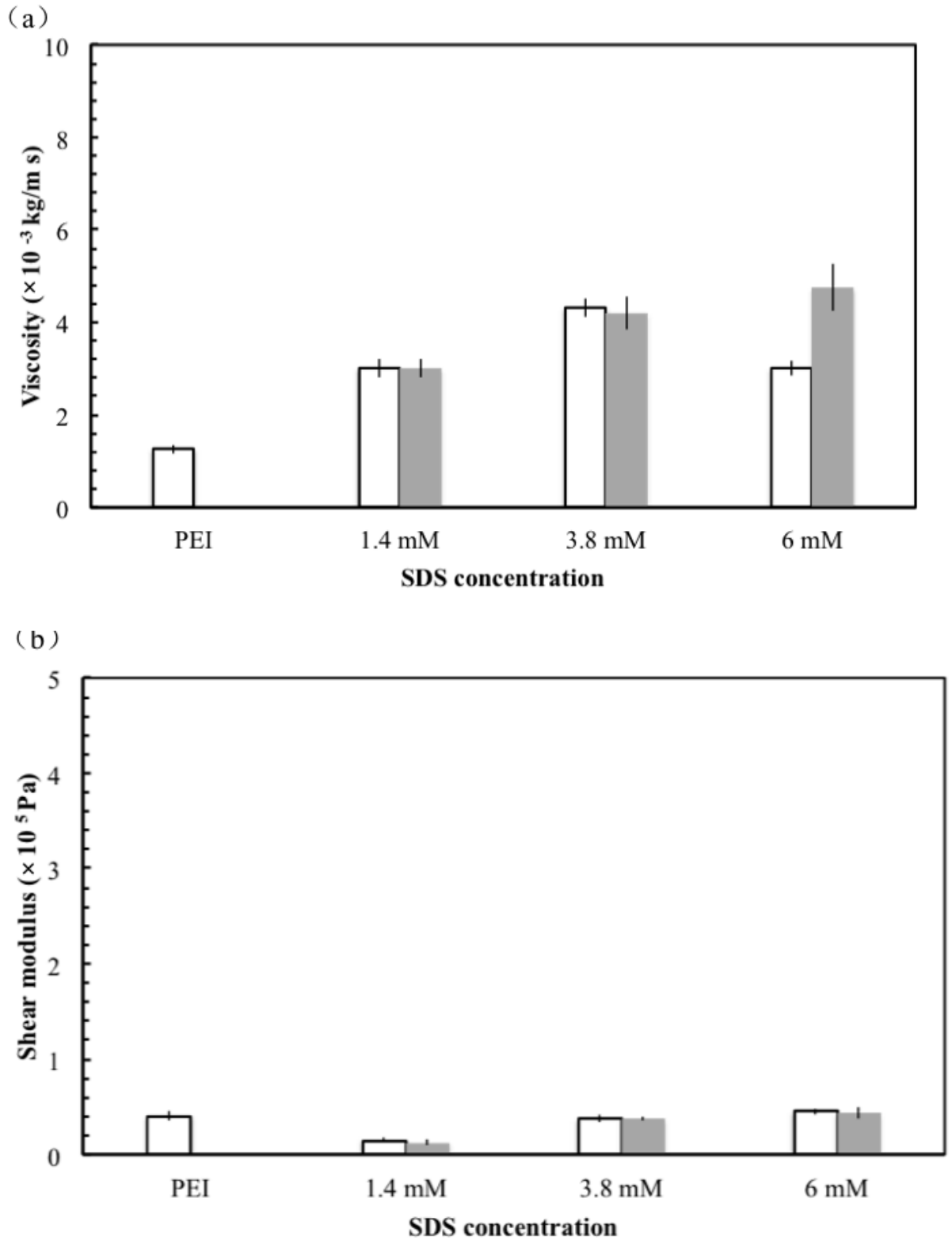

Figure 5.10 Results of viscoelastic properties from Voigt modeling for the adsorbed PEI/SDS nanoparticles on SiO_2, (a) shear viscosity (b) and shear modulus. The white columns represent the data after 1-2 hours adsorption, the grey columns represents the data after 20-22 hours of aging. The results show that the nanoparticles have higher values of shear viscosity than PEI, but the values of shear

modulus are either less (1.4 mM) or comparable (>1.4 mM) with that of PEI. After a long time of aging, both shear viscosity and shear modulus show little changes indicating surface layer does not change much at tow different time scales.

5.4.5 AFM imaging of PEI/SDS nanoparticles on Au and SiO_2

In order to further identify the phenomenon of adsorption of PEI/SDS nanoparticle on the different surface, the conformations of the adsorbed layer was monitored with AFM in Figure 5.11. Figure 5.11 (a) and (b) show AFM images of adsorbed layer on Au after the gold surface was kept in PEI/SDS nanoparticle solution for 1 hour, or overnight respectively. Figure 5.11 (c) and (d) provide the images during same time interval on SiO_2. In a shorter time, we observe some bright spherical spots on both surfaces, the average size of these dots are about 100-140 nm. The height of adsorbed PEI/SDS nanoparticles was only 15-25 nm. The configuration of film formed on Au is completely different from that on SiO_2 after a longer time of adsorption. The nanoparticles on Au may dissociate leading to significant configuration change and more adsorption whereas the nanoparticles on SiO_2 at low concentration on the surface remained scattered.

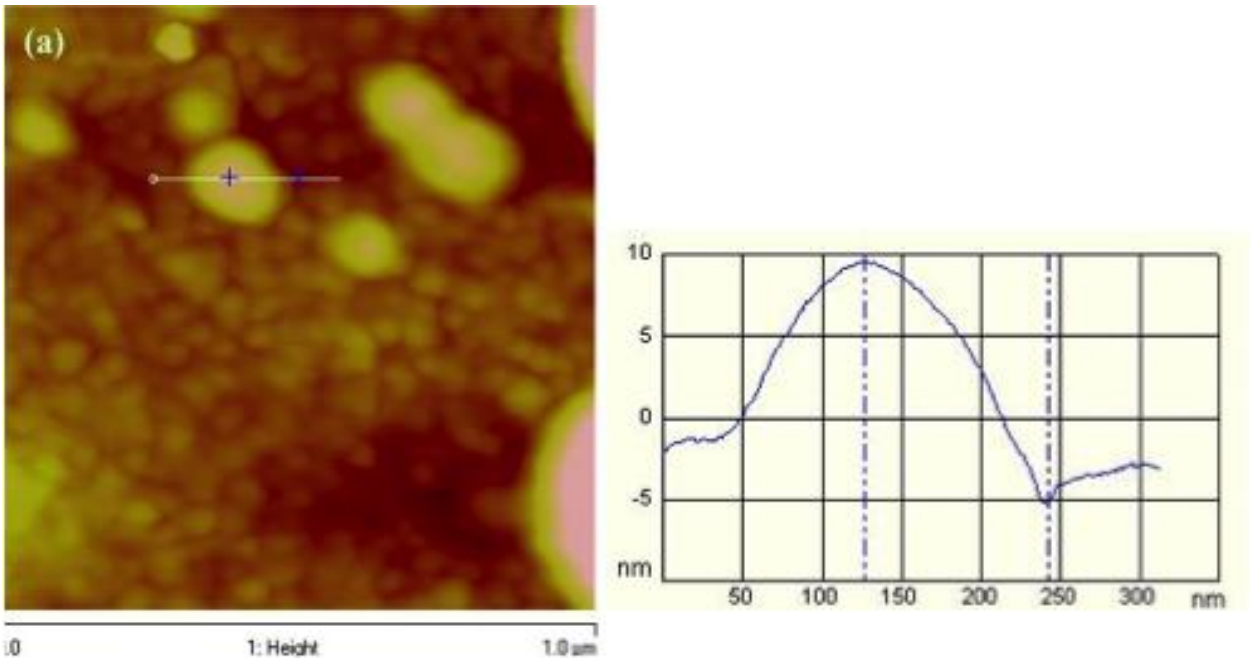

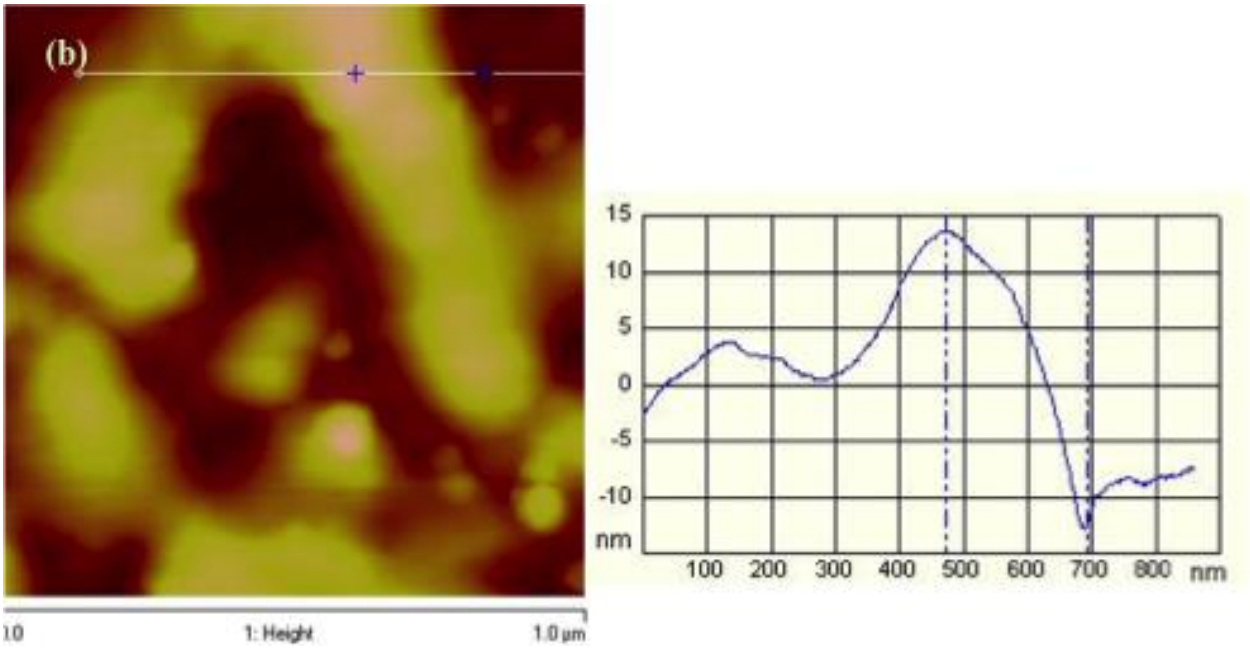
(b)
15
10
5
0
-5
-10
nm
100 200 300 400 500 600 700 800 nm
1: Height
1.0 µm

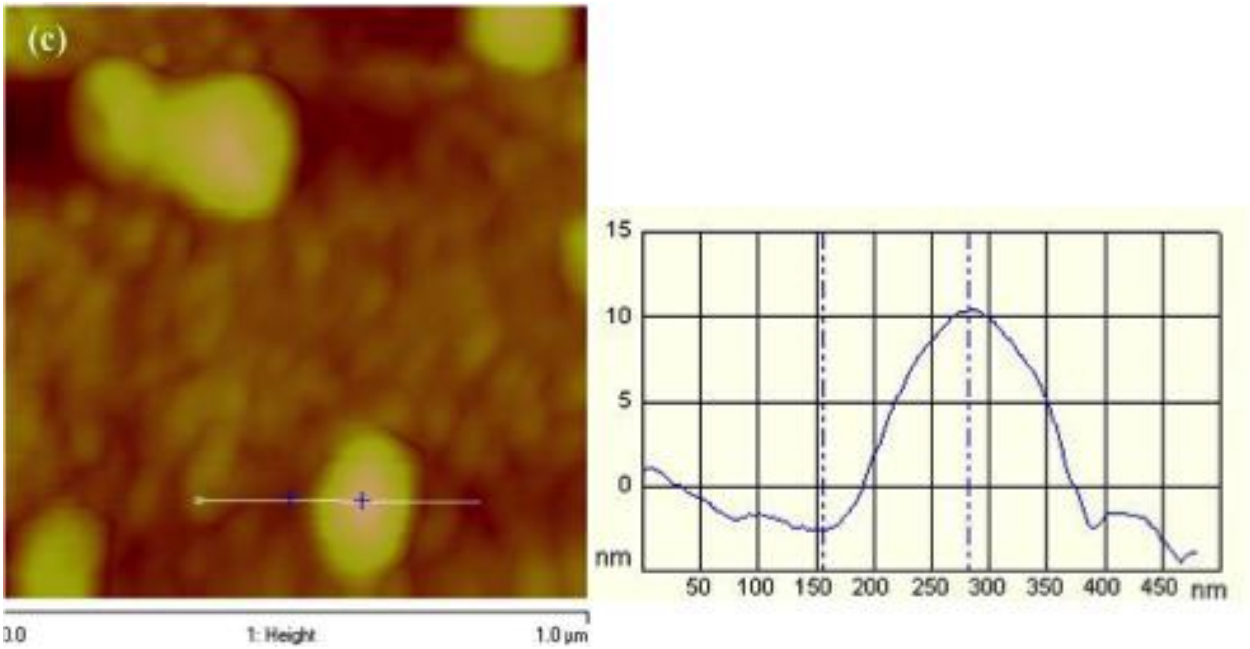
(c)
15
10
5
0
nm
50 100 150 200 250 300 350 400 450 nm
1: Height
1.0 µm

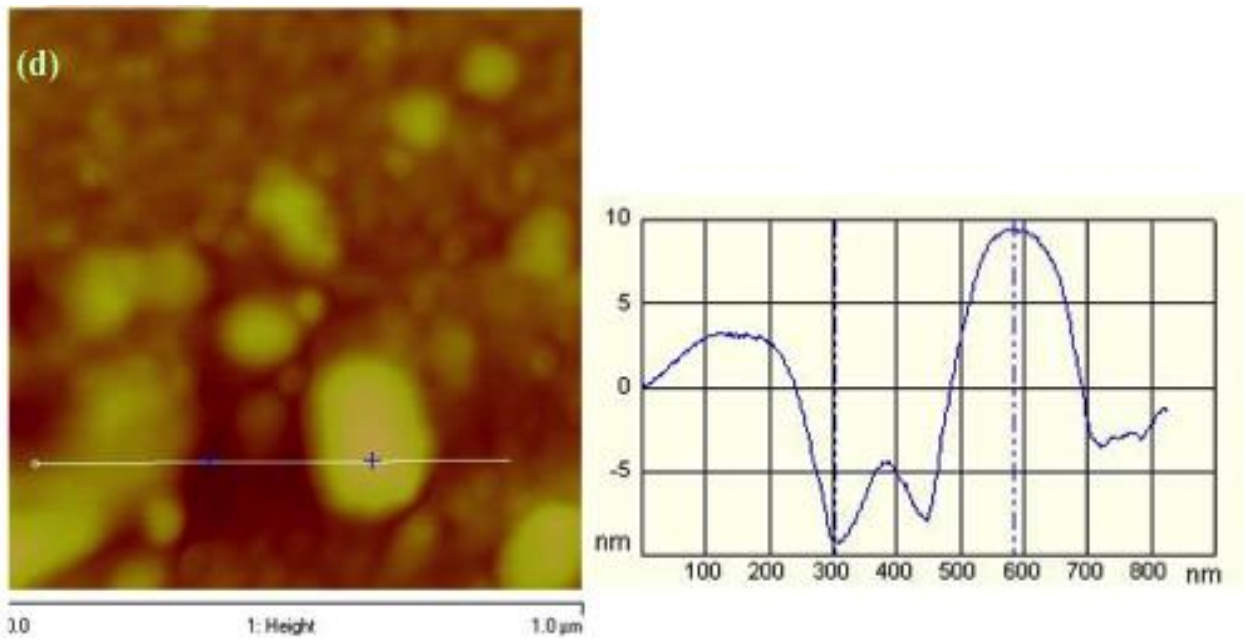

Figure 5.11 AFM images of PEI/SDS nanoparticle adsorption on Au (a) and (b), silicon oxide surfaces (c) and (d) after different time of adsorption (a and c: 1-2 hr; b and d: 20-22 hr(overnight)). The white spots on the images showed a maxium height around 25-30 nm. The separated spherical spots in a, c and d are the individual nanoparticles which have an average size of 100-150 nm. The irregular-shaped aggregates in b indicate more adsorption probably due to dissociation of the nanoparticles on Au surface. The location of the height profiles are shown in the height images on the right side

5.4.6 Effect of salts

Figure 5.12 shows an example of adsorption kinetics of nanoparticle with added salt. The adsorbed mass at final equilibrium for different SDS concentrations is listed in Table 5.3. The results show that the adsorption of PEI/SDS nanoparticles is strongly affected by the addition of salts. First, the added salts completely changed adsorption pattern on Au surface and the two-stage adsorption on Au surface is not observed anymore. Moreover, we observe the PEI/SDS nanoparticles in 25 mM NaCl yield adsorbed mass of 45mg/m^2 and 57 mg/cm^2 at 1 mM and 1.4 mM SDS concentration respectively. In 25 mM $CaCl_2$, the adsorbed amount increases to 53 ng/cm^2 at 1 mM SDS concentration and 63 mg/m^2 at 1.4 mM. When compared with the adsorption results without salts, it is found that the adsorption from PEI/SDS is significantly enhanced by addition of salts. On SiO_2 surface, the added salts do not change the adsorption

pattern but increase the mass adsorption on the surface. In addition, when the cells are flushed with salt solution, desorption of adsorbed nanoparticles is hardly observed.

Table 5.3 Adsorbed mass of 1.4 mM nanoparticle in presence of NaCl or $CaCl_2$ on Au and SiO_2 surface, the results are also compare with NP without salts at the same concentration

	Au		SiO_2	
	Mass (mg/m^2)	Thickness (nm)	Mass (mg/m^2)	Thickness (nm)
1 mM NP	27.3	27.3	23.85	23.85
1 mM NP+ 25 mM NaCl	45.0	45.0	-	-
1 mM NP+ 25 mM $CaCl_2$	53.25	53.25	40.0	40
1.4 mM NP	45.03		30.64	45
1.4 mM NP+ 25 mM NaCl	57.2	57.2	-	-
1.4mMNP+ 25 mM $CaCl_2$	63.86	63.86	45	45

（a）

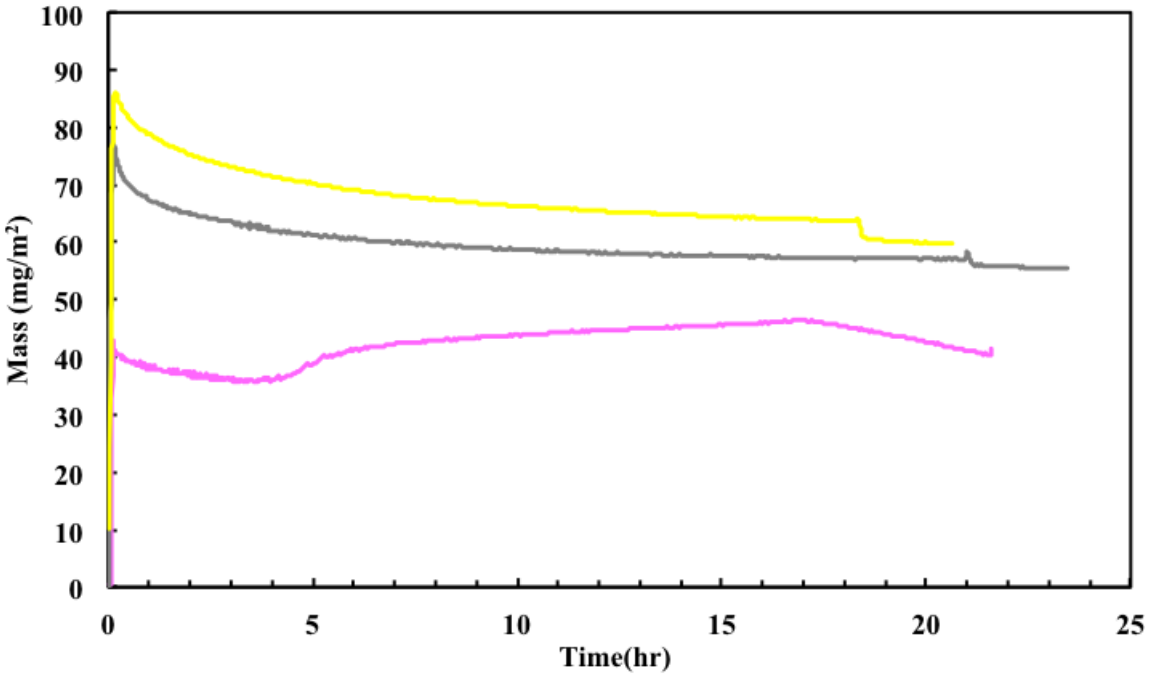

（b）

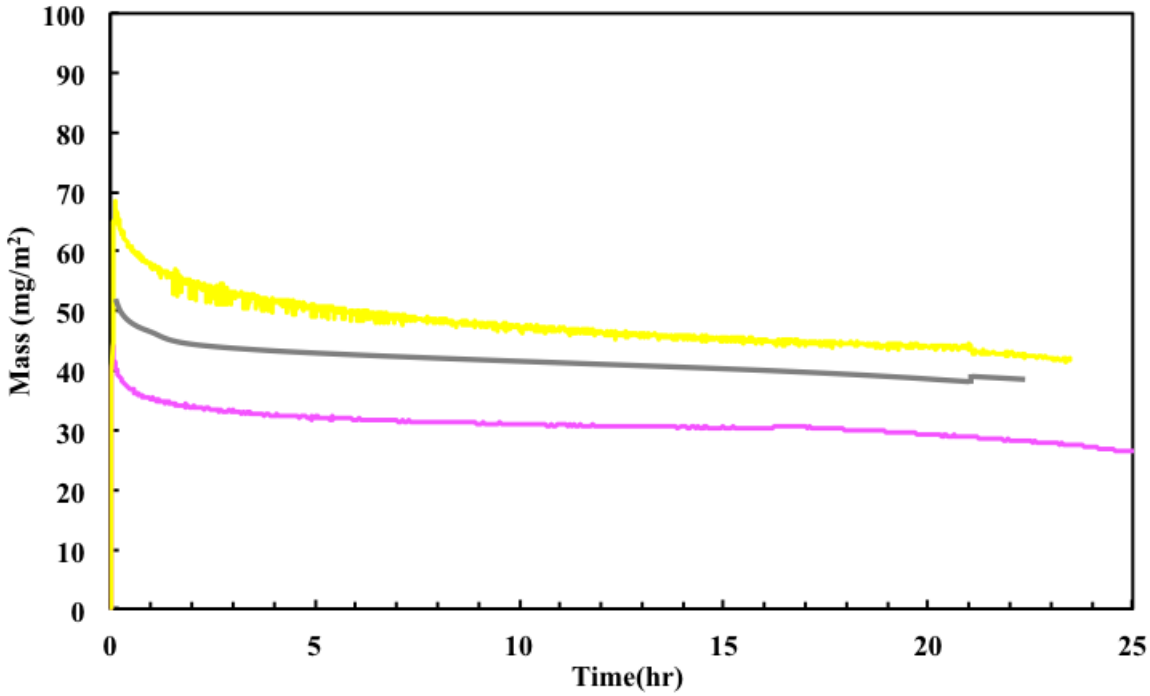

Figure 5.12 Adsorbed mass of 1.4 mM nanoparticle in presence of NaCl or $CaCl_2$ on a) Au and b) SiO_2 surface, violet curve is for 1.4 mM nanoparticles in absence of salts; grey curve is for 1.4 mM nanoparticles in 25 mM NaCl solution; yellow curve is for 1.4 mM nanoparticles in 25 mM $CaCl_2$ solution

5.5 Discussion

Comparison between PEI and SDS adsorption on different surfaces: PEI and SDS adsorption on both Au and SiO_2 surfaces are given as a reference for further comparison with adsorbed PEI/SDS nanoparticles. From Figure 5.1, we can see that both surfactant and polyelectrolyte have interactions with the gold surface. For SDS, the adsorption of such small molecules reaches equilibrium rapidly and the relaxation at the surface is on a time scale of minutes. The overlap of adsorption and desorption in ΔD vs Δf curve suggested that the adsorption is noncooperative and reversible as expected. A comparison of adsorption kinetics for PEI and SDS is clearly shown in Figure 5.1 (a) and (b). The adsorption equilibrium for PEI reaches more slowly than SDS. Such slow adsorption can be interpreted by the convective-diffusion process from the bulk to the surface as follows:1) the diffusion rate for polymer is usually one or two order of

magnitude lower than small surfactant molecules; therefore the adsorption is mostly limited by the transport from bulk to the surface; 2) Further adsorption of incoming polymer from the solution may be hindered or retarded by steric hindrance and electrostatic barrier created by the adsorbed large molecules [11, 36]. In Figure 5.1 (c), we find more detailed information about adsorption of PEI independent of aging time. Very little change of dissipation is observed until the frequency reaches - 4 Hz, indicating that a flat and rigid conformation forms initially. From this point, the dissipation increases proportionally to the decrease of frequency as a result of buildup of polymer layer via growth in thickness without conformation change [36]. When the ΔD reaches 4×10^{-6}, there is no more change in dissipation with increasing amount of PEI adsorption, this might be caused by a densification or conformational rearrangement of the polymer molecules that arrives at the interface at the later stage of adsorption or departure of water molecules from the adsorbed layer [36]. This result is consistent with previous observations on polyelectrolyte adsorption on gold surfaces [37].

On SiO_2 surface, SDS hardly absorbs on the surface whereas PEI adsorbs to a greater extent than SDS. The adsorption behavior for SDS is consistent with the fact that SDS does not adsorb on the surface of same charge due to the long-range electrostatic repulsion. Contrarily, positively charged PEI possesses considerable charge density at pH=7, the driving force for PEI adsorption on SiO_2 surfaces is attributed to both electrostatic attraction and hydrogen bonding [24]. The combination of these two interactions results in the strong adsorption of PEI on SiO_2. Moreover, the ratio between ΔD and Δf provides qualitative information on the viscoelasticity of the adsorbed layer. The lower ratio represents a stiffer film whereas a higher ratio indicates a more viscoelastic film [34]. When comparing ΔD vs Δf curve for between PEI and SDS on both Au and SiO_2 (Figure 5.1(c) and Figure 5.2(c)), we can see that SDS form a more rigid layer than

PEI. In addition, no decease of adsorbed PEI on SiO_2 is observed when the adsorbed film is washed with H_2O. This suggested that PEI is irreversibly adsorbed onto the negatively charged surface.

PEI/SDS nanoparticle adsorption on different surfaces: In Figure 5.3 and Figure 5.4, when compared to the adsorption of PEI and SDS on both Au and SiO_2 surfaces, the PEI/SDS nanoparticles have more adsorption than PEI; this can be explained by the fact that the nanoparticle complexes are dominant in the adsorption onto the surface. Due to their large dimension, a larger amount of nanoparticles are adsorbed whereas the structure is more compact than PEI as a result of smaller ratio of ΔD vs Δf [16]. We also find that the adsorption increases with the bulk concentration. This occurs when there is enough space for the nanoparticle to adsorb, the adsorption rate rises as a result of diffusion controlled adsorption [38]. Moreover, we noted that extremely long time is required for the PEI/SDS nanoparticles to reach their adsorption plateaus. On Au surface, the frequency continues to decrease and experiences two-step change indicating the overtaking of mass over the long-term aging. Contrarily, slight increase of Δf is observed on SiO_2 during the time of aging suggesting that there is mass loss on the surface. During desorption, the nanoparticle cannot be completely removed by H_2O and the desorption rates increased linearly with the bulk concentration. Such results indicate that the surface binding sites are limited, increase of bulk concentration causes more excess aggregates that may reside above saturated layer but are not tightly bound to it, then a loose multilayer of aggregates is easily rinsed off [19].

When we compare the curves of ΔD vs. Δf between Au and SiO_2 in Figure 5.5, the slopes of the curves are similar in the first region and the initial directions of the curves in both cases are pointing towards northwest, indicating an increase of mass. Then in the second region, they both

revert the directions towards southeast. Such phenomena can be explained as follows: 1) continuous adsorption of nanoparticles without restructuring and loosely packing onto the free space of the surfaces may contribute to the increase of adsorbed mass. Although we assume that the nanoparticles are initially adsorbed intact on the surface, the calculated thickness of the adsorbed layer in Figure 5.7 at the early time of adsorption is less than the hydrodynamic size of nanoparticles in bulk solution (130-150 nm [31]). Such inconsistency is further confirmed by the height measured by AFM images (see Figure 5.11). This may be attributed to the fact that the nanoparticles deformed and lost their shape when adsorbing on the solid substrates. Indeed, the shape of adsorbed nanoparticles was no long the same as that in the bulk solution. 2) After the curves switch the directions, the reorganization or restructuring of the adsorbed layer begins. Bingen et al. [39] and Keller et al. [40] both proposed that nanometer-sized particles (e.g. vesicles or protein) pack closely at the surface, the area occupied by the water surrounding the nanoparticles overlaps, resulting in lost of coupled water, this explains the decreases in both adsorbed mass and viscoelasticity. The similarity of the adsorption between Au and SiO_2 at the initial stage is further confirmed in terms of viscosity and shear modulus. When looking into viscoelastic analysis between Au and SiO_2 at early stage in Figure 5.9 and 5.10, we can see the results on both surfaces are quite comparable.

Important features of two-stage adsorption on Au shown in Figure 5.3 are also illustrated in Figure 5.5. Instead of terminating in region 2 like on SiO_2, the ΔD vs Δf curve for Au continues to extend. The adsorbed mass together with the viscoelasticity properties is compared between early time and longer times of adsorption in Figure 5.6, 5.7 and 5.9, 5.10. We noted that on Au surface, the adsorbed film has higher values of thickness, viscosity and shear modulus after longer time of adsorption. These observation suggest an increase of adsorption and stiffer

layers on Au at the second stage of adsorption probably due to configuration change of adsorbed nanoparticles at Au surface [34]. The AFM images in Figure 5.11 (a) and (b) also provide the evidence of evolution of the adsorbed layer on Au surface during the long-time aging. The nanoparticles start adsorbing on separated spots and eventually form large and irregular structure on the surface. However, the thickness together with viscosity and shear modulus for the adsorbed layer shows little change on SiO_2 during the long term of aging. In addition, the conformation of nanoparticles on SiO_2 does not change with time. These observations suggest different features of kinetic adsorption of nanoparticle between Au and SiO_2. Similar two-step adsorption is observed by Hodges et al. [19]. They studied the adsorption of the polyelectrolyte/surfactant complexes onto negatively charged silica surface. By combining the data from QCM and optical reflectometer, they claimed the two-step adsorption was a result of bulk properties instead of densification on the surface. More specifically, the free cations adsorbed on the surface initially and reversed the charge of surface at the first step, followed by further adsorption of polyelectrolyte/surfactant aggregates at the second step. However, in our system, there is no free surfactant or polyelectrolyte. Furthermore, the two-step adsorption is observed on Au not on SiO_2. Due to different bulk and surface properties of our system from Hodges' study, the mechanism of two-step adsorption for our system may be different from Hodges's system.

In order to find reasonable explanation for different surface-induced rearrangement of nanoparticles on these two surfaces, we performed two other experiments. Based on previous discussion about the surface properties of Au, it can be hydrophobic if slight amount of organics is adsorbed onto it. If the two-step adsorption were only attributed to the hydrophobicity of the Au surface, we would expect similar behavior on hydrophobic surface−polystyrene regardless of

the surface charge. However, such two-step adsorption is not seen on the polystyrene. We also tested the same nanoparticle solution on positively charged surface-$CaCO_3$. The two-step adsorption is not shown on $CaCO_3$ either and the adsorbed mass is even lower than that on SiO_2 (Figure 5.13). Based on these experimental results, we assume that the large change of thickness and viscoelasticity of adsorbed film on Au surface during long time experiment may be caused by dissociation of nanoparticles on the surface. The positively charged nanoparticles initially bind loosely to the neutral charged Au substrate. In the long-term measurement, the nanoparticles may dissemble at the surface after first stage of adsorption and induce multilayer adsorption. This hypothesis is evidenced by the increase of absorbed mass/thickness and decrease of viscoelasticity due to loss of coupled water during nanoparticle dissociation. For SiO_2, the particles are more tightly bound onto the surface because of negative charge on SiO_2, resulting in stronger electrostatic interaction of the nanoparticle with the surface and less mobility of the particles. Therefore, The particles do not experience much conformation change but a slow relaxation during the experiment. Besides, the viscoelastic properties do not change much in the cases of SiO_2.

(a)

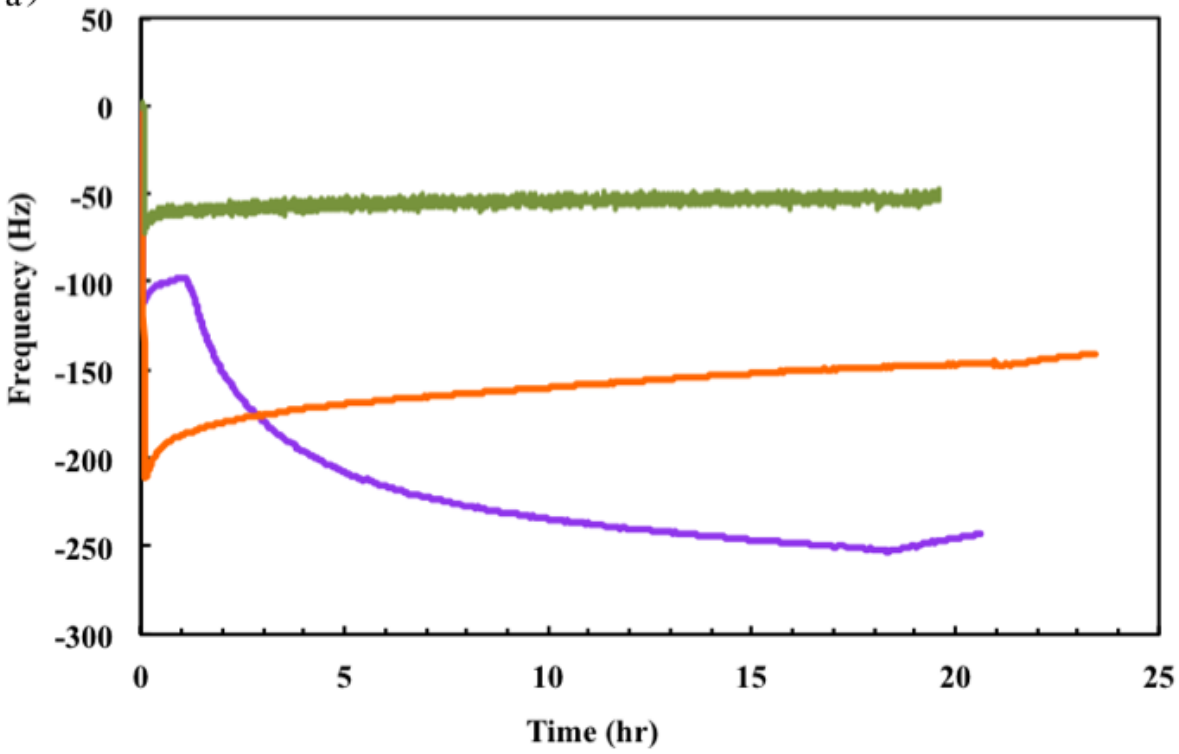
50
0
-50
-100
-150
-200
-250
-300
Frequency (Hz)
0
5
10
15
20
25
Time (hr)

(b)

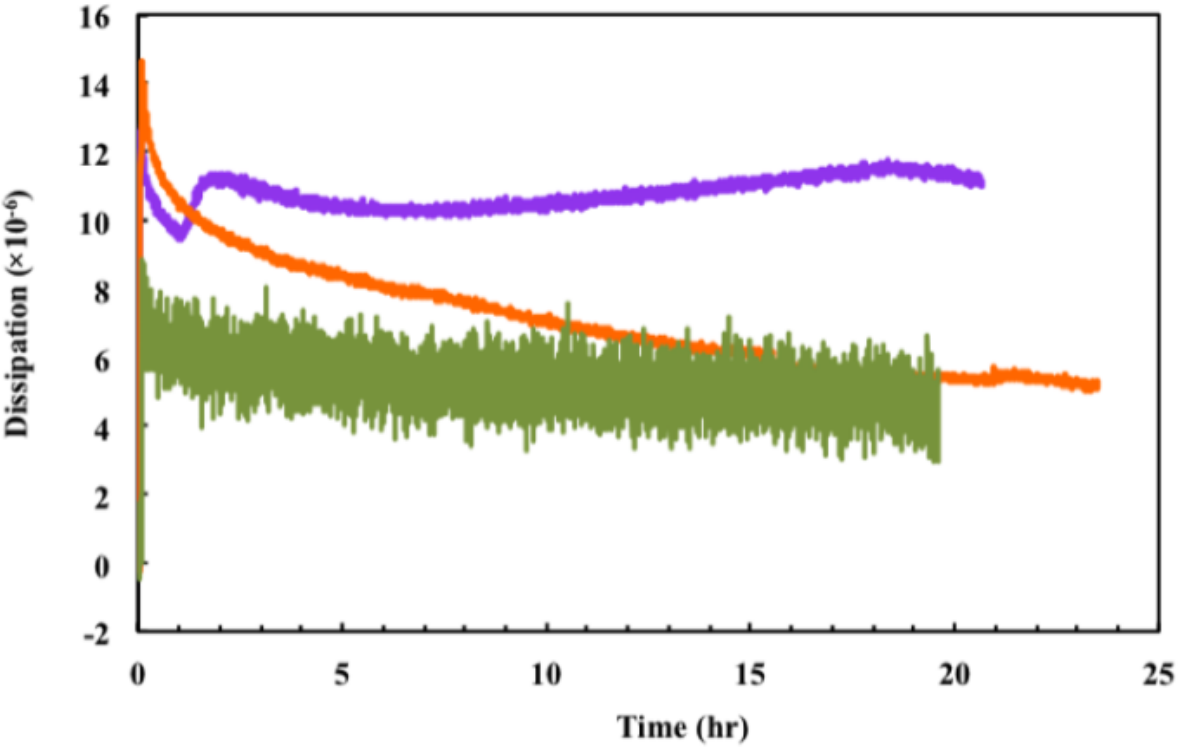
16
14
12
10
8
6
4
2
0
-2
Dissipation (×10⁻⁶)
0
5
10
15
20
25
Time (hr)

Figure 5.13 Representative QCM-D experimental results for the adsorption of 3.8 mM PEI/SDS nanoparticle on different surfaces. The purple color represents the results for Au, orange color for SiO_2, green color for $CaCO_3$. (a) Frequency change vs time (b) Dissipation change vs time

Salt effect: The salt effect is illustrated in Figure 5.12 and Table 5.3. The results show that for both surfaces, a larger amount of mass is adsorbed after addition of salts. This can be explained by the fact that the added salts decrease the repulsion between the adsorbed complex nanoparticles and incoming nanoparticles from the bulk. In addition, the salt may also increase the charge of SiO_2, therefore leading to more binding sites on the surface. Another significant feature after addition of salt is the lack of secondary adsorption on Au surface. This can be explained by the fact that the added salt accelerates the rate of further adsorption of PEI/ SDS nanoparticles and the equilibrium state is reached faster than that in the absence of salts.

5.6 Conclusions

The properties of refined nanoparticle adsorbed at the solid–liquid interface depend on the characteristics of the substrate. First, the adsorption of PEI/SDS nanoparticles on Au shows two-step adsorption during long time of aging, the viscoelastic properties of the adsorbed layer change accordingly. In contrast, the kinetic adsorption of the same nanoparticles shows only one plateau. By further investigation of the conformation change of surface layer on both substrates, we inferred that the distinction of adsorption behavior between two different surfaces is due to the flexibility of adsorbed nanoparticle on the surface. Weak interactions between nanoparticles and Au surface allow further disassembly of the surface layer and result in the formation of multilayers. While strong attraction between nanoparticles and SiO_2 provides less flexibility for nanoparticles, and the adsorbed layer remains almost unchanged during long-term aging. Moreover, the addition of salts enhances the adsorption on both surfaces and equilibrium state of

adsorption reaches faster. Rinse of the films with Millipore water confirms that the adsorption of PEI/SDS nanoparticles is irreversible and binding of excess nanoparticles at higher concentration is rinsed off more easily.

References

[1] M. Knag, J. Sjoblom, Journal of Dispersion Science and Technology 27 (2006) 277.

[2] G. M. Westwood, R. Parker, Macromolecules 43 (2010) 10582.

[3] S. Paria, K. C. Khilar, Advances in Colloid and Interface Science 110 (2004) 75.

4] K. Thalberg, K. Bergfeldt, Langmuir 7 (1991) 2893.

[5] D. W. McQuigg, P. L. Dubin, The Journal of Physical Chemistry 96 (1992) 1973.

[6] M. A. Winnik, C. Chassenieux, Langmuir 16 (2000) 4495.

[7] H. Dautzenberg, Macromolecular Chemistry and Physics 203 (2002) 2095.

[8] S. A. Agnihotri, T. M. Aminabhavi, Journal of Controlled Release 100 (2004) 5.

[9] A. Mezei, I. Varga, T. Gila´nyi, Langmuir 23 (2007) 4237.

[10] M. Y. Arteta, R. A. Campbell, T. Nylander, Langmuir 29 (2013) 5817.

[11] T. Nylander, B. Lindman, Advances in Colloid and Interface Science 126 (2006) 105−123.

[12]. A. Dedinaite, M. Bergström. , Langmuir 16 (2000) 5257−5266.

[13] R. A. Campbell, A. Angus-Smyth, T. Nylander, I. Varga, , The Journal of Physical Chemistry B 116 (2012) 7981.

[14] I. Varga, R.Meszaros, P. M. Claesson, Soft Matter 7 (2011) 10701.

[15] C. D. Bain, D. Langevin, R. Meszaros, T. Nylander, C. Stubenrauch, S. Titmuss, R. Von Klitzing, Advances in Colloid and Interface Science 155 (2010) 32.

[16] S. Ondaral, L. Odberg, L. Wagberg, Langmuir 26 (2010) 14606.

[17] Y.Chen. C. I. Cheng, Chemical Society Reviews 41 (2012) 1947.

[18]T. Roques-Carmes, S. Aouadj, C. Filiâtre, F. Membrey, A. Foissy, Journal of Colloid and Interface Science 274 (2004) 421.

[19] C. S. Hodges, S. Biggs, L. Walker, Langmuir 25 (2009) 4484.

[20] P. M. Claesson, M. L. Fielden, A. Dedinaite, Journal of Physical Chemistry B 102 (1998) 1270.

[21] J. Merta, T. Tammelin, P. Stenius, Colloids and Surfaces A: Physicochemical and Engineering Aspects 250 (2004) 103.

[22] A. Mohr, T. Nylander, L. Piculell, B. Lindman, V. Boyko, F. W. Bartels, Y. Liu, V. Kurkal-Siebert, ACS Applied Materials & Interfaces 4 (2012) 1500.

[23] M. Lundin, L. Macakova, A. Dedinaite, P. Claesson, Langmuir 24 (2008) 3814.

[24] R. Me´sza´ ros, L.Thompson, M. Bos, P. de Groot, Langmuir 18 (2002) 6164.

[25] M. Jaschke, H. J. Butt, H. E. Gaub, S. Manne, Langmuir 13 (1997) 1381.

[26] M. A. Plunkett, P. M. Claesson, M. W. Rutland, Langmuir 18 (2002) 1274.

[27] T. Reihs, M. Müller, K. Lunkwitz, Journal of Colloid and Interface Science 271 (2004) 69.

[28] K.A. Marx, Biomacromolecules 4 (2003) 1099.

[29] A. Dedinaite, P. M. Claesson, M. Bergström, Langmuir 16 (2000) 1951.

[30] R.Me´sza´ ros, L. Thompson, I. Varga, T. Gila´nyi, Langmuir 19 (2003) 9977.

[31] Y Gao , L.T. Duc , A. Ali , B. Liang , J. Liang , P. Dhar, Langmuir 29 (2013) 3654.

[32] P. M. Karlsson, A. E. C. Palmqvist, K. Holmberg, Langmuir 24 (2008) 13414.

[33] J. Kou, D. Tao, T. Sun, G. Xu, Minerals & metallurgical Processing 21 (2012) 47.

[34] A. Barrantesa, T. Arnebrant, L. Lindh, Colloids and Surfaces A: Physicochemical and Engineering Aspects 442 (2014) 56.

[35] K. F.Wang, R. Nagarajan, T. A.Camesano, Colloids and Surfaces B: Biointerfaces 116 (2014) 472.

[36] L. Alagha, S. Wang, Z. Xu, J. Masliyah, Journal of Physical Chemistry C 115 (2011) 15390.

[37] M. A. Plunkett, P. M. Claesson, M. Ernstsson, M. W. Rutland, Langmuir 19 (2003) 4673.

[38] A. Abudu, L. Goual, Energy & Fuels 23 (2009) 1237.

[39] P. Bingen, G. Wang, N. F. Steinmetz, M. Rodahl, R. P. Richter, Analytical Chemistry 80 (2008) 8880.

[40] C. A. Keller, K. Glasmästar, V. P. Zhdanov, B. Kasemo, Physical Review Letters 84 (2000) 5443.

6 Summary and Future Work

This dissertation focuses on the fundamental studies of bulk and interfacial properties of a refined self-assembled polyelectrolyte/surfactant nanoparticles [polyethylenimine (PEI) / sodium dodecyl sulfate(SDS)] with several applications in commercial and biomedical industries. The research work described in this dissertation can be summarized as follows:

1) In the bulk solution, the positively charged nanoparticles have an average particle size ranging from 110 -150 nm and excellent stability (no changes in particle size and zeta potential were observed) up to six months in pure water solution. However, the stability of the system had a strong dependence on the ionic strength of the solution. These refined nanoparticles acted as soft colloidal particles where the nanoparticle interacted with salts as a whole. These results were in contrast with the literature reports on the effect of salts on polyelectrolyte surfactant mixtures or polyelectrolyte surfactant complexes in the presence of excess surfactant or polyelectrolyte components, which typically resulted in the growth of micelles or reduction of interaction between polyelectrolyte and surfactant. Both the anions and cations affect the stability of cationic PEI/SDS nanoparticles in electrolyte solutions. The anion (counter-ion) caused precipitation at a critical concentration and this critical concentration showed a power-law dependence on its valence as predicated by the Schultz-Hardy rule. However, contrary to solid colloidal particles, which do not depend on the concentration of co-ions, the stability of our polyelectrolyte complexes was also affected by the charge on the co-ions. We found that these complex nanoparticles remained more stable at higher valence cations (coion). Furthermore, for anions or cations of same valence, the critical concentration is found to

follow the same trend as salts in the Hoffmeister series. Overall, these observations suggested that both electrostatic interaction and hydration forces are important contributors towards colloidal complex stability. These fundamental studies provide an insight into the ability of refined self-assembled systems to protect the encapsulated components from the environmental change in biomedical or other commercial applications. Also, for future work, PEI/SDS system can serve as a model of bulk and surface behavior studies on other different polyelectrolyte/surfactant nanoparticle system in more applications.

2) At the air/water interface (which in this dissertation serves as a model fluid/fluid interface), not only are PEI/SDS nanoparticles surface active, but for a certain range of SDS concentrations, the nanoparticles also undergo hydrophobic interface induced release, demonstrated by a two-stage adsorption to the air/water interface. This disassembly is also evidenced by direct visualization of the interface, as well as a sharp decrease in the surface shear viscosity at the interface. As a result, these nanoparticles can reduce the critical micelle concentration (CMC) of the solution by 6 times when compared to pure SDS. In addition, the kinetic adsorption behavior can be tuned by salts and the equilibrium can be reached faster with the addition of salts. Such adsorption behavior of refined PEI/SDS nanoparticles was in large contrast with PEI/SDS mixtures, which show competitive adsorption between free surfactant and polyelectrolyte/surfactant complexes. The primary application of these nanoparticles will be for controlled release of entrapped molecules at a hydrophobic interface. These nanoparticles can be also used in surfactant flooding and enhanced oil recovery, to protect the surfactant by entrapping it, and reducing the overall cost of surfactant delivery by (a) allowing controlled release

of the surfactant at the hydrophobic interface between oil/water and (b) by reducing the net amount of surfactant required, due to a reduction in the CMC. In the future, it would be interesting to test in details the effects of salts with different valency and/or hydration radius or even brines on the adsorption and rheological properties of the polyelectrolyte/surfactant system. These tests are important to ultimately employ these particles in enhanced oil recovery applications.

3) At a solid/liquid interface, the adsorption of refined PEI/SDS nanoparticles were compared on two different substrates: gold (Au) a model neutral control system and silicon dioxide (SiO_2), a model for the surface encountered in many oil wells. Two major findings are summarized as follows: (a) The kinetic adsorption of PEI/SDS nanoparticles depended on the surface properties of the substrates. While the nanoparticles adsorption to both surfaces, the mechanisms of adsorption were significantly different. The nanoparticles show a typical one-step adsorption curve onto SiO_2. However, a two-step adsorption of the refined nanoparticles was observed for the Au surface, suggesting differences in the conformation of the adsorbed nanoparticles on these two surfaces.The viscoelastic properties obtained by QCM-D were correlated with AFM images to obtain direct visual confirmation of conformation changes in these nanoparticles. Based on our observations, we conclude that the weak interactions between nanoparticles and Au allowed the particles to rearrange themselves allowing more particles to adsorb onto Au surface. The conformation showed little change on SiO_2 surface, which is probably due to the strong electrostatic interaction between the positive charged particles and negative charged surfaces that stabilized the nanoparticles. Further, the addition of salts enhanced the adsorption of refined nanoparticles on both substrates. This study provided

preliminary results for modifying the solid surface properties in various application, such as wettability change on porous media for enhanced oil recovery, coating for corrosion inhibition, as well as hair conditioning.